AFRL-PR-WP-TR-2000-2121

FUEL FORMULATION STUDIES
DELIVERY ORDER 6

B. ARNOLD, MARK BADGER,
BRUCE MILLER, AND CHUNSHAN SONG

ENERGY INSTITUTE AND DEPARTMENT OF MECHANICAL AND NUCLEAR ENGINEERING
THE PENNSYLVANIA STATE UNIVERSITY
UNIVERSITY PARK, PA 16802-2320

MAY 2000

FINAL REPORT FOR PERIOD OF 01 NOVEMBER 1997 – 15 JANUARY 2000

Approved for public release; distribution unlimited

PROPULSION DIRECTORATE
AIR FORCE RESEARCH LABORATORY
AIR FORCE MATERIEL COMMAND
WRIGHT-PATTERSON AIR FORCE BASE, OH 45433-7251

REPORT DOCUMENTATION PAGE	Form Approved OMB No. 0704-0188

Public reporting burder for this collection of information is estibated to average 1 hour per response, including the time for reviewing instructions, searching existing data sources, gathering and maintaining the data needed, and completing and reviewing this collection of information. Send comments regarding this burden estimate or any other aspect of this collection of information, including suggestions for reducing this burder to Department of Defense, Washington Headquarters Services, Directorate for Information Operations and Reports (0704-0188), 1215 Jefferson Davis Highway, Suite 1204, Arlington, VA 22202-4302. Respondents should be aware that notwithstanding any other provision of law, no person shall be subject to any penalty for failing to comply with a collection of information if it does not display a currently valid OMB control number. PLEASE DO NOT RETURN YOUR FORM TO THE ABOVE ADDRESS.

1. REPORT DATE (DD-MM-YYYY) 01-05-2000	2. REPORT TYPE Final Report	3. DATES COVERED (FROM - TO) 01-11-1997 to 15-01-2000

4. TITLE AND SUBTITLE
Fuel Formulation Studies Delivery Order 6
Unclassified

5a. CONTRACT NUMBER
F33615-98-D-2802

5b. GRANT NUMBER

5c. PROGRAM ELEMENT NUMBER

6. AUTHOR(S)
Arnold, B. ;
Badger, Mark ;
Miller, Bruce ;
Song, Chunshan ;

5d. PROJECT NUMBER

5e. TASK NUMBER

5f. WORK UNIT NUMBER

7. PERFORMING ORGANIZATION NAME AND ADDRESS
Energy Institute and Department of Mechanical and Nuclear Engineering
The Pennsylvania State University
University Park, PA16802-2320

8. PERFORMING ORGANIZATION REPORT NUMBER

9. SPONSORING/MONITORING AGENCY NAME AND ADDRESS
Propulsion Directorate
Air Force Research Laboratory
Air Force Materiel Command
Wright-Patterson AFB, OH45433-7251

10. SPONSOR/MONITOR'S ACRONYM(S)

11. SPONSOR/MONITOR'S REPORT NUMBER(S)

12. DISTRIBUTION/AVAILABILITY STATEMENT
APUBLIC RELEASE
,

13. SUPPLEMENTARY NOTES

14. ABSTRACT
Studies of industrial methods of producing coal-derived jet fuels were undertaken. The focus of the effort was on incorporating coal or coal components into the existing petroleum refinery infrastructure.

15. SUBJECT TERMS
Fuel; Coal Derived Fuel; Thermal Stability; High Temperature Fuels; coprocessing liquids; petroleum resudues; coal tar blending

16. SECURITY CLASSIFICATION OF:			17. LIMITATION OF ABSTRACT Same as Report (SAR)	18. NUMBER OF PAGES 135	19. NAME OF RESPONSIBLE PERSON Fenster, Lynn lfenster@dtic.mil
a. REPORT Unclassified	b. ABSTRACT Unclassified	c. THIS PAGE Unclassified			19b. TELEPHONE NUMBER International Area Code Area Code Telephone Number 703767-9007 DSN 427-9007

NOTICE

USING GOVERNMENT DRAWINGS, SPECIFICATIONS, OR OTHER DATA INCLUDED IN THIS DOCUMENT FOR ANY PURPOSE OTHER THAN GOVERNMENT PROCUREMENT DOES NOT IN ANY WAY OBLIGATE THE US GOVERNMENT. THE FACT THAT THE GOVERNMENT FORMULATED OR SUPPLIED THE DRAWINGS, SPECIFICATIONS, OR OTHER DATA DOES NOT LICENSE THE HOLDER OR ANY OTHER PERSON OR CORPORATION; OR CONVEY ANY RIGHTS OR PERMISSION TO MANUFACTURE, USE, OR SELL ANY PATENTED INVENTION THAT MAY RELATE TO THEM.

THIS REPORT IS RELEASABLE TO THE NATIONAL TECHNICAL INFORMATION SERVICE (NTIS). AT NTIS, IT WILL BE AVAILABLE TO THE GENERAL PUBLIC, INCLUDING FOREIGN NATIONS.

THIS TECHNICAL REPORT HAS BEEN REVIEWED AND IS APPROVED FOR PUBLICATION

C. Obringer

CYNTHIA OBRINGER
Fuels Branch
Turbine Engine Division
Propulsion Directorate

WILLIAM E. HARRISON III
Chief, Fuels Branch
Turbine Engine Division
Propulsion Directorate

John T. Datko

JOHN T. DATKO, JR.
Acting Chief of Technology
Turbine Engine Division
Propulsion Directorate

Do not return copies of this report unless contractual obligations or notice on a specific document requires its return.

REPORT DOCUMENTATION PAGE	*Form Approved* *OMB No. 0704-0188*

Public reporting burden for this collection of information is estimated to average 1 hour per response, including the time for reviewing instructions, searching existing data sources, gathering and maintaining the data needed, and completing and reviewing the collection of information. Send comments regarding this burden estimate or any other aspect of this collection of information, including suggestions for reducing this burden, to Washington Headquarters Services, Directorate for Information Operations and Reports, 1215 Jefferson Davis Highway, Suite 1204, Arlington, VA 22202-4302, and to the Office of Management and Budget, Paperwork Reduction Project (0704-0188), Washington, DC 20503.

1. AGENCY USE ONLY *(Leave blank)*	2. REPORT DATE May 2000	3. REPORT TYPE AND DATES COVERED FINAL, 11/01/97 – 01/15/00

4. TITLE AND SUBTITLE Fuel Formulation Studies Delivery Order 6	5. FUNDING NUMBERS C F33615-98-D-2802 PE 62203F PR 3048 TA 05 WU EX
6. AUTHOR(S) B. Arnold, Mark Badger, Bruce Miller, Chunshan Song	
7. PERFORMING ORGANIZATION NAME(S) AND ADDRESS(ES) Energy Institute and Department of Mechanical and Nuclear Engineering The Pennsylvania State University University Park, PA 16802-2320	8. PERFORMING ORGANIZATION REPORT NUMBER D.O. 0006
9. SPONSORING/MONITORING AGENCY NAME(S) AND ADDRESS(ES) Propulsion Directorate Air Force Research Laboratory Air Force Materiel Command Wright-Patterson AFB, OH 45433-7251 POC: Cindy Obringer, AFRL/PRTG, 937-255-6390	10. SPONSORING/MONITORING AGENCY REPORT NUMBER AFRL-PR-WP-TR-2000-2121

11. SUPPLEMENTARY NOTES

12a. DISTRIBUTION AVAILABILITY STATEMENT Approved for Public Release; Distribution Unlimited	12b. DISTRIBUTION CODE

13. ABSTRACT *(Maximum 200 words)*

Studies of industrial methods of producing coal-derived jet fuels were undertaken. The focus of the effort was on incorporating coal or coal components into the existing petroleum refinery infrastructure.

14. SUBJECT TERMS Fuel, Coal Derived Fuel, Thermal Stability, High Temperature Fuels, coprocessing liquids, petroleum residues; coal tar blending	15. NUMBER OF PAGES 138
	16. PRICE CODE

17. SECURITY CLASSIFICATION OF REPORT	18. SECURITY CLASSIFICATION OF THIS PAGE	19. SECURITY CLASSIFICATION OF ABSTRACT	20. LIMITATION OF ABSTRACT
UNCLASSIFIED	UNCLASSIFIED	UNCLASSIFIED	SAR

Standard Form 298 (Rev. 2-89) (EG)
Prescribed by ANSI Std. 239.18
Designed using Perform Pro, WHS/DIOR, Oct 94

THIS PAGE INTENTIONALLY LEFT BLANK

Table of Contents

Section Page
List of Figures v
List of Tables ix
1.0 CATALYTIC UPGRADING OF COPROCESSING LIQUIDS 1
1.1 Introduction 1
1.2 Experimental Section 2
1.3 Results and Discussion 4
1.4 Conclusions 11

2.0 ENHANCING STABILITY OF JET FUELS FROM COPROCESSING 12
2.1 Abstract 12
2.2 Introduction 12
2.3 Experimental 13
2.4 Results and Discussion 14
2.5 Conclusion 20

3.0 CATALYST CHARACTERIZATION 21
3.1 Introduction 21
3.2 Experimental 21
3.3 Results and Discussion 22
3.4 Conclusions 29

4.0 ASSEMBLY AND TESTING OF A 1-LITER STIRRED-TANK FLOW REACTOR 30
4.1 Hydrogen Delivery System 33
4.2 Slurry Feed System 34
4.3 Reactor Components 36
4.4 Data Acquisition System 37
4.5 Safety Issues 37

5.0 ASSEMBLY OF A LABORATORY-SCALE FIXED-BED FLOW REACTOR FOR CATALYTIC UPGRADING AND REFINING OF JET FUELS 40
5.1 Abstract 40
5.2 Introduction 40
5.3 Subtask Objectives 41
5.4 Literature Survey 41
5.5 Experimental 44

6.0 ASSEMBLY OF A HIGH-PRESSURE, HIGH-TEMPERATURE CELL FOR *IN SITU* FT-IR CHARACTERIZATION OF CATALYSTS AND REACTION INTERMEDIATES UNDER REACTION CONDITIONS 47
6.1 Introduction 47
6.2 Experimental 48
6.3 Results and Discussion 53
6.4 Conclusion 56

Table of Contents (continued)

Section Page
7.0 CO-COKING COAL AND PETROLEUM RESIDUES 57
  7.1 Goals 57
  7.2 Summary 57
  7.3 Introduction 57
  7.4 Experimental 58
  7.5 Results and Discussion 60
  7.6 Conclusions 77
  7.7 Future Work 78

8.0 COAL-BASED FUEL FORMULATION AND ENGINEERING 79
  8.1 Introduction 79
  8.2 Sources of Ultralow-Ash Coal 79
  8.3 Flowsheet Selection for Production of Ultralow-Ash Coal 80
  8.4 Evaluation of Co-Coking Test Coals (Phase II) 83
  8.5 Case Studies: Cost of Production of Ultralow-Ash Coal for Co-Coking Feedstock 84
  8.6 Summary and Conclusions 95

9.0 BLENDING OF COAL-TAR STREAMS WITH SUITABLE REFINERY STREAMS 96
  9.1 Goals 96
  9.2 Summary 96
  9.3 Introduction 96
  9.4 Experimental 97
  9.5 Results and Discussion 98
  9.6 Conclusions 113
  9.7 Suggestions for Future Work 113

10.0 REFERENCES 115
List of Symbols, Abbreviations, and Acronyms 122

List of Figures

Figure Page

1. Effect of the Sulfur/Pd Atomic Ratio on Naphthalene Conversion and Selectivity toward Tetralin and Decalin over Pd/USY12 in the Presence of Added Benzothiophene................5

2. Effect of the Sulfur/Pd Atomic Ratio on Naphthalene Conversion and Selectivity toward Tetralin and Decalin over Pd/USY20 in the Presence of Added Benzothiophene................5

3. Effect of the Sulfur/Pd Atomic Ratio on Naphthalene Conversion and Selectivity toward Tetralin and Decalin over Pd/USY40 in the Presence of Added Benzothiophene................6

4. Effect of the Sulfur/Pd Atomic Ratio on Naphthalene Conversion and Selectivity toward Tetralin and Decalin over Pd/USY80 in the Presence of Added Benzothiophene................6

5. TPR Profiles of Four Different Pd/USY Catalysts..........8

6. TPD Profiles of Four Different Pd/USY catalysts..........9

7. TPR Characterization Results..........17

8. Hydrogenation of 1-Naphthol over Pt+Pd/TiO_2 (Pt/Pd=0.3) 150 °C, 300 psi..........18

9. Hydrogenation of THNol over Pt+Pd/TiO_2 (1 wt percent, Pt/Pd=0.3)150 °C, 300 psi. 19

10. Hydrogenation of Tetralone over Pt+Pd/TiO_2 (1 wt percent, Pt/Pd=0.3)150 °C, 500 psi. 19

11. Reaction Network of 1-Naphthol Hydrogenation at Low Temperature..........20

12. TPR Profile of 2-wt percent Pt/Al_2O_3 Catalyst..........25

13. TPR Profile of 2-wt percent Pd/Al_2O_3 Catalyst..........26

14. TPR Profile of 2-wt percent Pt/MCM Catalyst..........26

15. TPR Profile of 2-wt percent Pd/MCM Catalyst. 27

16. XRD Patterns of Various 2-wt percent Pt Catalysts..........28

17. XRD Patterns of 2-wt percent Pd Catalysts. 29

18. Process Flow Diagram for a 1-L Stirred-Tank Flow Reactor. 31

19. Gas-Delivery System for a 1-L Stirred-Tank Flow Reactor. 32

20. Gas-Delivery Station..........34

List of Figures (continued)

Figure Page
21. Feed-System Components. 35

22. Reactors 3-5, Gas-Product Peripherals. 37

23. Panel and Instrumentation. 39

24. Fixed-Catalyst-Bed, High-Pressure, Liquid-FlowRreactor. 46

25. Schematic of the Analytical Setup of the FTIR. 49

26. Design of the High-Pressure, High-Temperature FTIR Cell. 50

27. Spectrum of Crystal as Provided by SpectraTech. 51

28. Spectrum of the Crystal in the Empty Cell (without purge) 52

29. Spectrum of the Empty Cell in the Presence of N_2 Purge. 52

30. Schematic Representation of Vented Reactor System. 59

31. Reaction Length and Feed-Ratio Effects on the Solid Coke Products Formed from Co-Coking Reactions at 465 °C with Powellton Coal and the Two Petroleum Resids. 63

32. Boiling-Point Distributions of Heated Treated Resids at 465 °C. 64

33. Boiling-Point Distributions of Co-Coking Reactions in Sealed Reactor at 465 °C. 65

34. Boiling-Point Distributions of Co-Coking Reactions in Vented Reactor at 465 °C. 65

35. Boiling-Point Distributions from Co-Coking Reactions at Different Temperatures. 66

36. Chromatogram of Hexane-Soluble Fraction from a Co-Coking Run at 465 °C in a Sealed Reactor. 67

37. Chromatogram of Hexane-Soluble Fraction from a Co-Coking Run at 465 °C in a Vented Reactor. 67

38. Boiling-Point Distributions of Hexane-Soluble Fractions form Co-Coking Experiments Using Different Resid Feeds 72

39. Photomicrographs of Solid Residues from Various Coking Experiments. 74

List of Figures (continued)

Figure Page

40. Distribution of Petroleum-Derived Carbon Textures in Residues from Petroleum-Fraction/Coal Blends Following Carbonization at 465 °C. 75

41. Distribution of Petroleum-Derived Carbon Textures in Residues from Petroleum-Fraction/Powellton Coal Blends after Carbonization at 465 °C. 77

42. Flowsheet Schematic for Low-Ash Coal Production........ 82

43. Balanced Flowsheet for Producing 3-Percent Ash Powellton-Seam Coal........ 86

44. Balanced Flowsheet for Producing 4-Percent Ash Pittsburgh-Seam Coal. 91

45. The Sulfur Removal after Hydrogenation of Different Blends at Varying Temperature and Pressure in a Micro-Reactor (a) DA/HT LCO:RCO 3:1; (b) DA/HT LCO:RCO 1:1; (c) DA/HT LCO:RCO 1:3; and (d) DA/HT LCO:RCO 0:1........ 99

46. The Nitrogen Removal after Hydrogenation of Different Blends at Varying Temperature and Pressure in a Micro-Reactor (a) DA/HT LCO:RCO 3:1; (b) DA/HT LCO:RCO 1:1; (c) DA/HT LCO:RCO 1:3; and (d) DA/HT LCO:RCO 0:1........ 100

47. The Increase in Hydrogen-to-Carbon Ratio of Hydrogenated Products from Different Blends at Varying Temperature and Pressure in a Micro-Reactor (a) DA/HT LCO:RCO 3:1; (b) DA/HT LCO:RCO 1:1; (c) DA/HT LCO:RCO 1:3; and (d) DA/HT LCO:RCO 0:1... 101

48. The Improvement in the Jet Fuel Range (180 to 330°C) of Hydrogenated Products from Different Blends at Varying Temperature and Pressure in a Micro-Reactor (a) DA/HT LCO:RCO 3:1; (b) DA/HT LCO:RCO 1:1; (c) DA/HT LCO:RCO 1:3; and (d) DA/HT LCO:RCO 0:1........ 102

49. The Conversion of Naphthalene to Tetralin in Hydrogenated Products from Different Blends at Varying Temperature and Pressure in a Micro-Reactor (a) DA/HT LCO:RCO 3:1; (b) DA/HT LCO:RCO 1:1; (c) DA/HT LCO:RCO 1:3; and (d) DA/HT LCO:RCO 0:1... 103

50. The Sulfur Removal after Hydrogenation of Different Blends at Varying Temperature and Pressure in a Stirred Batch Reactor (a) DA/HT LCO:RCO 3:1; (b) DA/HT LCO:RCO 1:1; (c) DA/HT LCO:RCO 1:3; and (d) DA/HT LCO:RCO 0:1........ 105

51. The Nitrogen Removal after Hydrogenation of Different Blends at Varying Temperature and Pressure in a Stirred Batch Reactor (a) DA/HT LCO:RCO 3:1; (b) DA/HT LCO:RCO 1:1; (c) DA/HT LCO:RCO 1:3; and (d) DA/HT LCO:RCO 0:1........ 106

List of Figures (continued)

Figure Page

52. The Increase in Hydrogen-to-Carbon Ratio of Hydrogenated Products from Different Blends at Varying Temperature and Pressure in a Stirred Batch Reactor (a) DA/HT LCO:RCO 3:1; (b) DA/HT LCO:RCO 1:1; (c) DA/HT LCO:RCO 1:3; and (d) DA/HT LCO:RCO 0:1. 107

53. The Improvement in the Jet-Fuel Range (180 to 330°C) of Hydrogenated Products from Different Blends at Varying Temperature and Pressure in a Stirred Batch Reactor (a) DA/HT LCO:RCO 3:1; (b) DA/HT LCO:RCO 1:1; (c) DA/HT LCO:RCO 1:3; and (d) DA/HT LCO:RCO 0:1. 108

54. The Conversion of Naphthalene to Tetralin in Hydrogenated Products from Different Blends at Varying Temperature and Pressure in a Stirred Batch Reactor (a) DA/HT LCO:RCO 3:1; (b) DA/HT LCO:RCO 1:1; (c) DA/HT LCO:RCO 1:3; and (d) DA/HT LCO:RCO 0:1 109

55. Yields of Conventional Fuels and Hydrogenated Fuels from Reaction at 1000 psig in a Stirred Batch Reactor after Thermal Stressing at 480 °C. 110

56. Yields of Conventional Fuels and Hydrogenated Fuels from Reaction at 1500 psig in a Stirred Batch Reactor after Thermal Stressing at 480 °C. 110

57. GC-MS Trace of Hydrogenated Product of DA/HT LCO:RCO 1:1 (under 1000 psig and 350 °C) before Stressing. 111

58. GC-MS Trace of Hydrogenated Product of DA/HT LCO:RCO 1:1 (under 1000 psig and 350 °C) after Stressing. 111

List of Tables

Table Page

1. Type of Support and its Nominal Properties 2

2. Pulse Chemisorption over Pd Supported on Different USY Supports 10

3. Types of Supports and Their Nominal Properties 13

4. Effects of Different Supports 14

5. Hydrogenation of 1-Naphthol over Pt and Pd Monometallic Catalysts 15

6. Hydrogenation of 1-Naphthol over Pt and Pd Bimetallic Catalysts 16

7. H_2 Pulse Chemisorption Results for TiO_2-Supported Pt, Pd Catalysts 17

8. Chemisorption Data for Al_2O_3-Supported Pt and Pd Catalysts 23

9. Chemisorption Data (metal dispersion in terms of H/M or CO/M) on TiO_2-Supported Pt and Pd Catalysts 24

10. Typical Operating Parameters of the 1-Liter Stirred-Tank Flow Reactor 30

11. Characteristics of Project Coals 58

12. Overall Product Distribution (in percent yield) for Sealed Co-Coking Reactions at 465 ^{o}C for 2 Hours 60

13. The Overall Product Distribution for the Various Vented Reactions (in percent yields) at 465 ^{o}C for 2 Hours 60

14. Feed Ratio and Reaction-Length Effects on Product Yields from Co-Coking Reactions with Powellton Coal and the Two Petroleum Resids at 465 °C 61

15. Feed Ratio and Reaction Length Effects on Hexane-Soluble Product H/C Ratios from Co-Coking Reactions with Powellton Coal and Various Petroleum Resids at 465 °C 62

16. Compound Distribution of Co-Coking Products 68

17. Compound-Distribution Yield in the Hexane-Soluble Fraction 69

18. Substituted-Compound Distribution and Yield for the Hexane-Soluble Fraction 69

19. Substituted-Compound Distribution and Yield for the Hexane-Soluble Fraction 70

List of Tables (continued)

Table Page

20. Solid H/C Ratios for Co-Coking Reactions at 465 °C in the Vented Reactor System......... 71

21. Liquid H/C Ratios for Co-Coking Reactions at 465 °C in the Vented Reactor System........ 71

22. Product Distribution for Co-Coking Reactions at 465 °C in the Vented Reactor System..... 71

23. Summary of Low-Ash Bituminous-Coal Production in the United States in 1996 and 1998 as Shipped to Power Stations (Energy Information Agency).. 80

24. Froth-Flotation Yield Versus Ash Results for Project Coal Samples.................................. 84

25. Estimated Operating Costs for Producing 3-Percent Ash Powellton-Seam Coal 87

26. Estimated Operating Costs for Producing 3-Percent Ash Powellton-Seam Coal 88

27. Cost of Production of 3-Percent Ash Powellton-Seam Coal... 89

28. Estimated Operating Costs forProducing 4-Percent Ash Pittsburgh-Seam Coal.................. 92

29. Estimated Operating Costs for Producing 4-Percent Ash Pittsburgh-Seam Coal 93

30. Cost of Production of 4-Percent Ash Pittsburgh-Seam Coal 94

32. Examples of Composition Analysis of Hydrogenated Fuels from Reaction at 1000 psig and 350 °C in a Stirred Batch Reactor before and after Stressing.................................... 112

33. Examples of Composition Analysis of Hydrogenated Fuels from Reaction at 1500 psig and 350 °C in a Stirred Batch Reactor before and after Stressing.................................... 113

1.0 CATALYTIC UPGRADING OF COPROCESSING LIQUIDS

1.1 Introduction

Aromatics in diesel fuel contribute greatly to the formation of harmful emissions from the exhaust gases of diesel engines; thus, a high aromatic content significantly lowers the quality of transportation fuels. With the implementation of strict environmental regulations for fuel composition and limitations on the aromatic content, deep hydrogenation of aromatic compounds in distillate fuels like jet fuel has received considerable attention.

Any fuel precursors inevitably contain small amounts of impurities that will deactivate catalysts and must be removed. Among the most common impurities are sulfur compounds. Conventional hydrotreating catalysts such as sulfide Ni-Mo and Co-Mo supported on alumina have the advantage of high tolerance to sulfur in the feedstock, but they become active only at relatively high temperatures. A reaction temperature >300 °C is typical for conventional hydrotreating processes [1]. Some undesirable reactions such as hydrocracking and dehydrogenation increase with temperature. On the other hand, hydrogenation of aromatics is highly exothermic, and is, therefore, thermodynamically favored at a lower reaction temperature. Hence, a high reaction temperature shifts the equilibrium toward a higher aromatic content in the equilibrium composition. Deep hydrogenation of aromatics requires a high concentration of hydrogen to offset the limitation of the thermodynamic equilibrium conversion at high temperature [1], thus making the process very uneconomical.

Noble-metal catalysts are active for the hydrogenation of aromatics, even at low temperatures, but they are susceptible to poisoning by sulfur-containing compounds. In current processing schemes, multiple catalyst beds are used to achieve deep desulfurization and deep hydrogenation. In the first stage, hydrodesulfurization takes place over a Ni-Mo or Co-Mo catalyst followed by intermediate byproduct gas removal, and finally, hydrogenation over the noble-metal catalyst occurs in the bottom bed where the concentrations of catalyst poisons (organosulfur and H_2S) are very low. There are no reports of noble-metal catalysts that can operate without such intermediate H_2S removal [2]. Noble-metal catalysts with high sulfur resistance, if possible to develop, will allow hydrotreating at substantially lower temperatures and pressures, and can lead to a major improvement in refining efficiency and economics. Because of its importance, sulfur resistance of noble-metal catalysts has been the subject of several recent publications [1, 3, 4]. When noble metals are supported on acidic materials like zeolite, the resistance to sulfur can be significantly increased.

This work focuses on the potential of zeolite-supported Pd catalysts for low-temperature hydrotreating of distillate fuels in the presence of organic sulfur compounds. Hydrogenation of naphthalene in n-tridecane was chosen as a model reaction for hydrotreating, and benzothiophene was added into the reaction system as a model organic sulfur compound. The zeolite supports, mordenite and ultra-stable Y zeolite, were selected because they are distinctly different from conventional supports such as alumina and titanium, and may offer several advantages.

The model-compound test will help the ongoing effort to develop advanced thermally stable jet fuels from coal-derived liquids and petroleum, where both complete and partial hydrogenation reactions of naphthalene-type compounds are important. Complete saturation of naphthalene gives decalins which show much higher thermal stability than long-chain alkanes, while partial saturation produces tetralin which can substantially inhibit the thermal degradation and solid-forming tendency of long-chain alkanes in jet fuels at high temperatures.

1.2 Experimental Section

1.2.1 Catalyst Preparation

Zeolite-supported Pt or Pd catalysts were prepared from the hydrogen form of the synthetic mordenite HM38 and the hydrogen form of a series of ultrastable Y zeolite (USY) support. Table 1 lists the supports and their nominal properties. The catalysts were prepared by incipient-wetness impregnation of an aqueous solution of tetraamminepalladium chloride ($[Pd(NH_3)_4]^{2+}$ Cl_2, Aldrich, 99.99+percent) dissolved in dilute hydrochloric acid (sufficient to form soluble $PdCl_4^{2-}$) to a nominal metal concentration of 2 wt percent. Following drying in a vacuum at 120 °C overnight, the catalysts were calcined in an air stream while the temperature was ramped from room temperature to 450 °C at the rate of 2.0 °C/min and held at 450 °C for 4 hours. The metal reduction was carried out *in situ* during naphthalene hydrogenation tests under a high pressure of hydrogen (1000 psig).

Table 1. Type of Support and Its Nominal Properties

support ID	material type	surface area m^2/g	SiO_2/Al_2O_3 mol ratio	Na_2O wt%	supplier and code
USY12	Y zeolite	730	12.0	0.05	PQ, CBV712
USY20	Y zeolite	780	20.0	0.03	PQ, CBV720
USY40	Y zeolite	750	40.0	0.03	PQ, CBV740
USY80	Y zeolite	780	80.0	0.03	PQ, CBV780

1.2.2 Hydrogenation Procedure

All catalysts were tested at 200 °C for 2 hours (unless otherwise mentioned) in a 25-mL stainless-steel microautoclave reactor. The reactor system is a T-shaped tubing bomb with most of the internal volume in the horizontal tube that contains the catalyst and the reactants.

Typically, the reactor was charged with approximately 0.1 g of catalyst, 1.0 g of naphthalene (Aldrich, 99 percent), 4.0 g of n-tridecane solvent (Aldrich, 99+percent), and 0.35 g of n-nonane (Aldrich, 99+percent, anhydrous) internal standard. Benzothiophene was added in a controlled amount for runs with sulfur. The charged reactor was flushed with H_2 (UHP) three times, then pressurized to 1000 psig of cold H_2 to start the test. The reactor was mounted on a holder and immersed in a fluidized sandbath preheated to a given temperature, usually 200 °C. Mixing was accomplished by shaking the reactor vertically.

After the reaction, the reactor was taken out of the sandbath and quenched in cold water, and allowed to cool to room temperature. After cooling, the gas headspace was collected for analysis, and the reactor was opened. The content was then filtered, and the liquid was analyzed by GC-FID and GC-MS. The solid was washed with acetone and dried.

1.2.3 Product Analysis

Two instrumental setups were used. First, a Perkin-Elmer (PE) 8500 GC equipped with a capillary column (DB-17) and an Flame ionization detector, and operated in the split-injection mode was used to analyze the liquid products quantitatively. The oven temperature was programmed from 40 to 200 °C at 5 °C/min with an initial isothermal time of 5 minutes to allow for the evaporation of the acetone solvent. The injection volume was 0.02 µl for all samples. The product identification was then based upon gas chromatography – mass spectrometry (GC-MS) using a Hewlett Packard (HP) 5890 II GC connected with a HP 5971A mass-selective detector. The GC column was DB-2, and the temperature program was the same as for the PE 8500 GC. In addition, the identifications were further confirmed by running standard compounds.

Since January 1999, the liquids obtained were analyzed quantitatively on a Schimadzu GC-MS. A Schimadzu GC-17A equipped with a Restek XTI-5 column was connected to a Schimadzu MC QP-5000 using a split ratio of 50 in which about 10 mg of liquid products were dissolved in 10 mL of dichloromethane solvent. The temperature program was the same as that used for the PE 8500 GC and HP GC-MS.

Both the GC and GC-MS indicate that cracking of n-tridecane and n-nonane, if any, was negligible under the conditions used (200 °C, 1000 psig cold H_2). The yield of products was determined by quantitative GC analysis using n-nonane as an internal standard, and the conversion was determined by the amount of naphthalene recovered after the reaction.

1.2.4 Catalyst Characterization

All catalyst characterizations, including Temperature-Programmed Reduction, Temperature-Programmed Desorption, and Pulse Chemisorption, were performed using an AutoChem 2910 Analyzer, an automated catalyst characterization system provided by the Micromeritics Instrument Corporation.

1.2.5 Temperature-Programmed Reduction (TPR)

The TPR was used to determine the number of reducible species present in the catalyst and to reveal the temperature at which the reduction occurs.

The TPR analysis begins by passing an analysis gas, a mixture of 5.12 percent H_2/Ar, over the sample, usually starting at ambient temperature. While the gas is flowing at 25 mL/min, the temperature is increased linearly with time from room temperature to 400 °C at the ramp rate of 10 °C/min, and the consumption of hydrogen by adsorption/reaction is monitored simultaneously. Changes in the concentration of the gas mixture are detected, and this information yields the hydrogen uptake on a volume basis.

1.2.6 Temperature-Programmed Desorption (TPD)

The TPD determines the number, type, and strength of active metal sites available on the surface of a catalyst from measurement of the amount of gas desorbed at various temperatures. After the sample has been outgassed in an argon flow, and reduced by pure hydrogen, or otherwise prepared, a steady stream of analysis gas (H_2) flows over the sample and reacts with the active sites. Then programmed desorption begins when the temperature is ramped linearly in time while a constant stream of inert carrier gas (Argon, 70 mL/min) passes over the sample.

At a certain temperature, the heat will overcome the activation energy, breaking the bond between the adsorbate and adsorbent. The adsorbed species will then desorb. If different active metals are present, they usually will desorb the reacted species at different temperatures. The desorbed molecules enter the stream of inert carrier gas and are swept to the detector, which measures the gas concentration. The volume of desorbed species, combined with the stoichiometry factor and the temperature at which pre-adsorbed species desorb, yields the number and strength of active sites.

1.2.7 Pulse Chemisorption

A pulse chemisorption analysis determines active surface area, percent metal dispersion, and active particle size by applying a measured pulse of reactant gas to the sample. Pulse chemisorption is performed in the same manner as TPD, except that the sample is dosed with the analysis gas using the injection loop until each active site has reacted. Once the active sites have completely reacted, the discretely injected gas volumes emerge unchanged. The amount chemisorbed is the difference between the total amount of reactant gas injected and the amount that did not react with the active sites of the sample.

1.3 Results and Discussion

The current study was focused on the effect of the SiO_2/Al_2O_3 ratio of the zeolite support on naphthalene hydrogenation in terms of naphthalene conversion and product selectivity.

1.3.1 Sulfur Tolerance of Pd Catalysts Supported on USY

A series of accelerated sulfur tolerance tests was designed where benzothiophene was added so that the sulfur-to-noble-metal atomic ratio ranged from about 1 to 10. The amount of sulfur added was large enough to cover almost all the metal particles even if they were ideally dispersed at the atomic level.

Figures 1-4 show the results of naphthalene hydrogenation over Pd/HY, using the four different catalyst supports USY12, USY20, USY40, and USY80, respectively, with sulfur addition in the form of benzothiophene. For the four different USY supports, the SiO_2/Al_2O_3 ratios are 12, 20, 40, and 80, respectively, increasing in the order of USY12 < USY20 < USY40 < USY80.

Figures 1 and 2 show that with increasing S/Pd atomic ratio, the catalytic activity decreases gradually in terms of naphthalene conversion from around 90 percent down to 20 percent or less. In addition, the selectvities toward tetralin are low. The sum of hydrogenation products is also far from unity, which implies that there were possibly many side reactions like coke formation during the process of naphthalene hydrogenation.

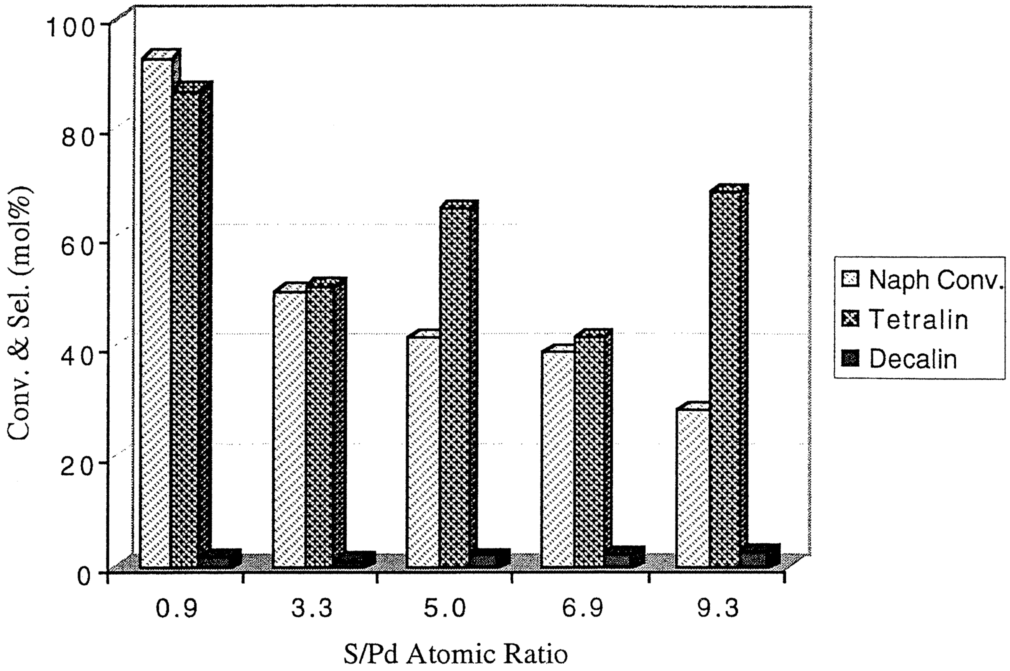

Figure 1. Effect of the Sulfur/Pd Atomic Ratio on Naphthalene Conversion and Selectivity toward Tetralin and Decalin over Pd/USY12 in the Presence of Added Benzothiophene

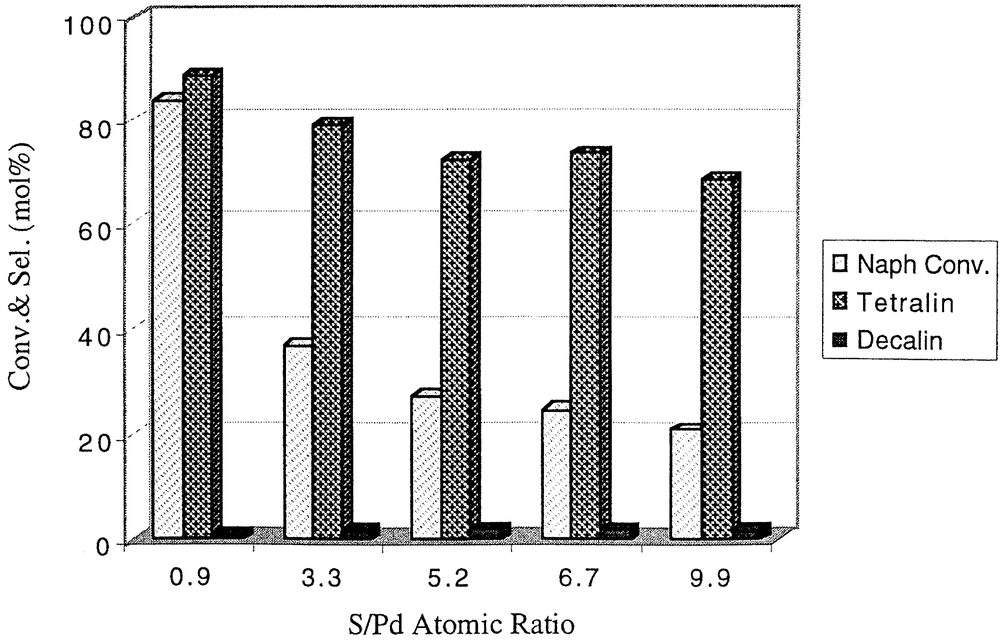

Figure 2. Effect of the Sulfur/Pd Atomic Ratio on Naphthalene Conversion and Selectivity toward Tetralin and Decalin over Pd/USY20 in the Presence of Added Benzothiophene

Figure 3 shows that with increasing sulfur addition in the form of benzothiophene, the naphthalene conversion drops rapidly, from 94.9 percent to 11.8 percent. However, the selectivities to tetralin are much higher than those in the case of Pd/USY12 and Pd/USY20. Moreover, the sum of the hydrogenation products is very near 100 percent, indicating fewer side reactions taking place in this hydrogenation process. The same trend was observed for Pd/USY80, which is shown in Figure 4.

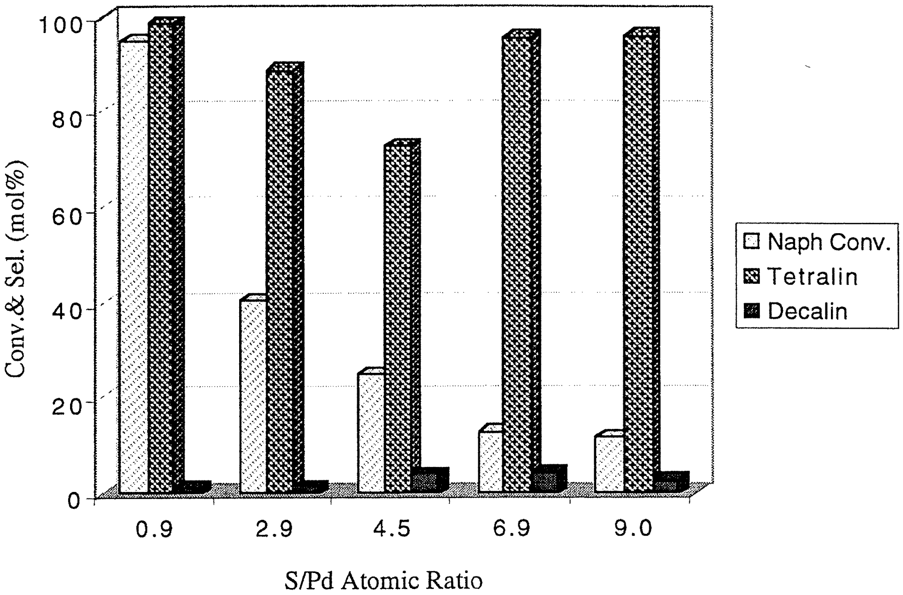

Figure 3. Effect of the Sulfur/Pd Atomic Ratio on Naphthalene Conversion and Selectivity toward Tetralin and Decalin over Pd/USY40 in the Presence of Added Benzothiophene

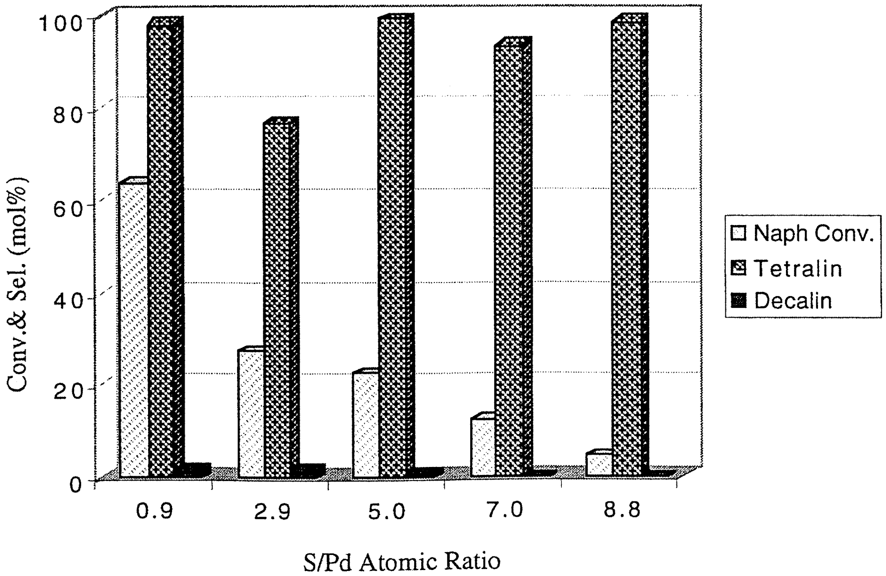

Figure 4. Effect of the Sulfur/Pd Atomic Ratio on Naphthalene Conversion and Selectivity toward Tetralin and Decalin over Pd/USY80 in the Presence of Added Benzothiophene

The best naphthalene conversion yields with respect to increasing sulfur loading were obtained for USY12, while the selectivity toward tetralin was higher for USY80.

The SiO_2/Al_2O_3 ratio is closely related to the acidity in the zeolite. Acid sites, especially Bronsted-acid sites, act as adsorption sites for aromatics. They can donate H^+ to activate aromatics via the formation of carbenium ions, which are involved in two kinds of reactions.

The desired hydrogenation reaction occurs when the carbenium ions are hydrogenated by the spillover hydrogen activated and dissociated on the metal sites. The other reaction is coke formation, where the carbenium ions react with other aromatics to form polynuclear aromatic hydrocarbon and coke, through polymerization and condensation reactions.

The USY12 and USY20 have stronger acidities than do USY40 and USY80, due to the larger acid site density caused by a lower SiO_2/Al_2O_3 ratio. When naphthalene is activated to form carbenium ions, the strong acid sites in USY12 and USY20 can capture carbenium ions more firmly, so that it is very difficult for them to escape from these sites. In this way, there is a higher probability for these ions to react and combine with each other, and finally form coke. Thus, there is a substantial number of side reactions occurring in the hydrogenation of naphthalene using USY12 and USY20. Therefore, in the hydrocarbon conversion reactions catalyzed by bifunctional catalysts, a balance between the concentrations of metal sites and acid sites has to be maintained for optimum activity and selectivity in metal/acid zeolite catalysts.

1.3.2 TPR Measurement

TPR curves for USY-supported palladium catalysts are shown in Figure 5. The TPR peak profiles can be divided into two groups: (i) positive sharp peaks near 70 °C, which are due to H_2 evolution from hydride decomposition, and (ii) negative broad peaks at high temperatures caused by H_2 consumption, corresponding to the complete reduction of Pd^{2+} to Pd^0.

The first positive hydrogen-production peak in the TPR is typical for palladium metals. In a hydrogen atmosphere at room temperature, Pd metal can form a hydride exothermally very easily. Two different kinds of hydride phase are normally distinguished: (i) α-Pd hydride, with a heat of solution of 6.0 – 8.8 kcal/mol (H_2), and (ii) β-Pd hydride, with a heat of solution of 9.7 kcal/mol (H_2). For bulk Pd, both phases can coexist in equilibrium at normal conditions. In zeolite, the β-Pd hydride, which decomposes at about 80 °C, is found only after significant sintering, e.g., when the Pd particles are quite large. The α-Pd hydride is observed with very small Pd clusters in zeolite, and it decomposes between 0 and 32 °C, depending on the cluster size.

The negative hydrogen-consumption peaks in TPR at higher temperatures are the target peaks we are interested in. The peak shifts from about 200 °C to 160 °C in the order of Pd/USY12, Pd/USY20, Pd/USY40, and Pd/USY80. For Pd/USY12, which has the highest reduction temperature, 201.3 °C, the USY12 support has more acid sites than does any of the other supports due to its having the smallest SiO_2/Al_2O_3 ratio, 12. The Pd/USY80, on the other hand, has the lowest reduction temperature, 162.3 °C, where the USY80 support has a smaller acid-site density due to its having the largest SiO_2/Al_2O_3 ratio, 80. In other words, palladium is

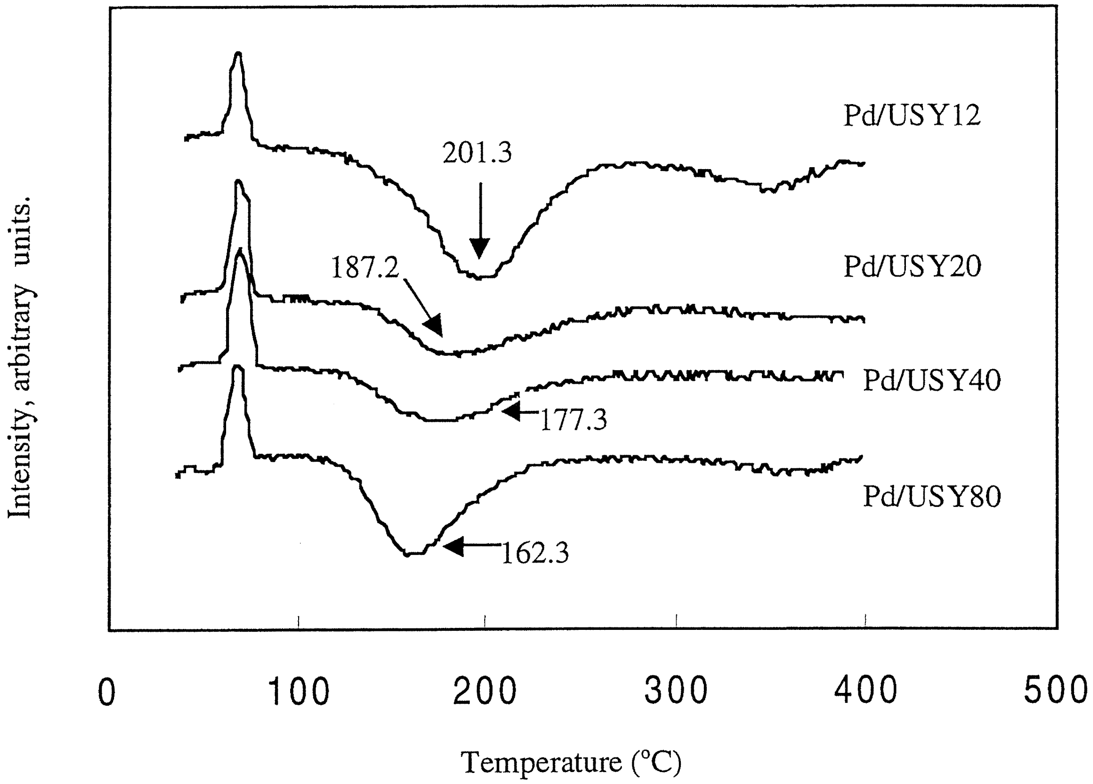

Figure 5. TPR Profiles of Four Different Pd/USY Catalysts

more easily reduced with an increase in the SiO_2/Al_2O_3 ratio due to a decrease in the density of acid sites present in the support.

After the introduction of palladium into zeolite during preparation, the Pd^{2+} ions are favorably coordinated to the framework oxygens during the following calcination. Hence, there is a strong interaction between the metal particles and the support. Zeolite protons can enhance the interaction by chemically anchoring small Pd particles. The reducibility of the supported metal is closely related to the interaction between metal and support, the stronger the interaction, the more difficult it is to reduce the metal. The USY12 has more acid sites than does any other USY support due to its small SiO_2/Al_2O_3 ratio, making the interaction between Pd and the support stronger, thereby causing the Pd^{2+} ions more difficulty in being reduced. The same reason can be used to explain the TPR results for the other three catalysts.

1.3.3 TPD Measurement

Figure 6 shows the TPD results of hydrogen over USY-supported palladium catalysts. There is only one single peak which corresponds to the desorption of H_2 from the surface of Pd metal particles. The TPD peak shifts from about 180 °C to 90 °C in the order of Pd/USY12, Pd/USY20, Pd/USY40, and Pd/USY80, with the same trend as for the TPR peaks. The Pd/USY12 shows a TPD peak at the highest temperature (185.3 °C), which implies that the hydrogen is adsorbed on the Pd metal surface more firmly and is more difficult to be desorbed.

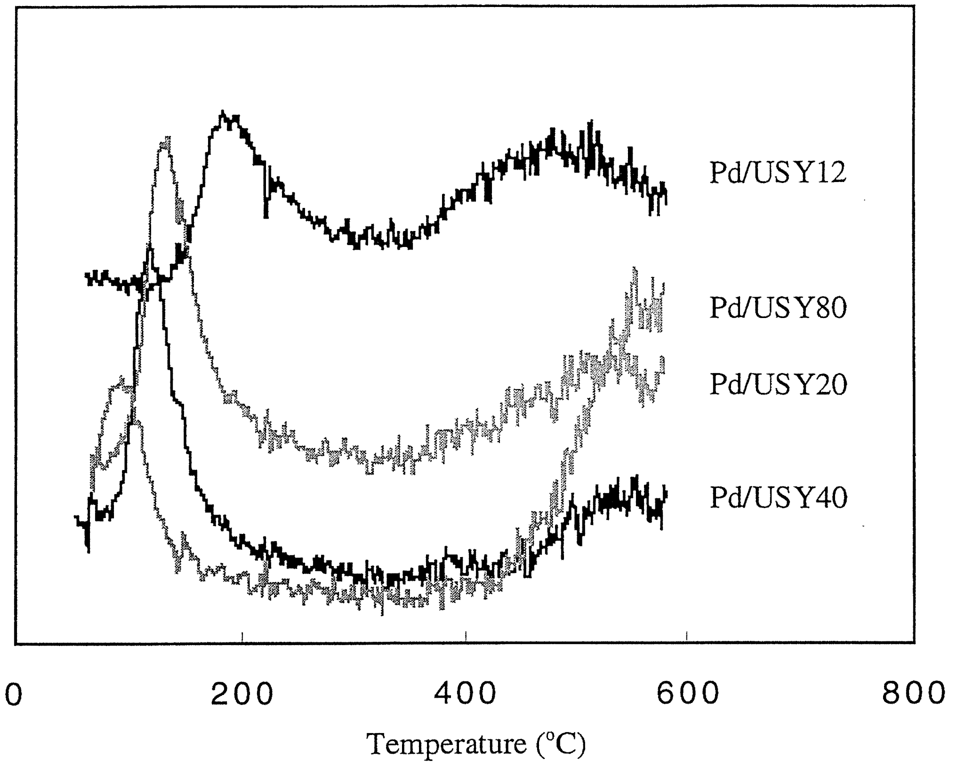

Figure 6. TPD Profiles of Four Different Pd/USY Catalysts

However, there is a much weaker bonding between the adsorbed hydrogen and Pd metal for Pd/USY80, since hydrogen is desorbed at a very low temperature (91.2 °C).

As mentioned before, reduction of Pd^{2+} ions in zeolite cavities by absorbed hydrogen results in the formation of Pd atoms and protons. While most hydrogen atoms are attached to the O^{2-} ions on the cage wall, some protons will remain attached to Pd atoms or form O^{2-}... H^{+}... Pd bridges. This interaction results in partial electron transfer, thus rendering the Pd clusters electron deficient. The electron-deficient Pd atoms are prone to capture electrons from the surroundings or other atoms like hydrogen, which strengthens the interaction between adsorbed hydrogen and reduced Pd atoms. Moreover, the higher the density of acid sites in the zeolite support, the more electron deficient the supported noble metal Pd will be, leading to the strong interaction between the Pd atoms and the adsorbed hydrogen.

The low SiO_2/Al_2O_3 ratio of 12 in the support USY12 generates more acid sites, which makes the Pd atoms in Pd/USY12 more electron deficient. This causes the Pd atoms to adsorb the hydrogen more firmly. Thus, the hydrogen desorption peak appears at a relatively high temperature.

The electron-deficient property of active sites also makes the metal more sulfur resistant. Zeolite protons enhance the metal dispersion by chemically anchoring small reduced Pd particles. The atomically dispersed Pd combines more strongly with hydrogen and also bonds less strongly to sulfur so as to inhibit further the poisoning reaction. This is the main reason why palladium is more sulfur resistant when supported on a more acidic support such as USY12 than when supported on another support.

1.3.4 Pulse Chemisorption Measurements

Pulse chemisorption is a good method to determine the percent metal dispersion, active surface area, and active-particle size which are very important factors in the catalytic reactions. Table 2 shows the pulse chemisorption results for the Pd/USY catalysts, USY12, USY20, USY40, and USY80. The Pd/USY40 catalyst has a higher metal dispersion than do the three other USY-supported palladium catalysts. The metal dispersion increases with increasing SiO_2/Al_2O_3 ratio until reaching a maximum of 70.9043 percent at a SiO_2/Al_2O_3 ratio of 40; the metal dispersion then decreases even though the SiO_2/Al_2O_3 ratio continues to increase.

Table 2 Pulse Chemisorption over Pd Supported on Different USY Supports

Catalyst ID	Metal Dispersion (%)	Metallic Surface Area		Active Particle Diameter (nm)
		(m^2/g sample)	(m^2/g metal)	
Pd/USY12	59.1777	5.2727	263.6354	1.893
Pd/USY20	63.2339	5.6341	281.7058	1.772
Pd/USY40	70.9043	6.3175	315.8773	1.580
Pd/USY80	67.0949	5.9781	298.9068	1.670

The four USY zeolite supports, USY12, USY20, USY40, and USY80, have almost the same acid strength. Thus, the USY12 support has a stronger acidity than the three other USY supports due to its larger acid-site density caused by a lower SiO_2/Al_2O_3 ratio. Because of the greater number of acid sites in the USY12 support, after the reduction of Pd^{2+} to Pd^0, acid sites in USY12 can hold Pd atoms more firmly and more closely, so that there is a greater chance for adjacent Pd atoms to touch, overlap, or even agglomerate to form larger particle clusters. This is a possible reason why the Pd/USY12 catalyst has the lowest metal dispersion and the largest active-particle size of the four USY-supported Pd catalysts.

The Pd/USY40 has a higher metal dispersion and smaller particle size because the USY40 support has the optimum number of acid sites. It is this optimum acidity which causes the Pd atoms to be distributed in the USY40 channels as evenly as possible. In other words, a balance between the concentrations of metal sites and acid sites has been optimized in the Pd/USY40 catalyst. This is also the reason why Pd/USY40 has a higher activity for naphthalene hydrogenation than does any other USY-supported Pd catalyst, as mentioned before. When the density of the acid sites decreases further, such as for Pd/USY80, the catalyst will have less metal dispersion and a larger active-particle size, which can be explained by the fact that there are too few acid sites to distribute the Pd atoms evenly in the zeolite channels.

With increasing sulfur poisoning, naphthalene hydrogenation with Pd/USY12 shows a higher sulfur resistance than with the other catalysts. Here, the electronic efficiency of active sites for this catalyst makes Pd less susceptible to sulfur poisoning. In addition, the metal dispersion seems to be another factor worthy of attention. Since Pd/USY12 has less metal dispersion than does Pd/USY40, there are more Pd atoms in the USY12 which are sufficiently close to one another so as to overlap or even agglomerate to form large particles. In other words, the percentage of the metal atoms which are located on the outermost channel surface and are directly exposed to sulfur poisoning in Pd/USY12 is less than in Pd/USY40. Therefore, more Pd atoms are temporarily protected from sulfur poisoning in Pd/USY12 than in Pd/USY40, so that Pd/USY12 is more sulfur resistant than any of its peer catalysts.

1.4 Conclusions

In the hydrogenation of naphthalene using the noble-metal palladium supported on zeolites, the activity, selectivity, and sulfur resistance of the catalysts were found to depend strongly on the type of support.

A balance between the concentration of metal sites and acid sites was achieved for Pd/USY40, where we determined the optimum activity and selectivity for the metal/acid zeolite catalysts.

For hydrogenation of naphthalene in n-tridecane at 200 °C in the absence of added sulfur, Pd/USY40 is more active and selective than any other catalyst with a different SiO_2/Al_2O_3 ratio. There were substantial numbers of side reactions taking place in the hydrogenation processes catalyzed by Pd/USY12 and Pd/USY20.

The addition of sulfur in the form of benzothiophene decreased the activity of all the catalysts tested. However, there appeared to be some improvement in the sulfur resistance of the noble metal when it was supported on USY12 due to its higher acidity.

2.0 ENHANCING STABILITY OF JET FUELS FROM COPROCESSING

2.1 Abstract

Supported Pt and Pd catalysts were examined for selective hydrogenation of 1-naphthol to form tetrahydronaphthol (THNol). Five kinds of supports were used: HY zeolite with a SiO_2/Al_2O_3 ratio of 40, HM zeolite with a SiO_2/Al_2O_3 ratio of 38, γ-Al_2O_3, SiO_2 and TiO_2. Among these five supports, only TiO_2-supported catalysts displayed selectivity for 1-naphthol hydrogenation to 1,2,3,4-THNol. Under the same reaction conditions, Pd/TiO_2 catalysts showed a much higher catalytic activity and higher selectivity to 1,2,3,4-THNol than did Pt/TiO_2 catalysts, and more tetralin was observed in the product distribution for Pd catalysts. On the other hand, Pt/TiO_2 showed a higher selectivity for 5,6,7,8-THNol. By using Pt and Pd bimetallic catalysts, a much higher selectivity to 1,2,3,4-THNol has been achieved. The product distribution depends strongly on the Pt/Pd ratio. The selectivity of 1,2,3,4-THNol decreases with an increase in the Pt/Pd mole ratio. The bimetallic catalyst with a Pt/Pd mole ratio of 0.33 shows the highest 1,2,3,4-THNol selectivity, 22.6 mol percent, at 150 °C, 500 psi, and 60 min. Tetralone was found to be an intermediate in the hydrogenation of 1-naphthol to 1,2,3,4-THNol. Further hydrogenation of 1,2,3,4-THNol to tetralin is much faster than that of 5,6,7,8-THNol.

2.2 Introduction

The present work deals with the catalytic production of specific hydroaromatic compounds as high-temperature stabilizers for jet fuels. Until recently, the major concern in jet-fuel stability involved only thermal oxidation stability and storage stability, because the current operating fuel temperature for all commercial and military jet fuels is below 300 °C, where fuel degradation is controlled by autoxidation reactions [5, 6]. With the development of high-Mach aircraft, fuel thermal stability has become crucial [7-10]. Fuel in such aircraft is expected to experience temperatures in the range of 400 to 500 °C [7-9]. One of the critical problems in developing thermally stable jet fuels for high-Mach aircraft is the thermal decomposition and formation of solids from hydrocarbon fuels in the pyrolytic regime [9-13]. Previous studies at Pennsylvania State University have demonstrated that during the pyrolytic degradation of coal- and petroleum-derived jet fuels, hydrogen transfer form hydrogen-donors, such as those present in coal-derived JP-8C jet fuel, could play an important role in suppressing thermal solid formation [10, 14]. In previous papers [15-18], it has been reported that the formation of carbonaceous materials in jet fuel can be retarded by hydrogen donors such as tetrahydronaphthalene (THN), tetrahydroquinoline (THQ), and tetrahydronaphthol (THNol); and aromatic alcohol-type molecules such as benzyl alcohol and benzenedimethanol. More recent work at Pennsylvania State University has shown that THNol (especially the 1,2,3,4-isomer) and THN as well as benzyl alcohol are effective hydrogen donors for capping aliphatic radicals formed at temperatures > 400 °C while being transformed into relatively stable products [19].

The present work is motivated by the need to produce effective hydrogen donors as high-temperature fuel stabilizers by selective hydrogenation of aromatic compounds that are abundant in coal-derived liquids [20]. Hydrogenation of aromatics is exothermic and, therefore, thermodynamically favored at a lower temperature [21, 22]. However, in conventional hydrotreating processes, a reaction temperature above 325 °C is typical, which consequently results in a relatively higher content of aromatics at equilibrium composition. Conventional supported Ni-Mo and Co-Mo catalysts become active only at relatively high temperatures. Consequently, hydrogenation of aromatics at higher temperatures requires higher hydrogen pressure to offset the limitation of thermodynamic equilibrium conversion.

This study examines the potential of supported Pt, Pd, and their bimetallic catalysts for low-temperature hydrogenation of 1-naphthol to produce tetrahydronaphthol, particularly 1,2,3,4-tetrahydro-1-naphthol. The results reveal that by using proper support and bimetallic species, we can selectively promote the hydrogenation to 1,2,3,4-tetrahydro-1-naphthol.

2.3 Experimental

2.3.1 Catalyst Precursor and Reactant

Catalysts with one metal precursor loaded on different supports were prepared from HY zeolite with an SiO_2/Al_2O_3 ratio of 40, HM zeolite with an SiO_2/Al_2O_3 ratio of 37.5, gamma-Al_2O_3, SiO_2 and TiO_2, used as received (see Table 3).They were prepared by incipient-wetness impregnation of an aqueous solution of either tetraammineplatinum chloride ($[Pt(NH_3)_4]Cl_2$, Aldrich, 99.995 percent Pt, metal base) or tetraamminepalladium chloride ($[Pd(NH_3)_4]Cl_2$, Aldrich, 99.995 percent Pd, metal base). Bimetallic catalysts were prepared by the co-impregnation method using both $[Pt(NH_3)_4]Cl_2$ and $[Pd(NH_3)_4]Cl_2$. Following drying in vacuo at 100 °C for 3 hours, the catalysts were calcined in air at 450 °C for 3 hours. For all the catalysts used, the metal loading was kept at 1 wt percent.

Table 3. Types of Supports and Their Nominal Properties

Support ID	Material Type	Surface Area m^2/g	SiO_2/Al_2O_3 mol. Ratio	Na_2O wt%	Supplier and Code
HY	Y-zeolite	750	40	0.03	PQ-CBV-740
HM	mordenite	512	37.5	0.07	PQ CBV-30A
TiO_2	titania	50			Degussa. P-25
Al_2O_3	γ-alumina	203			KF S-1
SiO_2	Silica-gel	500			Aldrich

2.3.2 Catalyst Characterization

Characterization by TPR was carried out for all the catalysts on a Micromeritics AutoChem 2910 (USA) analyzer. In a typical TPR experiment, about 0.4 g of catalyst was loaded in a U-shaped quartz adsorption cell. Before a TPR run, the sample was heated in Ar for 30 minutes at 350 °C to remove moisture and impurities and then cooled to room temperature in an Ar flow (10 ml/min). The TPR profile of catalyst sample was recorded by following the temperature program with a heating rate of 10° C/min between 25 and 500 °C in a 5.12 percent H_2-Ar gas mixture.

2.3.3 Catalyst Evaluation

Catalyst tests were done in a 25-mL stainless-steel microautoclave reactor. The reactor system is T-shaped with most of the internal volume residing in the horizontal tube that contains the catalyst and reactants. The reactor was charged with 0.05 g catalyst, 0.5 g 1-naphthol (TCI, 99.99+ percent), and 2.0 g of n-tridecane solvent. The charged reactor was flushed with H_2 to the desired pressure to start the test. The reactor was then mounted on a holder and immersed in a fluidized sandbath heater. Mixing was accomplished by vertical agitation. At the end of the test, the reaction was quenched by immersing the reactor in cold water. After cooling, the contents of the reactor were washed with acetone onto a filter, and the solid was dried. Solution products were identified by GC-MS (HP5890 GC-HP 5971 MSD) and quantitatively analyzed by GC-FID. For both GC instruments, the column was a 30 m by 0.25 mm i.d. DB-17 fused-silica capillary column, and the oven-temperature program was 80 to 290 °C at 6 °C/min. The GC-MS analysis indicates that the cracking of n-tridecane, if any, was negligible under the conditions used. Additional details of the analytical procedures are available elsewhere [23].

2.4 Results and Discussion

2.4.1 Effect of Different Supports

Table 4 shows the results of 1-naphthol hydrogenation over monometallic Pt and Pd catalysts prepared using different kinds of support. All reactions were performed under 500 psi at 150 °C; the reaction time was 90 minutes for Pt catalysts and 30 minutes for Pd catalysts. It is obvious that even over shorter reaction times, a Pd catalyst with a given support shows a higher catalytic activity than does a Pt catalyst with the same type of support. Both kinds of zeolite-supported catalysts displayed no selectivity for 1,2,3,4-THNol. Under the conditions employed, TiO_2-supported catalysts appeared to be the only ones showing selectivity for 1,2,3,4-THNol and a much higher selectivity for total THNL (1,2,3,4-THNol + 5,6,7,8-THNol).

Table 4. Effects of Different Supports

	Naphthol	Product Yield Distribution (mol%)			
Catalysts	Conv. wt%	1,2,3,4-THNol	5,6,7,8-THNol	Tetralone	THN+DeHN
Pt/HY	33	0	7.6	14.3	7.2
Pt/HM	58.4	0	23.9	16.3	15.4
Pt/Al_2O_3	36.9	0	24.2	10.6	2
Pt/TiO_2	84	2.8	55.5	12.2	6.6
Pd/HY	59.8	0	15.9	15.4	28.3
Pd/HM	100	0	23.2	13.1	57
Pd/Al_2O_3	100	1.6	28.2	13.7	55.7
Pd/TiO_2	97.8	11.2	34.2	20.5	29.4
Pd/SiO_2	100	0	35.2	0	64.8

All reactions were done at 150 °C, 500 psi

Pt catalysts: 90 minutes; Pd catalysts: 30 minutes

In an attempt to compare the present results with previous literature data on effects of the support or supported catalyst, we conducted a literature search using the SCI-Expanded data base (1986-1999) of the Institute of Scientific Information, but this search yielded no publications on the hydrogenation of 1-naphthol [24]. Therefore, we cannot compare our results with the literature. On the other hand, it is known in the literature that TiO_2-supported catalysts may have a metal-support interaction that favors the hydrogenation of oxygen-containing compounds. For example, Vannice has demonstrated that metal-support interactions (MSI) in Pt/TiO_2 can markedly shift selectivity toward the formation of and retention of high selectivity for the intermediate unsaturated alcohols [25]. It is possible that the MSI between TiO_2 and metal atoms caused the regioselective hydrogenation of 1-naphthol.

2.4.2 Hydrogenation of 1-Naphthol over TiO_2-Supported Pt and Pd Monometallic Catalysts

Results of 1-naphthol hydrogenation for the TiO_2-supported Pt and Pd monometallic catalysts are shown in Table 5. The product distribution depends strongly on the type of metal used as well as the reaction conditions. It is apparent that a Pd catalyst exhibits a much higher activity for 1-naphthol conversion than does a Pt catalyst. On the other hand, the Pd catalyst yielded more hydrogenolysis products such as tetralin. It should be noted that a Pd catalyst has a higher selectivity for 1,2,3,4-THNol than does a Pt catalyst, whereas a Pt catalyst presents a higher selectivity for 5,6,7,8-THNol. By controlling the reaction conditions (200 °C, 300 psi or 150 °C, 500 psi), the selectivity of a Pd catalyst for 1,2,3,4-THNol can reach 8 mol percent.

Table 5. Hydrogenation of 1-naphthol over Pt and Pd monometallic catalysts

	Temp.	Pressure	Time	Naphthol	Product Yield Distribution (mol%)				
Catalysts	°C	psi	min.	Conv.%	DeHN	THN	Tetralone	1,2,3,4-THNol	5,6,7,8-THNol
Pt/TiO_2 1 wt%	200	300	90	84.2	4.3	13.4	23.7	1.6	52.9
	200	500	90	100.0	7.6	25.6	1.9	1.4	47.5
	200	500	60	55.4	3.7	9.4	24.6	2.0	58.6
	150	500	60	36.7	5.6	1.0	25.2	2.4	65.7
Pd/TiO_2 1 wt%	200	500	30	100.0	4.3	62.6	1.0	4.1	28.1
	200	300	30	100.0	2.2	59.4	4.0	7.2	31.5
	200	300	60	100.0	1.8	59.3	3.6	8.1	33.2
	150	500	60	100.0	2.1	52.6	0.4	8.0	42.0

The observed product distribution indicates competitive adsorption during simultaneous ring hydrogenation and C-O bond-cleavage reactions. Process selectivity is interpreted in terms of reactant/catalyst interactions where naphthol-ring adsorption is viewed as occurring via the aromatic pi-electron system and/or near the hydroxyl group where the latter interaction promotes either hydrogenation or hydrogenolysis; the latter represents a direct loss of selectivity with respect to THNol formation.

2.4.3 Hydrogenation of 1-Naphthol over TiO_2-Supported Pt and Pd Bimetallic Catalysts

Results for 1-naphthol hydrogenation at 150 °C over Pt and Pd bimetallic catalysts are shown in Table 6. It is clear that bimetallic catalysts display a much higher selectivity for 1,2,3,4-THNol. Product distribution depends strongly on the Pt/Pd ratio. With an increase of the Pt/Pd mole ratio, the selectivity for 1,2,3,4-THNol decreases. Relative to the monometallic Pd catalyst, the bimetallic catalyst with a Pt/Pd ratio of 0.33 (total metal loading kept at 1 wt. percent) shows the highest 1,2,3,4-THNol selectivity, reaching 22.6 percent at 150 °C, 500 psi, and 60 minutes, even though the 1-naphthol conversion decreased by roughly 10 percent.

Table 6. Hydrogenation of 1-Naphthol over Pt and Pd Bimetallic Catalysts

Catalysts	Pressure psi	Time min.	Naphthol Conv.%	Product Yield Distribution (mol%)				
				DeHN	THN	Tetralone	1,2,3,4-THNol	5,6,7,8-THNol
	300	60	71.6	5.0	10.9	23.1	3.5	54.6
$Pt+Pd/TiO_2$	300	90	74.2	7.4	12.6	24.9	3.9	52.3
1 wt%	500	60	69.0	3.0	9.3	22.4	3.6	59.6
Pt/Pd = 3	500	90	89.1	2.4	16.1	12.5	8.8	57.0
	300	60	90.3	2.7	12.4	33.1	12.6	38.1
$Pt+Pd/TiO_2$	300	90	99.2	1.9	27.8	9.0	17.6	41.9
1 wt%	500	60	90.8	2.3	24.5	8.2	22.6	40.8
Pt/Pd = 0.33	500	90	100	2.1	40.7	7.8	11.0	38.3

All reactions were done at 150 °C.

TPR characterization results are shown in Figure 7. For single-metal catalysts, Pt displays a much higher reduction temperature (376.29 °C) than that of Pd (283.14 °C); this is consistent with the reaction result where the Pd catalyst shows a higher catalytic activity in terms of 1-naphthol conversion, since all reactions were carried out at a low temperature, 150 °C. When the two metals are loaded into bimetallic catalysts, the reduction temperatures fall between the corresponding monometallic ones. There are two possible effects involved in the bimetallic catalyst system. One is that one metal can prevent the other from agglomerating; the other is that the two metals can combine and form new species different from the parental ones. It is worth mentioning that there is a specific peak for the bimetallic catalysts, particularly for the one with a Pt/Pd ratio of 0:33. The TPR peak has a higher temperature than even the highest single-metal reduction temperature (Pt, 376.29 °C). This observation suggests that a new bimetallic phase is formed in this catalyst system, which induces the higher selectivity for the 1,2,3,4-isomer of THNol.

If Pd is the main metal species in the bimetallic catalytic system that guides the reaction toward the formation of 1,2,3,4-THNol, the presence of Pt will prevent the agglomeration of Pd particles during the catalyst preparation and reaction processes. THE H_2 pulse chemisorption characterization for both monometallic and bimetallic catalysts was done in order to measure metal dispersion and metal particle size; the results are shown in Table 7. It is obvious that bimetallic catalysts display a much higher metal dispersion and smaller metal-particle size compared with monometallic catalysts; the one with a Pt-to-Pd ratio of 0:33 has the highest metal dispersion of all the catalysts tested.

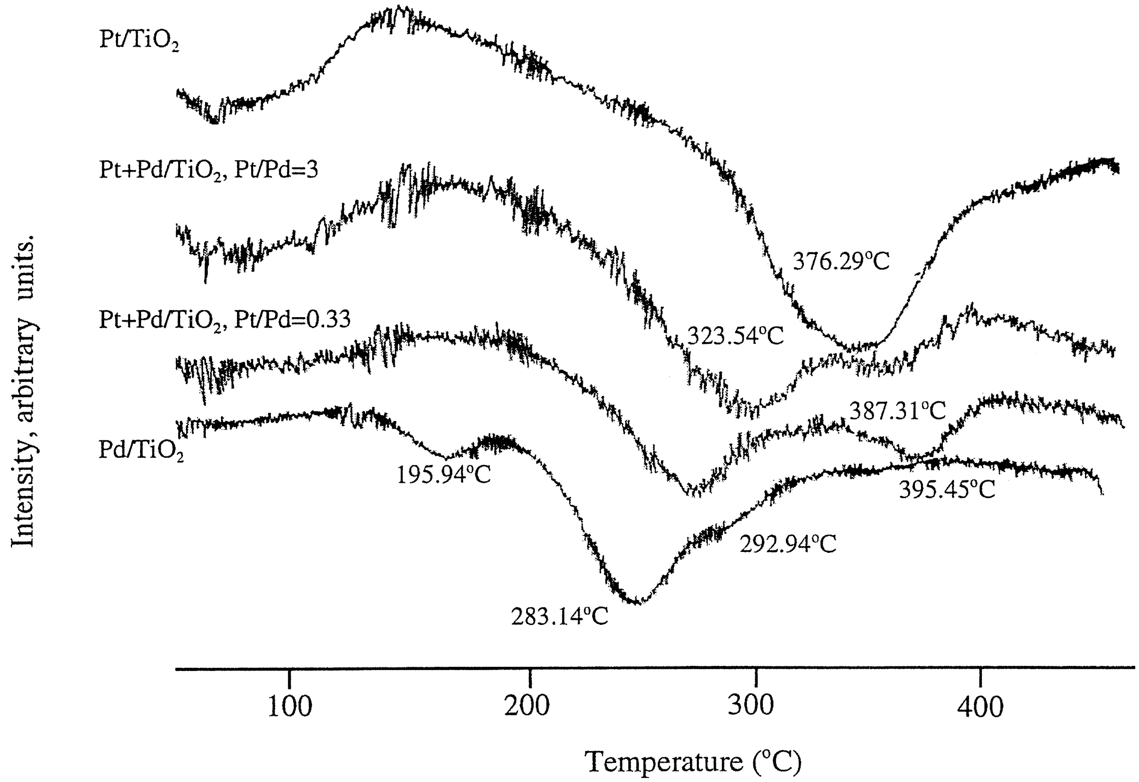

Figure 7. TPR Characterization Results

Table 7. H_2 Pulse Chemisorption Results for TiO_2-Supported Pt, Pd Catalysts

Catalysts	Metal Dispersion	Particle Diameter (nm)	Metal Surface Area (m^2/g sample)
Pt/TiO_2	30.54	3.71	0.76
Pd/TiO_2	18.84	5.95	0.84
$Pt+Pd/TiO_2$ (Pt/Pd=3)	66.72	1.70	1.64
$Pt+Pd/TiO_2$(Pt/Pd=0.3)	106.06	0.89	5.62

2.4.4 Reaction Network

Product analysis for reactions under various conditions indicated that there are three types of by-products (tetralin, decalin, and tetralone) in the reaction system. In order to understand the way in which these products are formed, reactions with different time periods, ranging from 2 to 50 minutes, were carried out; the results are shown in Figure 8 for the reaction of 1-naphthol with hydrogen at 150 °C and 300 psi. At the beginning of the reaction, at 2 minutes with a 1-naphthol conversion of 22 percent, the yield of THN is zero, and the yield of 1,2,3,4-THNol is very low, about 1 percent. On the other hand, the yield of both tetralone and 5,6,7,8-THNol is relatively high compared with other products found; that of 5,6,7,8-THNol is close to 20 percent.

The results suggest that 1-tetralone and 5,6,7,8-THNol are primary products. The curves representing 1-tetralone, 1,2,3,4-THNol, and 5,6,7,8-THNol pass through a maximum, which means that these compounds are intermediates, being converted into one of the other compounds in the network. At about 15 minutes, the 1-tetralone concentration starts to drop sharply, while at the same time the concentration of 1,2,3,4-THNol increases significantly. This suggests that 1,2,3,4-THNol may be formed by the further hydrogenation of tetralone. This is confirmed by the tetralone hydrogenation results shown in Figure 9 . At 25 minutes, as the concentration of 1,2,3,4-THNol decreases, the concentration of THN starts to increase dramatically. The 5,6,7,8-THNol also contributes to the formation of THN, but in very small amounts since the curve representing 5,6,7,8-THNol stays relatively steady during the reaction time.

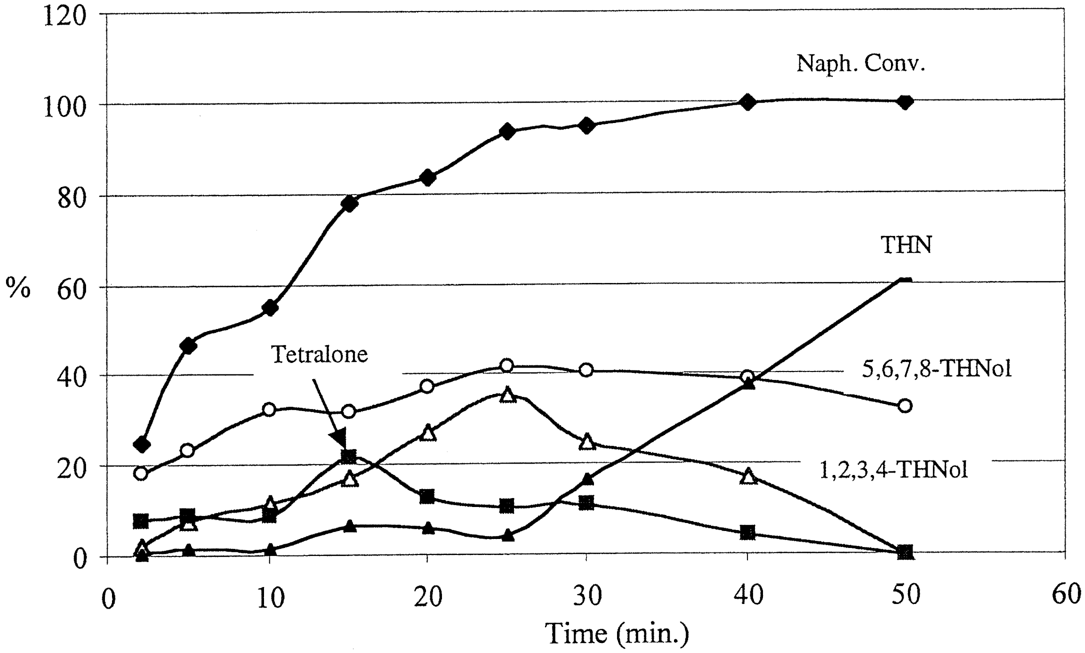

Figure 8. Hydrogenation of 1-Naphthol over Pt+Pd/TiO_2 (Pt/Pd=0.3) 150 °C, 300 psi

To clarify further the relative reactivity of the intermediates, hydrogenation of the mixture of the two tetrahydro-naphthol isomers was carried out at the same reaction conditions, 150 °C and 300 psi. The results are shown in Figure 10. Starting with equal amounts of each isomer, the concentration of 1,2,3,4-THNol dropped to near 0 while the concentration of THN increased to about 60 percent within the first 5 minutes. On the other hand, the concentration of 5,6,7,8-THNol stayed relatively stable. A small amount of DeHN was found after 10 minutes. The relatively higher stability of 5,6,7,8-THNol compared with 1,2,3,4-THNol is the result of the conjugation effect between the hydroxyl group and the benzene ring.

Hydrogenation of tetralone was carried out using a Pt and Pd bimetallic catalyst with a Pt/Pd ratio of 0.3 at 150 °C, 500 psi; the reaction results are shown in Figure 9. The 1,2,3,4-THNol and THN were the only products observed under the conditions employed. It is apparent that 1,2,3,4-

THNol is an intermediate during the hydrogenation, and its further hydrogenation leads to the formation of THN.

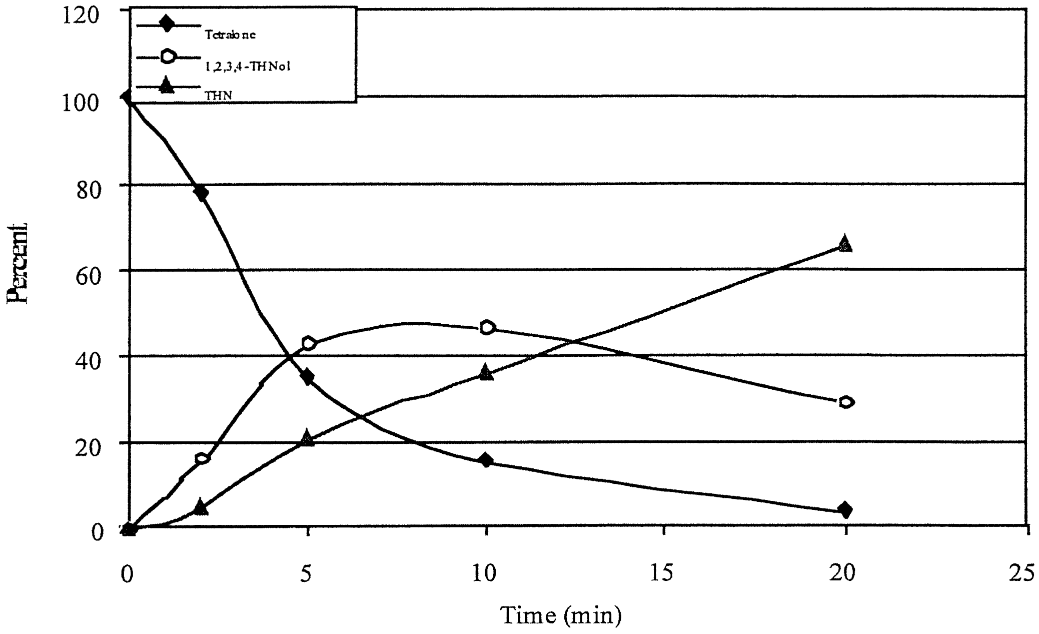

Figure 9. Hydrogenation of Tetralone over Pt+Pd/TiO_2 (1 wt%, Pt/Pd=0.3)150 °C, 500 psi

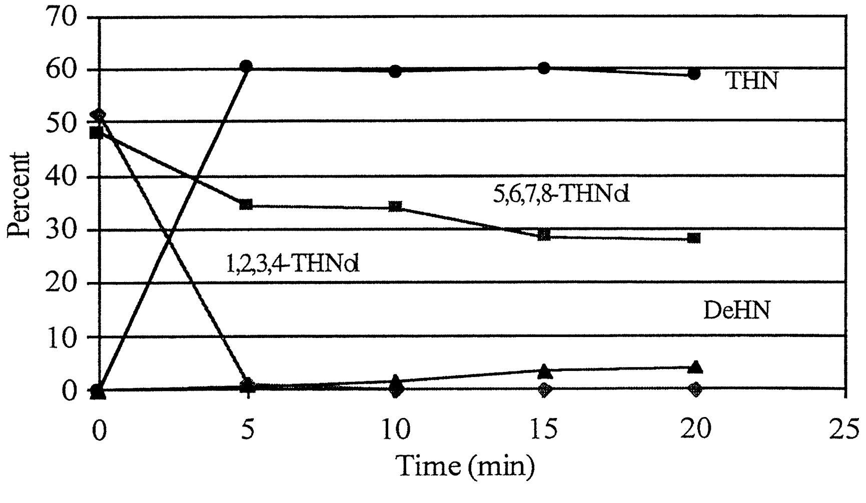

Figure 10. Hydrogenation of THNol over Pt+Pd/TiO_2 (1 wt%, Pt/Pd=0.3)150 °C, 300 psi

According to these results, we proposed the reaction network for the hydrogenation of 1-naphthol shown in Figure 11. The reaction pathway is consistent with the one proposed by others [26-28] for the hydrodeoxgenation of 1-naphthol, except that no 1,2,3,4-THNol was observed because of the constant H_2 pressure during the reaction.

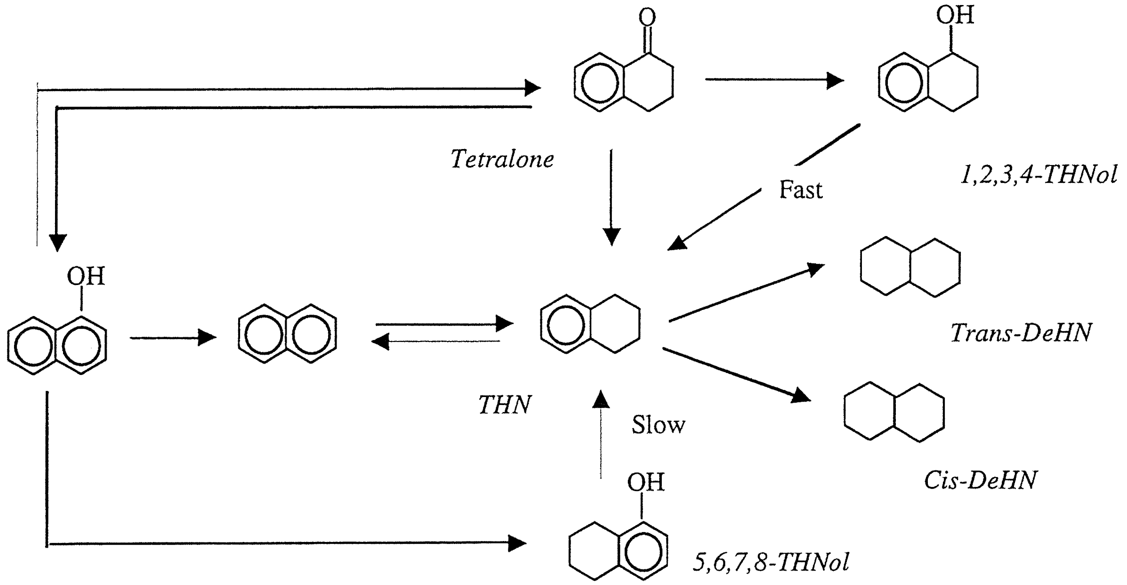

Figure 11. Reaction Network of 1-Naphthol Hydrogenation at Low Temperature

On the basis of the results from this study, a reaction mechanism involving the adsorption of 1-naphthol on the sites surrounding the interface between the noble-metal particles and the support is proposed. The hydrogenation of phenol to cyclohexanone over Pd/MgO and Pd/Al_2O_3 was reported by Neri *et al.* [26]. A higher selectivity for cyclohexanone was found with Pd/MgO compared with Pd/Al_2O_3, which is explained by different forms of adsorbed phenol. In this study, they concluded that the acidity of the support also plays an important role in the selective hydrogenation of the benzene ring, rather than removal of the hydroxyl group.

2.5 Conclusion

We have established that the catalytic hydrogenation of 1-naphthol can be tailored to produce more 1,2,3,4-THNol by selecting an appropriate support and noble-metal species. The catalyst in which Pd is supported on TiO_2 shows a higher selectivity than does the Pt catalyst. Relative to hydrogenation with monometallic catalysts, the selectivity for 1,2,3,4-THNol can be tripled by using the bimetallic catalyst Pt+Pd/TiO_2 with an appropriate Pt/Pd ratio. Tetralone was found to be the intermediate in the hydrogenation of 1-naphthol to 1,2,3,4-THNol. Further hydrogenation of THNol to tetralin and decalin can occur more easily for 1,2,3,4-THNol than for 5,6,7,8-THNol. Therefore, the control of H_2 pressure, reaction temperature, and time period is also very important in order to achieve a high 1,2,3,4-THNol selectivity.

3.0 CATALYST CHARACTERIZATION

3.1 Introduction

Deep hydrogenation of aromatics in distillate fuels reduces the aromatic content of fuels. This generates decalins, which are desirable components in jet fuels because of their higher thermal stability and higher density than long-chain alkanes [29-31]. Conventional catalysts for fuel hydroprocessing are sulfided Co-Mo and Ni-Mo supported on alumina. However, such catalysts are only active at high temperatures (> 300 °C). Because of the exothermic nature of hydrogenation, deep hydrogenation at lower temperatures is preferred. Noble metals are the catalysts of choice for deep hydrogenation and low-temperature hydrotreating. Song and co–workers found that noble metals can be active and selective for the low-temperature hydrogenation of aromatics in distillate fuels [32, 33]. The activity of these catalysts mainly depends on their respective metal dispersion, structure, and morphology. During this reporting period, we have characterized a series of supported Pt and Pd catalysts by CO and H_2 chemisorption, temperature-programmed reduction, and X-ray diffraction methods.

3.2 Experimental

3.2.1 Catalyst Preparation

The supports used were Al_2O_3, TiO_2, HM-38, HY zeolite, and MCM-41. Most of the support materials were obtained from commercial vendors: Al_2O_3 from Degussa (Aluminum Oxide C); TiO_2 from Degussa (Titania P25); HM-38 mordenite from PQ Corporation (CBV 30A); and HY zeolite from Linde (LZ-Y52). The mesoporous aluminosilicate molecular sieve MCM-41 type structure was synthesized using aluminum isopropoxide as the Al source and then converted to the ammonium form by ion exchange. The platinum catalysts were prepared by impregnation from an aqueous solution of hexachloroplatinate (IV) hydrate, $H_2PtCl_6.xH_2O$ (Aldrich, 99.995 percent Pt, metal basis). The Pd catalysts were prepared by impregnation of $PdCl_2$ (Aldrich, 99.999 percent Pd, metal basis) dissolved in dilute hydrochloric acid (sufficient to form soluble $PdCl_4^{2-}$). In both cases, water was removed by rotary evaporation at about 60 °C. The catalyst precursors were dried in an oven at 60 °C overnight, and calcined in an electric furnace at 450 °C for 4 hours.

3.2.2 CO and H_2 Chemisorption

Hydrogen and carbon monoxide chemisorption experiments on Pt and Pd supported on Al_2O_3 were carried out using a Micromeritics AutoChem 2910 instrument. From the experimental results, metal dispersions were determined. For this purpose, optimum catalyst pretreatment/pre-reduction conditions had to be determined. Before a chemisorption experiment, 0.5 g of catalyst sample was loaded into a quartz adsorption cell. The catalyst was pretreated by flowing H_2 (20 mL/min) following the temperature program: 120 °C: 10 °C/min: hold 30 min/220 °C: 10 °C/min: hold 30 min/350 °C: 10 °C/min: hold 120 minutes. After the reduction, H_2 was replaced by a He flow, and the sample was treated in He for 90 min at 350 °C to remove any residual hydrogen still present on the sample. After passivating with He, the sample was cooled to room temperature. A 10.3- or 5-percent H_2-Ar mixture was used for hydrogen chemisorption, and a 10.1-percent CO-

He mixture was used as a probe gas for carbon monoxide chemisorption. Both mixtures were auto-pulse injected onto the catalyst sample.

For the Pt/TiO_2 and Pd/TiO_2 catalysts, the experimental procedure was the same as above, except that these catalysts were pretreated by low-temperature reduction (LTR) at 250 °C and high-temperature reduction (HTR) at 500 °C to study the implications of a strong metal-support interaction (SMSI) effect.

3.2.3 Temperature-Programmed Reduction (TPR)

The TPR of various Ni catalysts was carried out on a Micromeritics 2910 AutoChem (USA) analyzer. In a typical experiment about 0.2 g of a catalyst sample was dried for 12 hours at 120 °C and then loaded into a U-shaped quartz adsorption cell. Before the TPR run, the sample was heated in Ar for 30 minutes at 350 °C and then cooled to room temperature in an Ar flow (10 mL/min). The TPR profile of the catalyst sample was recorded using the following temperature program: 25 to 450 °C/ 10 °C/min in a 5.12-percent H_2-Ar mixture.

3.2.4 X-Ray Diffraction (XRD)

X-ray diffraction patterns of the catalysts were recorded on a Philips PW 3040 diffractometer using CuK_α radiation. The tube voltage was 40 kV, the current was 40 mA, and the scanning rate was 10 °C/min. The sample was carefully ground and fully packed into the X-ray diffraction cell.

3.3 Results and Discussion

The H_2 and CO chemisorption experiments were carried out on the standard 0.5-wt percent Pt/Al_2O_3 catalyst using the pulse-chemisorption method. The 0.5-wt percent Pt/Al_2O_3 standard was supplied by Micromeritics Instrument Corporation (USA), who makes the AutoChem 2910 instrument. Both CO and H_2 chemisorption showed 42 percent Pt dispersion on Al_2O_3. These experimental values were within the range of ± 2 percent compared with the reference value given by Micromeritics (40 percent).

Table 8 shows the chemisorption results for Pt and Pd supported on amorphous supports (e.g., Al_2O_3 and TiO_2) as well as zeolites (HY and MCM-41). The chemisorption in terms of H/Pt follows the order: $Pt/MCM > Pt/HM38 > Pt/Al_2O_3 > Pt/HY$. A similar trend can be seen for CO chemisorption. On the other hand, the Pd catalysts show the following order: $Pd/HM38 > Pd/MCM > Pd/Al_2O_3 > Pd/HY$. However, the difference between Pd/HM38 and Pd/MCM is very small (Pd/HM38=0.64; Pd/MCM=0.61). The chemisorption results obtained on individual Pt and Pd catalysts are described below.

It can be seen from Table 8 that for 2-wt percent Pt/Al_2O_3, the Pt dispersion in terms of the H/Pt value is 0.65, considering the stochiometry of H_2 chemisorption on Pt to be unity. The difference in the obtained dispersion values between H_2 and CO chemisorption, 0.14, can be ascribed to the dual nature of CO chemisorption on platinum. It is well known that CO can be chemisorbed on Pt via linear or bridged bonding. At a similar metal loading level for Pd/Al_2O_3, a value of 0.41 for H/Pd is obtained. This may be due to the formation of palladium hydride during H_2 chemisorption. Close observation of the data in Table 8 shows that there is a clear support effect on the Pt and Pd dispersions. For the MCM-41 support, Pt is better dispersed (H/Pt=0.82) than Pd (H/Pd=0.61), whereas on HY zeolite both Pt and Pd show poor metal dispersion, Pd being higher (H/Pd=0.33) than Pt (H/Pt=0.21). For the HM38 support, Pt (H/Pt=0.71) is better dispersed than Pd (H/Pd=0.64). The differences in CO chemisorption among the various supports for Pt and Pd can be attributed to the dual nature of CO bonding to the metal (linear and bridged).

Table 8. Chemisorption Data for Al_2O_3-Supported Pt and Pd Catalysts

Catalyst	H/Metal(=Pt or Pd)	CO/Metal (=Pt or Pd)
2-wt% Pt/Al_2O_3	0.65	0.51
2-wt% Pt/MCM	0.82	0.85
2-wt% Pt/HY	0.21	0.23
2-wt% Pt/HM38	0.71	0.55
2-wt% Pd/Al_2O_3	0.41	0.46
2-wt% Pd/MCM	0.61	0.63
2-wt% Pd/HY	0.33	0.35
2-wt% Pd/HM38	0.64	0.61

For the 2-wt percent Pt/MCM, the Pt dispersion in terms of hydrogen per Pt atoms (H/Pt) is 0.82, considering the stochiometry of H_2 chemisorption on Pt to be unity. At a similar metal-loading level for the Pd/Al_2O_3 catalysts, H/Pd=0.61. This may be due to the formation of palladium hydride during H_2 chemisorption [34].

It can be seen from Table 8 that in 2-wt percent Pt/HY, the Pt dispersion in terms of H/Pt is 0.21. At a similar metal-loading level for Pd/HY, a value of 0.33 for H/Pd is obtained.

Table 8 shows that in 2-wt percent Pt/HM38, the Pt dispersion in terms of H/Pt is 0.71. At a similar metal-loading level for Pd/HM38, a value of 0.64 for H/Pd is obtained. The lower Pd dispersion might be due to the formation of palladium hydride during H_2 chemisorption. For the Pt/HY and Pd/HY catalysts, CO chemisorption values of 0.55 and 0.61 were obtained, respectively.

Table 9. shows the H/metal and CO/metal values from H_2 and CO chemisorption for the Pt/TiO_2 and Pd/TiO_2 catalysts. The catalysts were pretreated by LTR at 250 °C and HTR at 500 °C in separate experiments. This was carried out to determine the implications of a SMSI effect on these catalysts.

It can be seen from Table 9 that for the 2-wt percent Pt/TiO_2 treated by LTR, the Pt dispersion is 0.16. For the HTR-treated 2-wt percent Pt/TiO_2, the dispersion decreases significantly (0.04). The difference in the dispersion values obtained for LTR and HTR can be ascribed to a SMSI for metals supported on reducible oxides (e.g., TiO_2). Similar trends can be seen in CO chemisorption and also for 2-wt percent Pd/TiO_2 treated under LTR and HTR conditions. A SMSI results in larger metal particles because of metal site agglomeration on the support, thus a significant decrease in metal dispersion is observed.

Table 9. Chemisorption Data (metal Dispersion in Terms of H/M or CO/M) on TiO_2-Supported Pt and Pd Catalysts

Catalyst	H/M (LTR)	H/M (HTR)	CO/M (LTR)	H/M (HTR)
2-wt% Pt/TiO_2	0.16	0.04	0.18	0.02
2-wt% Pd/TiO_2	0.14	0.02	0.15	0.02

An important consideration when interpreting CO-chemisorption behavior is that bridge-bonded CO could be present on the monometallic catalyst. Dorling and Moss [35] found that on Pt/silica catalysts, the CO chemisorption data in conjunction with XRD and electron microscopy showed that the ratio of Pt surface atoms to CO molecules varied from 1 to 2 with an increase in the Pt loading of the catalysts, which modified the size of the platinum particles. However, the chemisorption of CO at lower metal loading is dominated by linear bonding rather than bridged bonding. On the other hand, hydrogen dissociatively chemisorbs on platinum at ambient temperature requiring adjacent sites on the platinum [36]. Because the hydrogen chemisorption stochiometry for each metal site is unity (H/metal=1), a more accurate measure of metal dispersion is available for hydrogen compared with CO chemisorption. For Pd catalysts, the analysis is again complicated by the fact that hydrogen chemisorption leads to palladium hydride formation. Because of these factors, it is desirable to characterize each catalyst with a different characterization method in choosing the most suitable catalyst for a specific application. Temperature-programmed reduction and x-ray diffraction are two important characterization methods.

3.3.1 Temperature Programmed Reduction (TPR)

The TPR of the standard compound AgO was carried out using a 10.3 percent H_2-He gas mixture and heating from room temperature to 300 °C at a rate of 10 °C /min. A peak maximum at 110 °C was observed for AgO, which was within the experimental error when compared with the reference of 115 °C provided by Micromeritics. Hence, the peak maximum of the catalyst analyzed has a ± 5 °C condition range.

The TPR profiles of the 2-wt percent Pt/Al_2O_3 and 2-wt percent Pd/Al_2O_3 are presented in Figures 12 and 13. It can be seen from Figure 12 that the reduction pattern of the Pt/Al_2O_3 catalyst shows two peaks, one at 195 °C and the other at 341 °C. A comparison of the intensities of both peaks shows that most of the Pt is reduced from Pt^{IV} to Pt° whereas some Pt undergoes a two-step reduction, from Pt^{IV} to Pt^{II} and then from Pt^{II} to Pt° at 341 °C. The TPR profile of the 2-wt percent Pd/ Al_2O_3 catalyst is presented in Figure 13. It can be seen that Pd is reduced at 80 °C, resulting in a single reduction peak. The reduction profiles in Figures 12 and 13 show that Pd is easily reduced at a lower temperature compared with Pt. In the case of palladium, adsorption of H_2 gives rise to PdH formation; this may promote its rate of reduction [34].

TPR profiles of 2-wt percent Pt/MCM and 2-wt percent Pd/MCM catalysts are presented in Figures 14 and 15. It can be seen from Figure 15 that the Pd/MCM catalyst produces a single reduction peak at 97 °C. On the other hand, the Pt/MCM catalyst in Figure 14 shows two reduction peaks, one broad peak at 77 °C and a high-intensity peak at 317 °C. Comparison of the peak intensities in Figures 14 and 15 shows that most of the Pt is reduced from Pt^{IV} to Pt° at 317

°C, whereas some Pt undergoes a two-step reduction, from Pt ^{IV} to Pt^{II} at 77 °C and from Pt^{II} to Pt^{o} at 317 °C. It is known that H_2 dissociates on the metal surface and adsorbs with a metal-to-hydrogen stochiometry of unity (H/M=1). The reduction profiles show that Pd is easily reduced at a lower temperature compared with Pt.

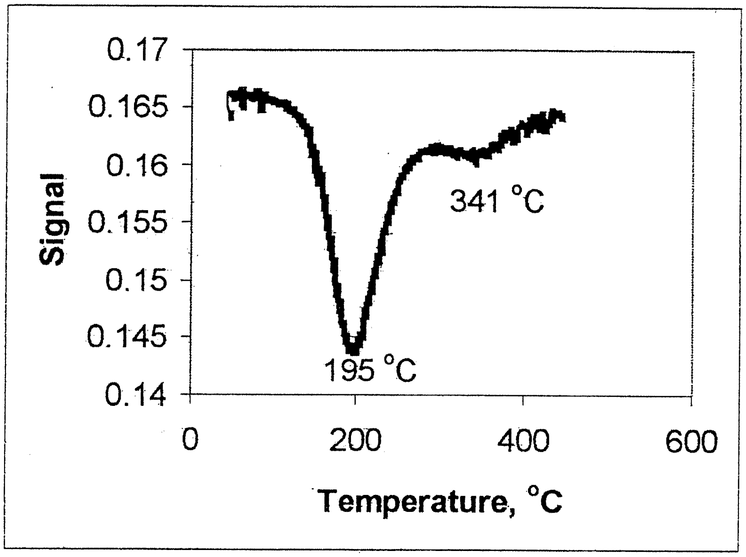

Figure 12. TPR Profile of 2-wt% Pt/Al_2O_3 Catalyst

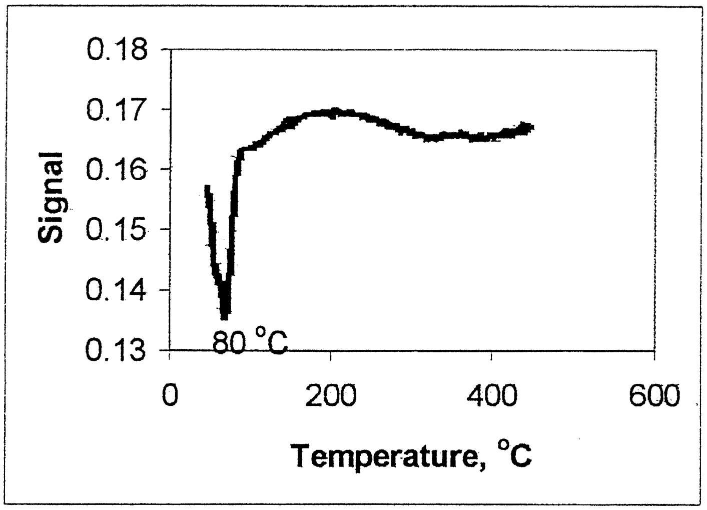

Figure 13. TPR Profile of 2-wt% Pd/Al_2O_3 Catalyst

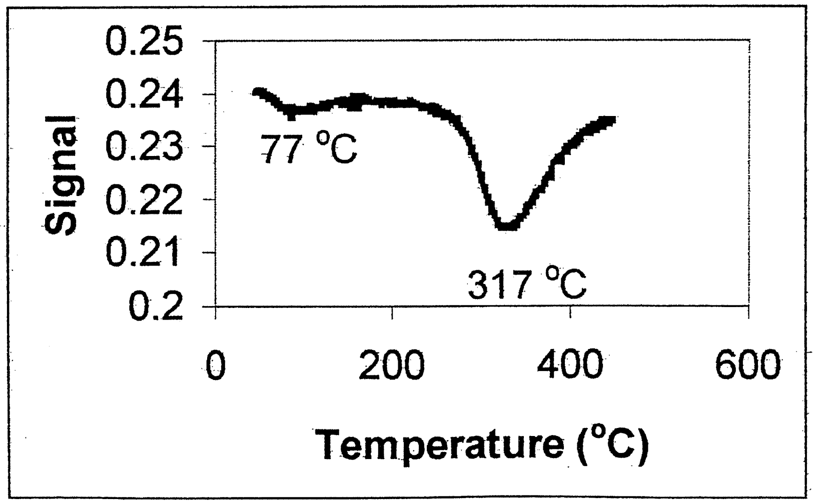

Figure 14. TPR Profile of 2-wt% Pt/MCM Catalyst

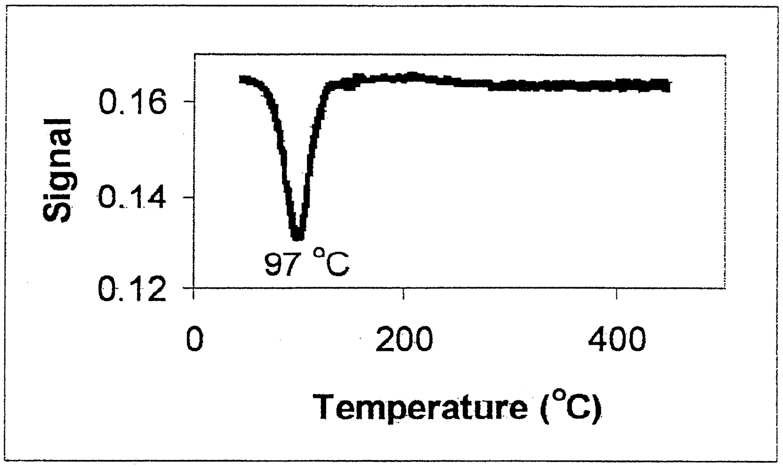

Figure 15. TPR Profile of 2-wt% Pd/MCM Catalyst

X-ray Diffraction (XRD)

X-ray diffraction patterns of various Pt catalysts are presented in Figure 16. The XRD patterns of the various Pt catalysts show no characteristic peaks due to platinum. This indicates that Pt is in a highly dispersed form on these supports. Even if Pt crystallites are formed, they are too small to be detected by X-rays, i.e., below 40-Å crystallite size. In the XRD pattern of the Pt/Al_2O_3 catalyst, only peaks due to Al_2O_3 are seen (d=1.394, 1.990, 2.444) [37]. In the case of Pt/TiO_2, peaks due to the anatase form of TiO_2 are present (d=3.509, 1.895) [38]. In Pt supported on MCM, HY, and HM38 mordenite samples, only the characteristic patterns of MCM, HY, and HM38 are present, indicating a high Pt dispersion on these supports. A comparison of the XRD results with the chemisorption findings shows that Pt is in a dispersed form in all these catalysts.

X-ray diffraction patterns of various Pd catalysts are presented in Figure 17; no characteristic peaks due to palladium are present. This indicates that Pd is highly dispersed on all of these supports. Even if Pd crystallites are formed, they are too small to be detected by X-rays, i.e., below 40 Å. In the XRD pattern of the Pd/Al_2O_3 catalyst, only peaks due to Al_2O_3 are seen (d=1.394, 1.990, 2.444) [37]. In the case of Pd/TiO_2, peaks due to the anatase form of TiO_2 are present (d=3.509, 1.895) [38]. In Pd supported on MCM, HY, and HM38 mordenite samples, only the characteristic patterns of MCM, HY, and HM38 are seen, indicating a high Pd dispersion. A comparison of the XRD results with the chemisorption findings shows that Pd is in a dispersed form in all these catalysts.

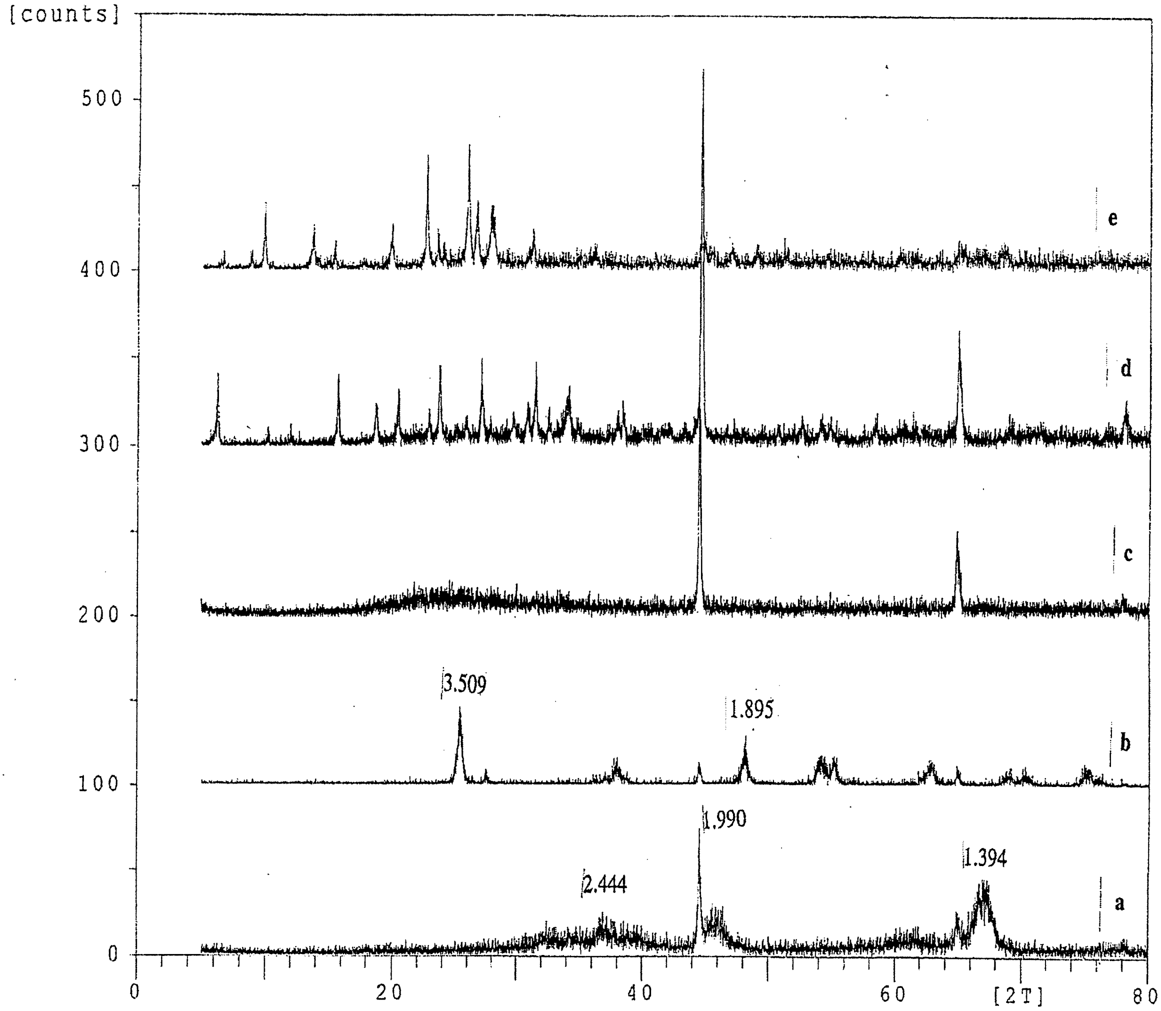

Figure 16. XRD Patterns of Various 2-wt% Pt Catalysts.
(a) Pt/Al_2O_3 (b) Pt/TiO_2 (c) Pt/MCM-41 (d) Pt/HY (e) Pt/HM38

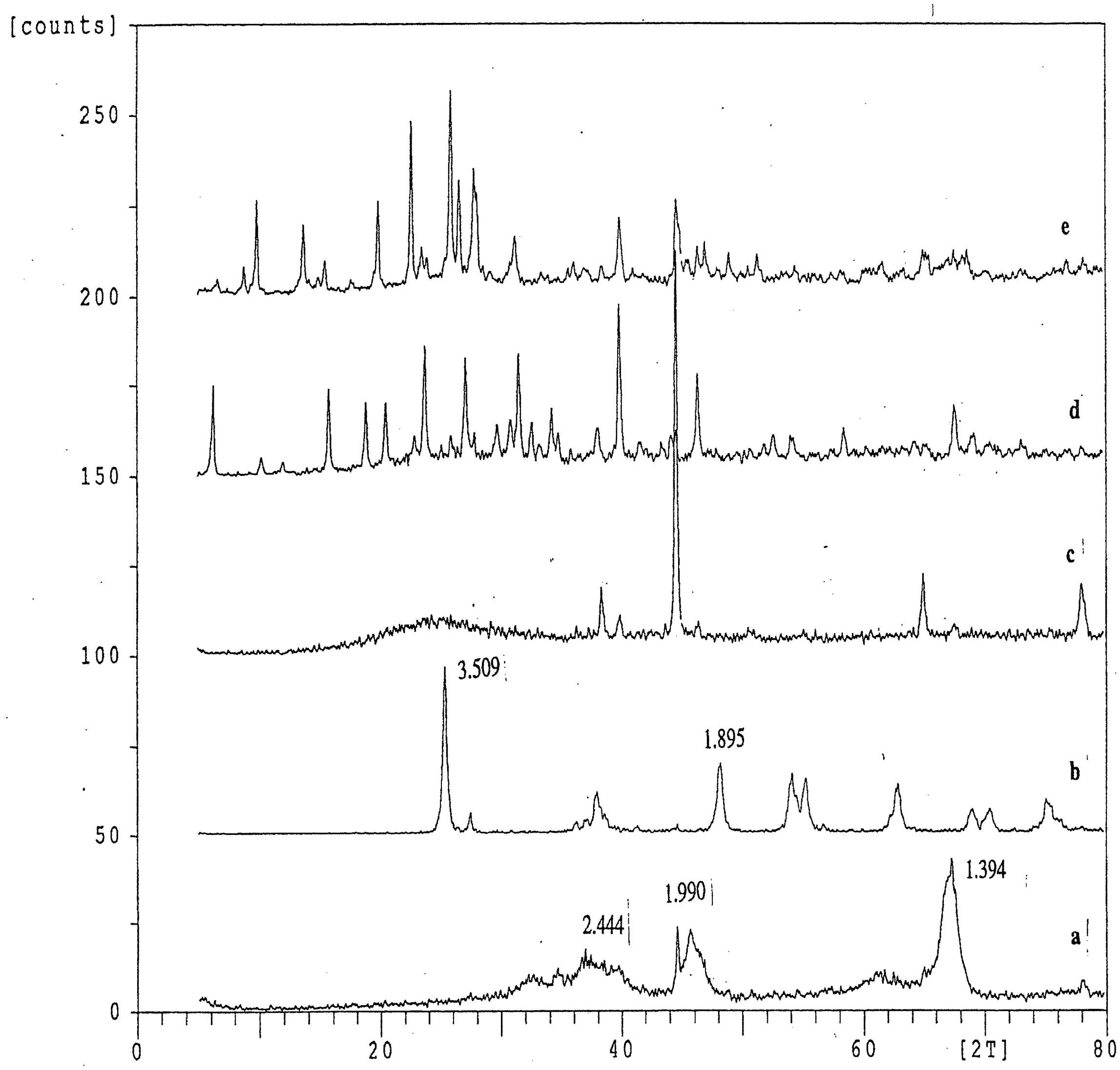

Figure 17. XRD Patterns of 2-wt% Pd Catalysts
(a) Pd/Al_2O_3 (b) Pd/TiO_2 (c) Pd/MCM-41 (d) Pd/HY (e) Pd/HM38

3.4 Conclusions

The observed H/Pt values follow the order: Pt/MCM>Pt/HM38>Pt/Al_2O_3>Pt/HY. A similar trend was observed for CO chemisorption. The Pd catalysts show the trend: Pd/HM38>Pd/MCM>Pd/Al_2O_3>Pd/HY. The chemisorption data for Pt and Pd supported on TiO_2 imply a strong metal-support interaction (SMSI) following low-temperature and high-temperature reduction of the catalysts. The Pt and Pd catalysts supported on the zeolites MCM-41 and HM38 show a higher metal dispersion than that for Al_2O_3 and TiO_2. Temperature-programmed reduction studies show that Pd can be reduced easily and at lower temperatures compared with Pt. The XRD characterization of the Pt and Pd catalysts shows no crystalline peaks due to Pt and Pd, indicating a high degree of dispersion for both metals.

4.0 ASSEMBLY OF A 1-LITER STIRRED-TANK FLOW REACTOR

A continuous flow–process reactor system for the direct liquefaction of coal and upgrading of coal liquids was designed and assembled. The process flow diagram of the system is shown in Figure 18 while the gas-delivery system is shown in Figure 19. The typical operating conditions of the system are given in Table 10. Details of this continuous-mode process reactor system along with its peripheral units are presented below.

The size of the coal particles utilized is small (≤ 60 – 200 mesh) in order to reduce mass-transfer limitations. The solvent used can be a process solvent (middle distillate, decant oil, etc.) or petroleum resid. A dispersed catalyst will be used instead of a traditional supported catalyst. The advantages are the need for less catalyst, good control of retrogressive reactions at pre-conversion conditions thus reducing char formation and catalyst deactivation, reduced reaction severity, a faster hydrogen transfer rate, improved economics due to enhanced yields of desired products, and a higher coal conversion.

Table 10. Typical Operating Parameters of the 1-Liter Stirred-Tank Flow Reactor

	Coal Liquefaction Reactor	Coal Liquids Upgrading Reactor
Reactor Feed	Subbituminous Coal/ Bituminous Coal	Coal Liquids Product from Liquefaction Reactor
Solvent	Middle Distillates	Middle Distillates
Catalyst	MoS_2 Catalyst from Soluble Precursors (Dispersed State)	Mesoporous Supported Catalysts
Reactor Temperature	1st Stage: 350 to 400 °C 2nd State: 400 to 440 °C	375 to 440 °C
Reactor Pressure	2,500 psig	2,500 psig

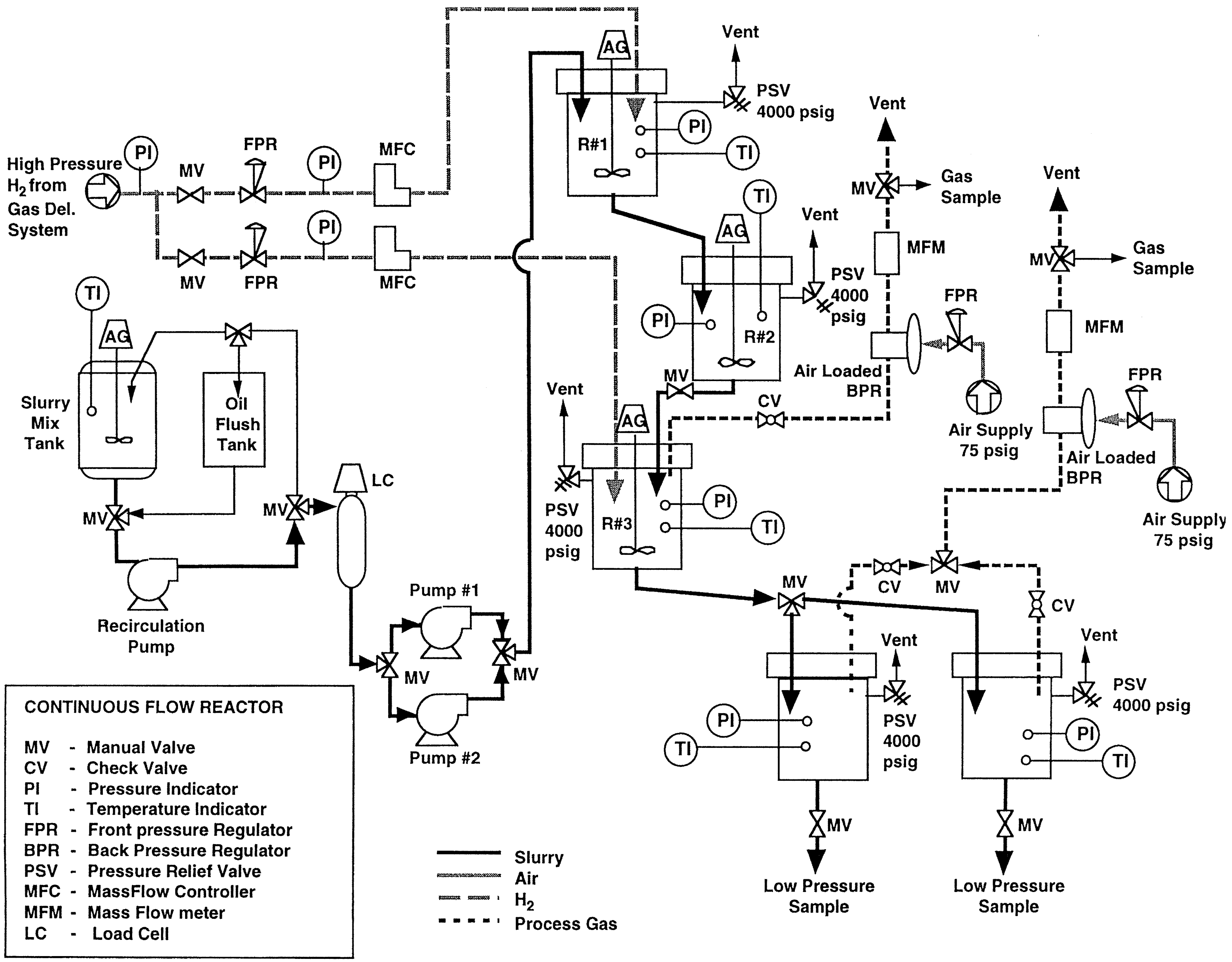
High Pressure H$_2$ from Gas Del. System
PI
MV
FPR
PI
MFC
MV
FPR
MFC
TI
AG
Slurry Mix Tank
Oil Flush Tank
MV
MV
Recirculation Pump
LC
Pump #1
Pump #2
MV
MV
AG
R#1
PSV 4000 psig
Vent
PI
TI
AG
R#2
TI
PI
Vent
PSV 4000 psig
MV
AG
R#3
Vent
PSV 4000 psig
PI
TI
Vent
MV
Gas Sample
MFM
FPR
Air Loaded BPR
Air Supply 75 psig
CV
Vent
MV
Gas Sample
MFM
FPR
Air Loaded BPR
Air Supply 75 psig
MV
CV
MV
CV
Vent
PSV 4000 psig
PI
TI
MV
Low Pressure Sample
Vent
PSV 4000 psig
PI
TI
MV
Low Pressure Sample
CONTINUOUS FLOW REACTOR
MV - Manual Valve
CV - Check Valve
PI - Pressure Indicator
TI - Temperature Indicator
FPR - Front pressure Regulator
BPR - Back Pressure Regulator
PSV - Pressure Relief Valve
MFC - MassFlow Controller
MFM - Mass Flow meter
LC - Load Cell
Slurry
Air
H$_2$
Process Gas

Figure 18. Process Flow Diagram for 1-L Stirred Tank Flow Reactor

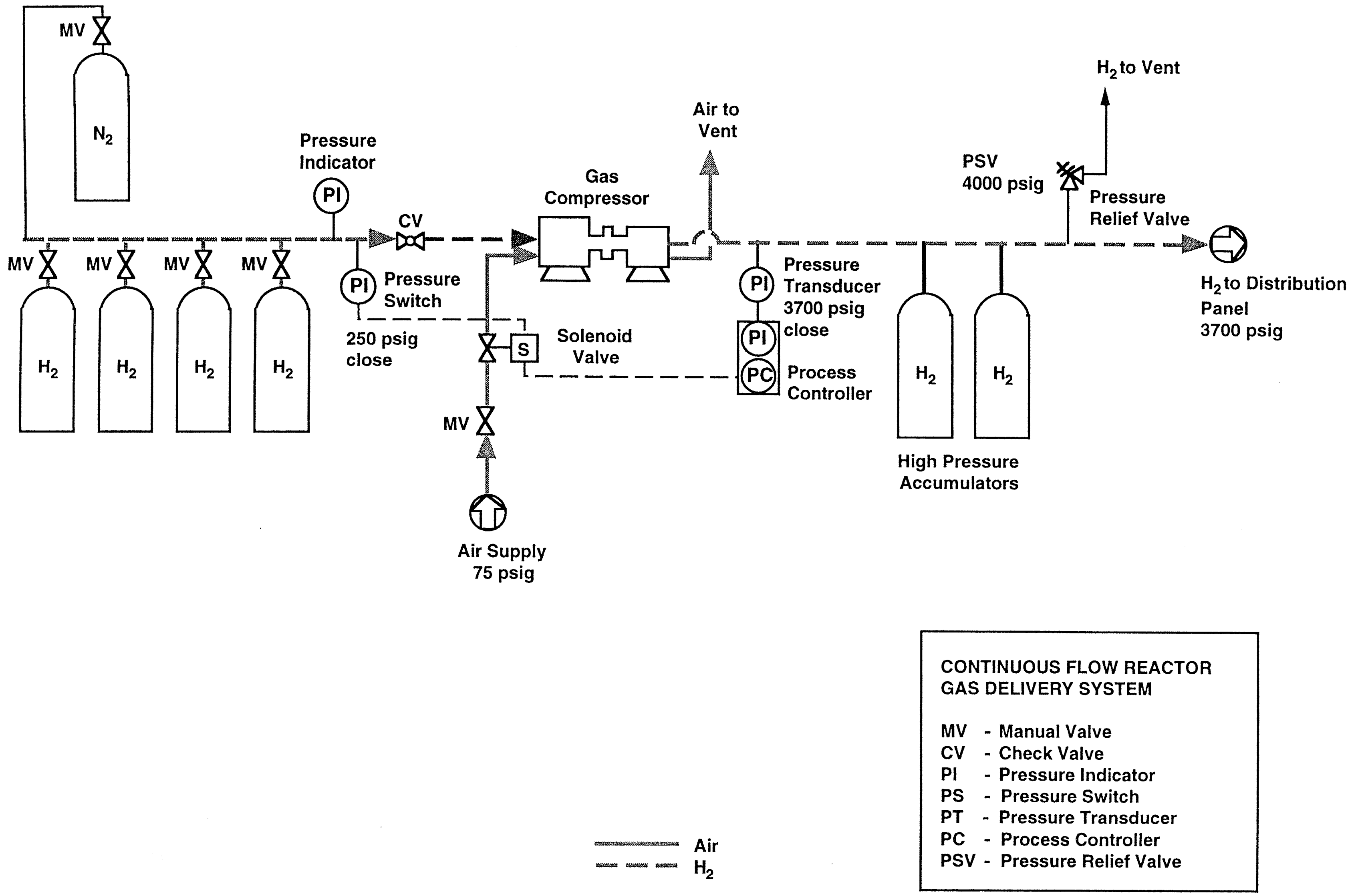
MV
N$_2$
MV
MV
MV
MV
H$_2$
H$_2$
H$_2$
H$_2$
Pressure Indicator
PI
PI
Pressure Switch
250 psig close
CV
Gas Compressor
Air to Vent
Solenoid Valve
S
MV
Air Supply 75 psig
PI
Pressure Transducer 3700 psig close
PI
PC
Process Controller
H$_2$
H$_2$
High Pressure Accumulators
PSV 4000 psig
Pressure Relief Valve
H$_2$ to Vent
H$_2$ to Distribution Panel 3700 psig
Air
H$_2$
CONTINUOUS FLOW REACTOR GAS DELIVERY SYSTEM
MV - Manual Valve
CV - Check Valve
PI - Pressure Indicator
PS - Pressure Switch
PT - Pressure Transducer
PC - Process Controller
PSV - Pressure Relief Valve

Figure 19. Gas Delivery System for 1-L Stirred-Tank Flow Reactor

4.1 Hydrogen Delivery System

The system requires a steady flow of feed gas at pressures of approximately 2,500 psig. Since the manufacturer's gas cylinders have a maximum pressure of 2,500 psig, it was necessary to design a feed-gas compression system. The H_2 feed gas will flow from the gas cylinders into an air-driven gas compressor (Haskel, model No. AGT-30/75), where it is compressed to pressures between 3,400 and 3,700 psig and stored in the compressed-gas storage tanks. The compressor is capable of compressing the inlet feed gas to pressures as high as 5,000 psig, depending on the inlet pressure and the desired exit flow rate to the compressed-gas storage tanks. Air is used as the drive air and supplied through a solenoid valve (Omega, model No. SV-202). A pressure switch (Omega, model No. PSW-133) measures the pressure remaining in the H_2 cylinder manifold. When the manifold pressure decreases to 275 psig, the pressure switch energizes the gas solenoid valve and shuts it off, thus stopping the flow of gas to the compressor and effectively turning it off. Downstream of the compressor, a pressure transducer (Omega, model No. PX-213) measures the H_2 pressure in the high-pressure accumulators. A process controller (Omega, DP-25E), using the input from the pressure transducer, opens and closes the gas solenoid valve (effectively turning the compressor on and off) to maintain the pressure in the gas accumulators between 3,400 and 3,700 psig. A process diagram for the H_2 delivery system is shown in Figure 19.

Safety was first and foremost in the design of the H_2 delivery system. A separate structure was built outside of the building that houses the reactor components to accommodate the compressor, H_2 cylinders, and accumulators. Figure 20 shows the gas-delivery station and exhaust fan. A check valve between the H_2 gas manifold and the gas compressor prevents the flow of H_2 back into the manifold. An inert-gas cylinder (N_2) is connected prior to the gas manifold for flushing and leak-detection purposes. Finally, a pressure-relief valve was placed between the high-pressure accumulators and the distribution panel, so that in the event the H_2 pressure exceeds 4,000 psig, the relief valve would burst thereby allowing the H_2 to vent.

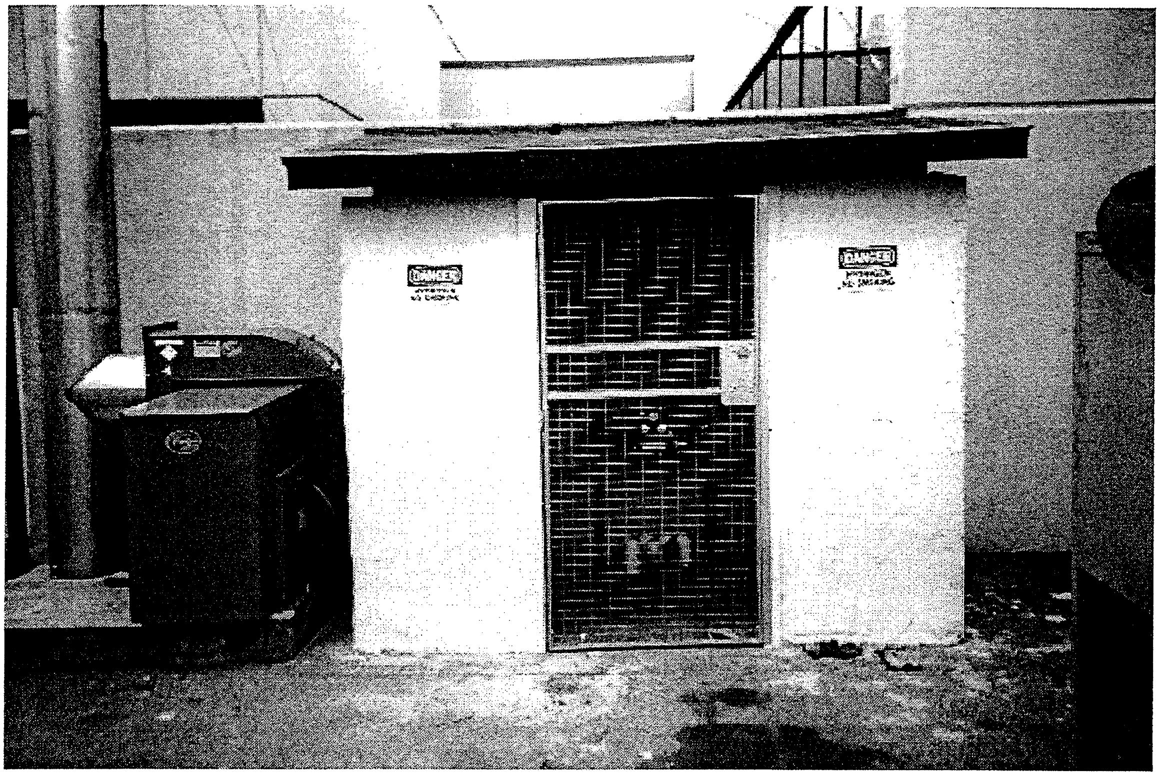

Figure 20. Gas-Delivery Station

Hydrogen from the gas-delivery station is brought into the liquefaction laboratory by 1/4 inch stainless-steel tubing. At the control panel, there are two manual valves that are used to determine the flow of reaction gas. Depending on the orientation of the valves, H_2 can be introduced to reactor 1 or reactor 3, or both. Front pressure regulators (Tescom, model No. 26-1023-24-002-008) control the pressure of H_2, and mass-flow controllers (Brooks, model No. 5850TR) and a power supply (Brooks, model No. 0152E) control the flow of H_2. Pressure gauges downstream from the pressure regulators display the H_2 pressure.

4.2 Slurry Feed System

The slurry feed system consists of the feed mix tank, flush tank, recirculation pump, load cell, and dual slurry feed pumps. The individual components are described below.

The feed slurry to the reactors consisting of coal, dispersed catalyst, and solvent or petroleum resids, is thoroughly mixed in the 3-gallon slurry-feed mix tank equipped with an agitator and variable-speed dc motor. The 3-gallon stainless-steel pressure vessel (Pope Scientific, model No. 10692316) also has a level indicator for visual determination of slurry levels. The temperature and the pressure in this vessel are maintained at 80 to 100 °C and 50 to 80 psig. The agitator maintains the slurry in suspension along with the recirculation pump. Directly under the feed-mix tank is the Moyno recirculation pump. This pump, capable of delivering a 250-psig discharge, works in conjunction with the feed-tank agitator to maintain solids in suspension.

A Totalcomp load cell is used to measure accurately the flow of slurry to the pumps. The load cell measures the weight of the slurry in the holding tank as it is fed to the slurry pumps. A manual valve upstream controls the flow of feed to the holding tank. When the load cell registers that the holding tank is nearly empty, the manual valve upstream is opened and feed is diverted from the recycle loop into the holding tank. After filling the tank, the manual valve is closed. Currently the system is not automated, thereby requiring diligence on the part of the operators. However, contingencies are being made to automate this system.

Slurry from the feed mix tank is fed to the reactors by the slurry pumps (Braun & Luebbe, model No. N-P31). Each pump is capable of handling a high concentration of solids loading in slurry (35 wt. percent) at a 3,500-psig maximum discharge pressure and a 315 °C maximum pumping temperature. The pumps are mounted on a two-tier stand to facilitate a parallel-flow orientation. Three-way manual valves before and after the pumps allow the operators to change pumps quickly in the event that one becomes plugged. This design insures minimal disruption to process runs, as a plugged pump can be cleaned and serviced while the other pump is on-line.

The 5-gallon stainless-steel flush tank (Pope Scientific, model No. 10694316) is used to flush the entire reactor system between process runs. A light oil is used as the flushing agent. Figure 21 shows the feed-system components.

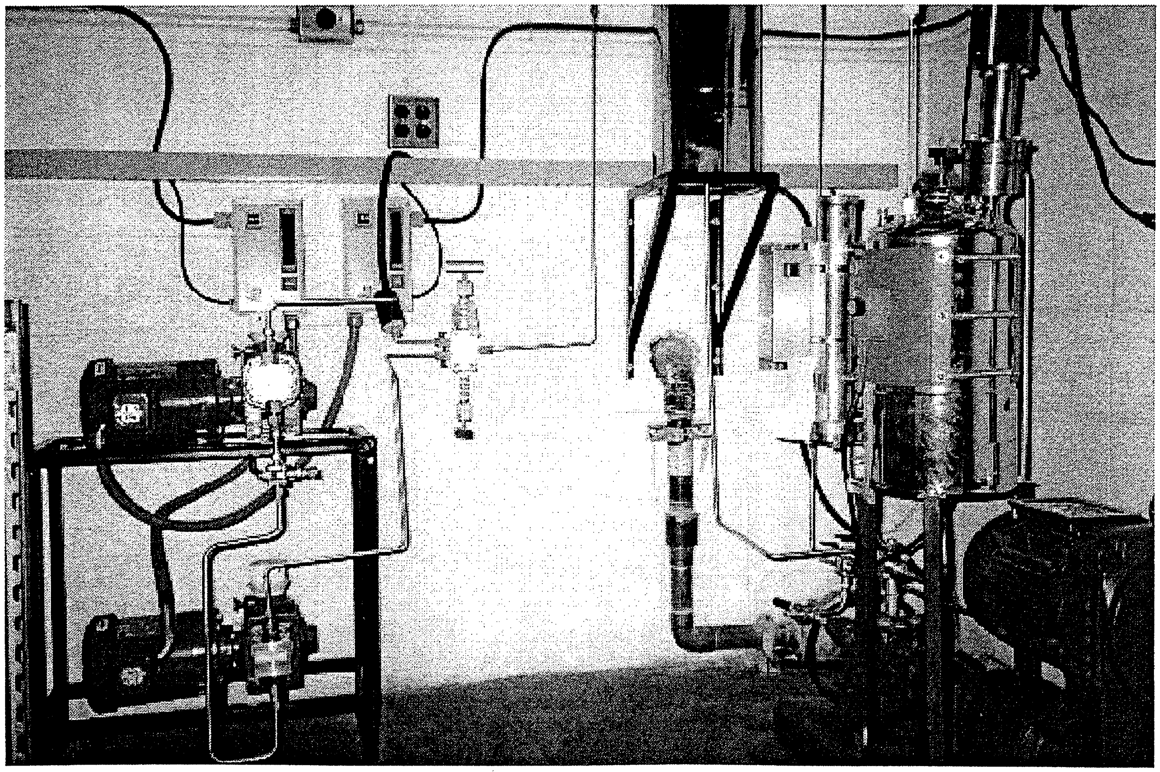

Figure 21. Feed-System Components

4.3 Reactor Components

The main components of the liquefaction system are the 1-L stirred autoclaves (Autoclave Engineers, model no. 95107403). Each vessel is equipped with a dispersimax turbine-type impeller that provides agitation. A dc motor controls the speed of the impeller, and an analog readout displays the revolutions per minute (RPM). Type-K thermocouples, located in thermowells, measure the temperature in each reactor. Pressure taps are installed on each reactor so that pressures can be observed from the pressure gauges mounted on the panel. Ceramic heating jackets encircle each reactor, capable of heating to temperatures of approximately 500 °C. Currently, only the first three reactors are wired with solid-state relays and process controllers (Omega, model No. CN76000) in order to control temperature. Each reactor is equipped with a pressure-relief valve rated at 4,000 psig at 25 °C (MAWP: 2900 psig, 480 °C). The outlets to the pressure-relief valves are hard-plumbed with 1/4 inch stainless-steel tubing leading to the exhaust hoods.

The first reactor in Figure 18 is the 1st Stage Coal Liquefaction Reactor. Process temperatures for this reactor are approximately 350 °C. Hydrogen is fed from the H_2 delivery system to the reactor through the impeller to increase gas-liquid contact. The H_2 reacts with the slurry to form primary products, which include the product vapors and the coal liquids, which remain in the slurry. The unreacted gas, product vapors, and slurry, along with the product liquids, flow from the first reactor into the 2nd Stage Coal Liquefaction Reactor.

The 2nd Stage Coal Liquefaction Reactor is the location where the gas and slurry undergo secondary reactions to form more coal liquids. Process temperatures for this reactor are approximately 400 to 440 °C. The products from this reactor flow through a manual valve into the 3rd Stage Coal Liquefaction Reactor.

In the 3rd Stage Coal Liquefaction Reactor, more coal liquids are formed through secondary reactions that did not occur in the 2nd stage reactor. This reactor is maintained at the same process temperature as is the 2nd stage reactor. Hydrogen can be fed from the gas-delivery system to the reactor, if so desired, by the operator to help facilitate secondary reactions. The product vapors exiting this reactor flow through an air-driven back-pressure regulator (Tescom, model No. 54-2325Z212A-013 Peek) and a flow meter (Omega, model No. FMA-869-V-H2), before being vented to the atmosphere. A three-way valve allows a gas sample to be taken prior to venting.

The final two units are unheated (They have heating jackets if the need to heat them arises in the future) and are used as collection vessels. A three-way valve controls the flow of products to either reactor, thereby allowing one reactor to collect samples continuously at process pressures (2,500 psig) while in the other, the pressure can be let down and the sample collected for analysis. Vapor products from these reactors flow through an air-driven back pressure regulator and flow meter similar to the products from the 3rd stage reactor. Reactors 3 through 5, along with the back-gas-product peripherals, are shown in Figure 22.

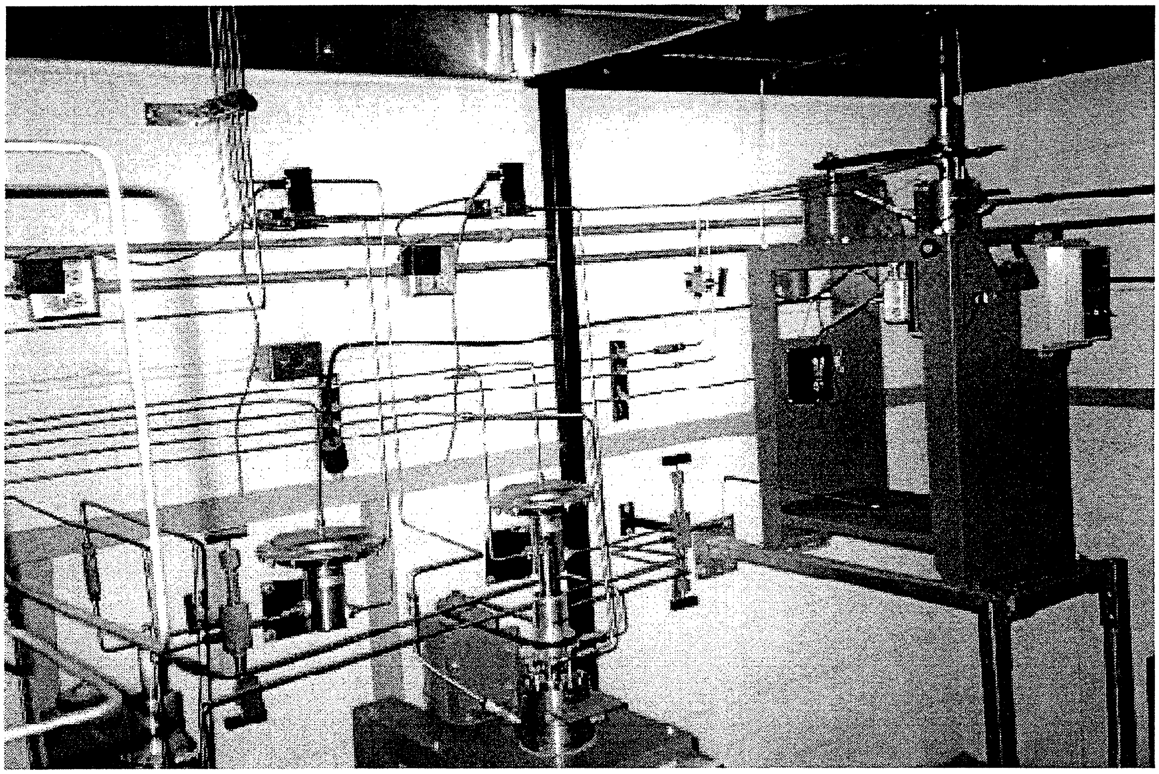

Figure 22. Reactors 3-5, Gas-Product Peripherals

4.4 Data Acquisition System

Process variables, including temperatures, pressures, and load-cell weights, are recorded periodically with a data acquisition (DAC) system. The DAC system consists of a computer (AMD K-6 II, 450 MHz), DAC card (National Instruments, model No. 6024E), and software (National Instruments, LabView).

Temperatures from the five reactors and feed tank, along with the pressure of the accumulators and the weight of the load cell measuring the holding tank, are recorded at specified intervals. Reactor pressures are currently logged manually, but there is some consideration being given to measuring these signals digitally in the future.

4.5 Safety Issues

In addition to the above-mentioned safety features, several other amendments were made in order to ensure the safety of the operators.

Two large (2.5 by 5 feet) stainless-steel vent hoods were installed above the reactors, one above the mezzanine level and the other above the sample-collection reactors. An exhaust fan was purchased and installed outside the liquefaction room adjacent to the gas-delivery station. The exhaust fan (Hartzel, model No. 032-18-BCI3) is a belt-driven, backward-curved centrifugal fan, powered by a 1.5 HP, 1,800 RPM motor, capable of delivering 2,800 cubic feet of air per minute at 2 inches w.c. Based on the volume of the room (roughly 2,200 cubic feet), this fan delivers a little over one air exchange per minute. This also provides a face velocity at each hood of approximately 100 ft/min, well within OSHA acceptable limits.

Continuous toxic-gas air monitors were installed and calibrated. Three sensors, monitoring hydrogen (Bacharach, model No. 51-8311), hydrogen sulfide (Bacharach, model No. 51-8307), and combustibles (Bacharach, model No. 51-8317), were mounted near the ceiling in the center of the room. The hydrogen sensor has a range of 0-2,000 ppm, the hydrogen-sulfide sensor a range of 0-100 ppm, and the combustibles sensor a range of 0-100 percent. Two Bacharach gas-sentinel dual-channel control units are wired to the individual sensors and provide readouts and alarm conditions in the event of a gas release.

Another safety precaution taken was the division of the liquefaction lab by means of a blast wall. Quarter-inch-thick plate steel was welded to a 2 by 2 inch steel square tube that was mounted horizontally across the room at a height of 8 feet. This effectively separates the room into two "partitions"; 2/3 of the room is for reactors and peripherals while the remaining 1/3 is for control and instrumentation. The blast wall contains the instruments and controls and shields the operators from the reactor equipment. Figure 23 shows the blast wall (with instrumentation) as well as the data-acquisition computer and toxic-gas monitors.

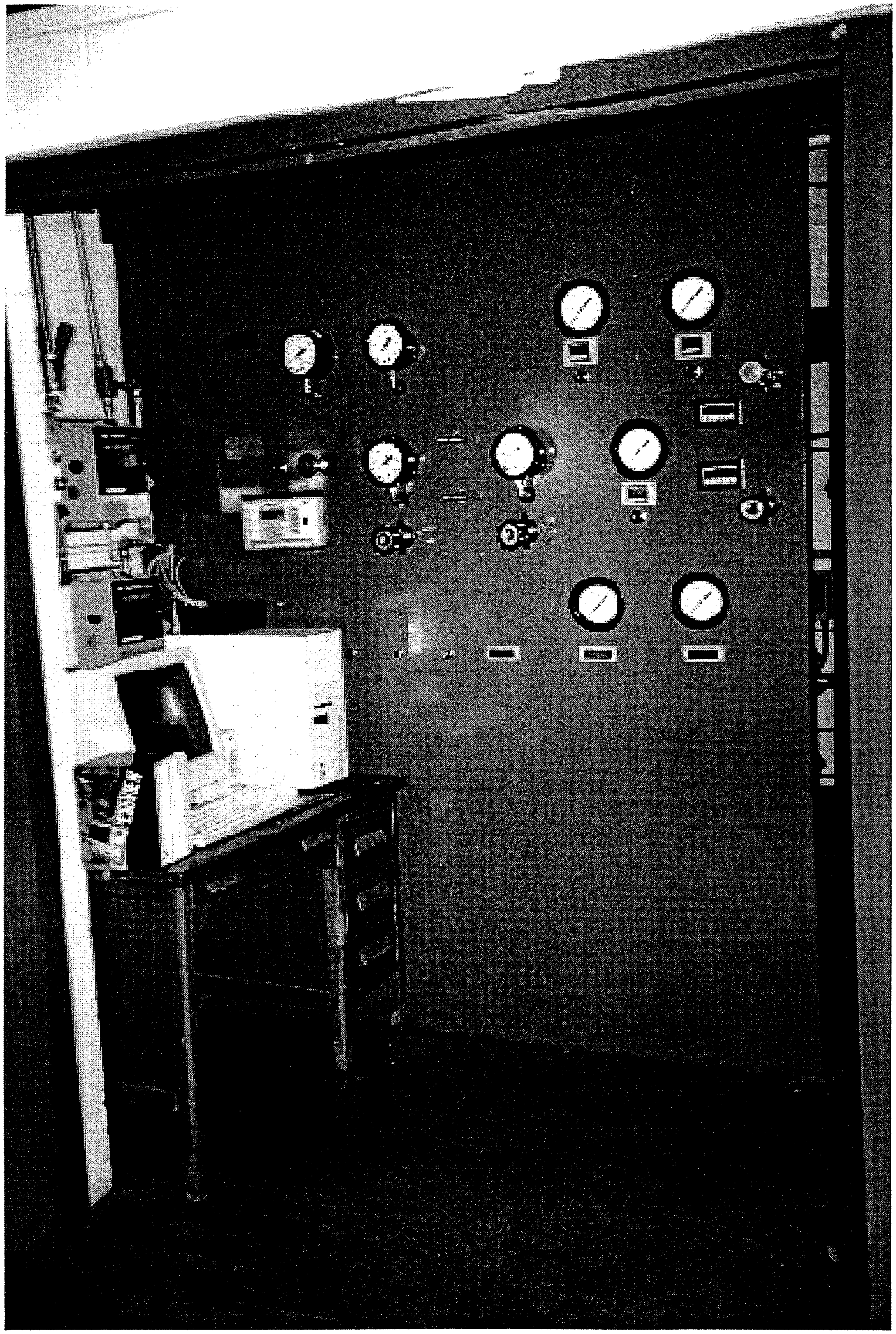

Figure 23. Panel and Instrumentation

5.0 ASSEMBLY OF A LABORATORY-SCALE FIXED-BED FLOW REACTOR FOR CATALYTIC UPGRADING AND REFINING OF JET FUELS

5.1 Abstract

Hydrotreating is a critical step in the production of coal-derived, thermally stable advanced jet fuel. Hydrotreating is important for economic, environmental, and operational reasons. The professed objectives of this subtask include identifying commercial catalysts of optimal activity for hydrotreating the prototype jet fuel and generating kinetic data and protocols for the scale-up of hydrotreating activity for large-scale production of jet fuel. These objectives are to be achieved by performing experimental studies using a high-pressure, multi-phase flow reactor. A critical literature survey and the assembly of this reactor were the key aspects of work accomplished as part of this subtask during the reporting period.

5.2 Introduction

The role of downstream hydrotreating in the quest for coal-derived, thermally stable fuel for advanced jet aircraft cannot be overestimated. Coal-derived liquids such as the prototype for JP-900 can be expected to contain substantial amounts of heteroatoms such as sulfur and nitrogen. As a representative example, certain middle-distillate fuels produced from direct coal-liquefaction processes contain as much as 0.89-wt percent sulfur and 2.04-wt percent nitrogen [39]. The use of such heteroatom-containing jet fuels will be severely limited for environmental, economic, and operational reasons. For example, Mushrush *et al.* [40] in a recent paper allude to the possibility of fuel instability because of the presence of organo-nitrogen compounds. The removal of these heteroatoms from jet fuel via downstream hydrotreating is, therefore, a critical imperative.

The process of removing heteroatoms, such as sulfur and nitrogen, is generically referred to as hydrotreating [41-53]. Sulfur removal, specifically, is known as hydrodesulfurization (HDS), while hydrodenitrogenation refers to removal of nitrogen. Heteroatoms in jet fuel exist as sulfur (thiophenes, benzothiophenes, dibenzothiophenes, and substituted dibenzothiophenes) and nitrogen (pyridines, quinolines, and carbazoles) containing organic molecules [54]. Hydrotreating technology was initially, then frequently and extensively, applied to produce clean petroleum-derived liquid fuels. Hydrotreating catalysts are usually sulfided molybdenum on alumina promoted by either cobalt or nickel depending on the exact heteroatom being targeted. Cobalt favored hydrodesulfurization while nickel was effective for hydrodenitrogenation.

Hydrotreating for sulfur- and nitrogen-removal in coal-derived jet fuels will be accomplished best by multiple-step hydrotreating. This is because of the high concentrations of heteroatom constituents which can be removed only by using several different types of catalysts to produce jet fuel that meets environmental and compositional regulations. The necessity for such a multiple-step hydrotreating protocol is, however, not unique to coal-derived liquid fuels. Several studies, including two at Penn State [46, 55-57], have demonstrated a similar multistep hydrotreating protocol to produce clean fuels from petroleum-derived light cycle oil.

5.3 Subtask Objectives

The specific objectives of this subtask include:

1. Evaluation and identification of commercial catalysts for effective hydrotreating of coal- derived, thermally stable, liquid jet fuel

2. Generation of preliminary kinetic data for scale-up of downstream hydrotreating of coal- derived liquids to produce jet fuel meeting environmental and compositional regulations

There was a need for a comprehensive literature survey on this subject before any experimental endeavors could be initiated. Thus for most of the reporting period the major pieces of work executed by the investigators included design, modification, and assembly of the liquid-flow reactor which would be required for this subtask along with a comprehensive literature survey.

5.4 Literature Survey

Hydrotreating conversions of the prototype jet fuel and the light cycle oil provided by British Petroleum are to be carried out. For such conversions, it is important to better understand their detailed composition from the viewpoint of desirable components which should be retained during deep desulfurization conversions and the sulfur and nitrogen species which have to be treated to extinction. Although a plethora of sophisticated analytical techniques and procedures is now widely available, most reported literature on compositional fuels has focussed on petroleum-derived jet fuels. Most of this literature has been reviewed and attempts to correlate this to the hydrotreatment of coal-derived jet fuel are underway.

5.4.1 Compositional Features of Jet Fuels

Atmospheric gas oil (AGO) has been the focus of our studies because petroleum-derived jet fuels best resemble this petroleum fraction which needs to be regulated for sulfur content [53, 58]. Gas oil refers to a petroleum-derived hydrocarbon liquid having a particular boiling range. There are two types of gas oils—atmospheric and vacuum—distinguished by their boiling ranges. The AGO has an initial boiling point (IBP) of 228 to 232 °C and end boiling point (EBP) of 339 to 377 °C as defined by American Society for Testing and Materials. Vacuum gas oils (VGO) have a boiling range of 340 to 530 °C.

The AGO is primarily composed of straight-chain saturated hydrocarbons with aromatic hydrocarbons forming the second major class of constituents. Sulfur species form about 5 percent of all molecules in AGO. The presence of other polar, heteroatom (nitrogen and oxygen) containing molecules (referred to as polars) is minimal [53]. The LCO, obtained primarily as a byproduct from fluid catalytic cracking (FCC) units, contains nearly equal amounts of saturates and aromatics. In this case too, sulfur species constitute about 5 percent of all molecules in LCO. The presence of polars is minimal in LCO. By combining several liquid- chromatography (LC) separations with GC-MS and using specific GC detectors for sulfur compounds, it has been possible to identify the majority of individual sulfur species in middle-distillate fuels (which characterizes jet fuel).

Pioneering work by the Chemical Inspection and Testing Institute of Japan [53] separated a light gas oil using conventional LC contacting silica gel to yield three fractions: saturates, monoaromatics (single-ring aromatics), and multiring aromatics. The fraction containing multiring aromatics was further separated into sulfur-free and sulfur compound–containing fractions using a procedure developed by Nishioka *et al.* [59]. This method uses the ligand exchange interactions of $PdCl_2$ supported on silica gel for effective separation of sulfur species. For the fraction containing saturates, the carbon number of the components varied from 12 to 25. The single ring–aromatics fraction was more complicated. The sulfur-free multiring aromatics fraction was shown to be composed of five classes of alkyl-substituted aromatics.

For the sulfur-containing multi-ring aromatics fraction, more than 70 individual sulfur compounds, dominated by alkylbenzothiophenes and alkyldibenzothiophenes (both were present in equal concentrations) were identified using gas chromatography-(AED) and GC-MS. The number of carbon atoms on benzothiophenes did not exceed 25 and the dibenzothiophene substituents did not exceed 7.

5.4.2 Reactivity of Polyaromatic Sulfur Compounds

Several research reports have focussed on identifying individual sulfur species in liquid middle-distillate fuels, their contribution to total sulfur content, and their individual rate constants at differing reaction conditions. It was observed that the overall kinetics for the HDS of these species could be described by lumping the rate constants for the individual sulfur species into four reactivity groups [60-64]. These groups, listed in order of decreasing reactivity, are as follows:

1. benzothiophenes with no substituents in 2- or 7-position
2. dibenzothiophenes with no substituents in the 4- or 6-position
3. dibenzothiophenes with one substituent in the 4-position
4. dibenzothiophenes with two substituents in the 4- and 6-positions

For these distillates to meet the mandated sulfur specifications, all compounds in groups 1, 2, and 3 will have to be completely desulfurized, and at least half of those in the least-reactive fourth group will also have to be converted. Several studies using different types of catalysts and operating conditions have identified 4-methyldibenzothiophene (4-MDBT) and 4,6-dimethyldibenzothiophene (4,6-DMDBT) as the most refractory sulfur compounds which will have to be eliminated to achieve deep desulfurization [49, 50, 63-70].

Conversion of sulfur compounds in heavier oils will be much more difficult since dibenzothiophenes in this cut are present in about twice the concentration of the alkylbenzothiophenes. The reactivity of thiophenes fused to polyaromatic ring systems, contrary to popular perception, is higher than those of DBTs because :

- molecules containing more than three condensed aromatic systems are easy to hydrogenate since the puckered hydrogenated ring system will have little steric hindrance for HDS
- the thiophene ring is probably fused at the end of the ring system, analogous to several biological thiophene systems which would have a rate constant of HDS similar to that of benzothiophene, i.e., higher than dibenzothiophene
- a higher degree of condensation does not necessarily lead to higher steric hindrance since the ring systems may be bent as in the case of 1,2-benzanthracene rather than the straight 2,3-benzanthracene

Most of the literature on HDS includes studies on model compounds dissolved in inert solvents. HDS as a commercial process, however, will involve removal of polyaromatic sulfur compounds (PASCs) from a mixture containing a wide range of molecules and distillation cuts. The PASCs in fact represent only a small (less than 2 percent of all molecules in a distillate fraction) portion of the entire fuel. Thus it is important to understand the behavior of other feed components during HDS in both qualitative and quantitative terms. For example, high temperatures may lead to the following:

- cracking of coexisting fragile molecules such as linear paraffins
- alkyl substituents on aromatic rings being cleaved
- dehydrogenation and condensation reactions producing gum and polyaromatic hydrocarbons which impart undesirable color to the product fuel

Similarly, high hydrogen pressures may lead to nonselective hydrogenation of all aromatics, thus consuming expensive hydrogen in excess [71-76].

Also, it has been reported that nonsulfur compounds affect the HDS rate by competitive adsorption on the catalytic sites. It has been reported that diaromatic systems, like naphthalene, inhibit HDS of a variety of PASCs. For feedstocks like VGO, the presence of polars in high concentrations will have a strong inhibiting effect on hydrogenation and HDS reactions [63,77].

It has been known for many years that the ease of sulfur extrusion from a thiophenic compound is affected by the presence of alkyl substituents. Almost three decades ago, Givens and Venuto [78] clearly demonstrated that the position and number of substituents present on benzothiophene strongly influenced the overall reactivity of the molecule and the degree of desulfurization. Although this research effort was for hydrocracking applications, its relevance to hydrotreating jet fuel cannot be questioned. A general trend of reduced reactivity of sulfur compounds with increasing degree of substitution can be observed. This trend is particularly pronounced in the case of dibenzothiophenic structures. The initial reports by Houalla *et al.* [79] produced clear evidence that ring substitution in the remote positions such as the 2-, 7-, and 8- on dibenzothiophenes did little to reduce reactivity. It has been recently proposed that steric inhibition of adsorption on catalyst surfaces is the major cause of such reduced reactivity. Very recent literature has challanged this hypothesis [66].

5.4.3 Promoter Effect on HDS

The role of promoters such as cobalt in hydrotreating studies is of great scientific interest. Cobalt may be present in one of the following three forms after sulfidation:

1. Co_9S_8 crystallites on the support

2. cobalt ions adsorbed on the edges of the MoS_2 crystallites (known popularly as the Co-Mo-S phase)

3. cobalt ions in tetrahedral sites in the γ–alumina lattice [42, 43, 48, 50, 80-82]

Depending on the relative proportions of cobalt and molybdenum and on the pretreatment, a sulfided catalyst contains either a relatively large amount of Co_9S_8 or a large amount of the Co-Mo-S phase. Mössbauer spectroscopic experiments have revealed that the structure of the catalyst in the sulfided state is a function of the oxidic precursor.

5.4.4 Hydrotreating Flow Reactors

The assembly and design of different hydrodesulfurization/(HDN) reactors have been studied in detail. Various aspects such as heat and mass transfer, kinetic measurements, and diffusion limitations were clarified. The literature was also surveyed to determine the best reactor configuration for this study [83-87].

Vanrysselberghe and Froment [88] studied the hydrodesulfurization of dibenzothiophene on a commercial $CoMo/Al_2O_3$ catalyst using a multiphase reactor. The operating conditions were varied over the following range: temperature, 513-517 K; total pressure, 50-80 bar; molar hydrogen to hydrocarbon ratio, 1.1-4.1. They used a multi-phase Robinson-Mahoney stainless-steel upflow reactor capable of handling temperatures of 623 K and pressures of 140 bar. Temperatures were measured by thermocouples; a back pressure regulator was installed after the cyclone; and a mist eliminator was used for gas-liquid separation. The feed was pumped using a high-pressure Spectra-Physics pump, and the feed measurements were carried out using Brooks mass-flow controllers. An online GC was also present.

Other researchers [84, 86] studied hydrodesulfurization of Kuwait atmospheric residuum using a series of alumina-aluminum phosphates (AAP) in a cocurrent down-flow trickle-bed reactor at 663 K and 7582 kPa. The reactor used a Mity-Mite back pressure regulator and a Lewa proportioning pump for the feed, which was measured using Brooks mass-flow controllers. This reactor was unique in using a wet-test meter after the back-pressure valve to measure the extent of gas-liquid separation.

5.5 Experimental

The principal feedstocks for this work will be the prototype for JP-900 being produced from coal-tar blending and petroleum-derived jet-fuel base stock, i.e., LCO provided by British Petroleum (BP) for baseline, reference experiments. Commercial catalysts, chosen after considering the desired properties of the product fuel in consultation with commercial catalyst suppliers, will be used for these studies. Two particular commercial catalysts have already been acquired.

All studies will be carried out on a fixed-catalyst-bed, high-pressure, liquid-flow reactor as outlined in Figure 24. The liquid feed, jet fuel in this case, is pumped through a high pressure liquid-chromatography pump into the reactor using hydrogen pressure. Hydrogen-sulfide gas is used for *in situ* sulfidation of the commercial catalyst. Methane is to be used as an internal standard for gas-chromatography analysis. Gas flows are to be controlled and measured by mass-flow controllers while the pump will measure the liquid feed. The high pressure in the reactor will be developed using a back pressure regulator. The reactor effluents are characterized and analyzed using an off line GC.

The reactor is planned to be controlled using a data-acquisition system. This reactor system was designed after an extensive review of available commercial reactor systems and components, and experimental reactor systems involving high-pressure and liquid flow already in operation at Penn State. A commercial high-pressure equipment manufacturer delayed the reactor design and assembly because of a flawed reactor-tube fabrication. The reactor tube had to shipped back for changes which caused considerable delay.

It is now well established that 4-methyldibenzothiophene and 4,6-dimethyldibenzothiophene are the sulfur-containing organic compounds with the lowest reactivity and without whose desulfurization jet fuel will not meet requisite regulatory and compositional standards. Consequently these sulfur-containing molecules will be used as model compounds for obtaining hydrodesulfurization conversion, selectivity, and kinetic data for commercial catalysts. However, these model compounds are not commercially available and will need to be synthesized in-house. Experimental apparatus design and chemicals were ordered to carry out these organic syntheses during the reporting period.

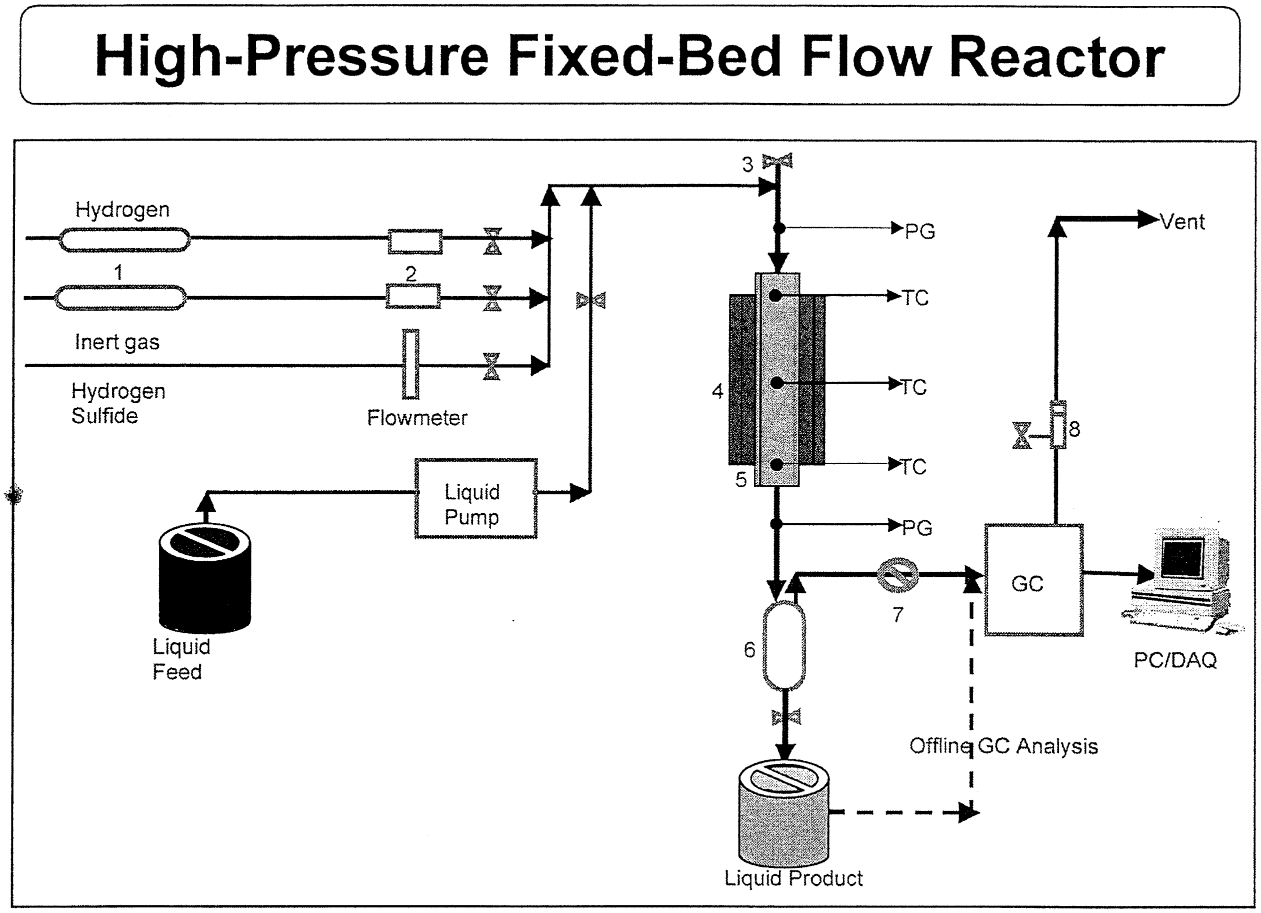
High-Pressure Fixed-Bed Flow Reactor
Hydrogen
1
2
Inert gas
Hydrogen Sulfide
Flowmeter
Liquid Pump
Liquid Feed
3
PG
TC
TC
TC
4
5
PG
6
7
GC
Vent
8
PC/DAQ
Offline GC Analysis
Liquid Product

Figure 24. Fixed-bed, high-pressure, liquid-flow reactor for catalytic hydroprocessing. 1. Oxygen Traps / Gas Purifiers; 2. Gas Mass Flow Controllers (MFCs); 3. Valves; 4. Furnace; 5. Reactor; 6. Liquid sampling; 7. Back Pressure Regulator; 8. NaOH Scrubber (before venting off H_2S gas)

5.6 Conclusions

The reactor assembly is virtually complete, and detailed experimental studies are in progress. The comprehensive literature survey executed during the reporting period, glimpses of which have been provided above, provides a sound basis for developing an accurate and scalable hydrotreating protocol for the large-scale commercial production of advanced jet fuel.

6.0 ASSEMBLY OF A HIGH-PRESSURE, HIGH-TEMPERATURE CELL FOR *IN SITU* FT-IR CHARACTERIZATION OF CATALYSTS AND REACTION INTERMEDIATES UNDER REACTION CONDITIONS

6.1 Introduction

The elucidation of the nature of active sites on solid catalysts and the estimate of their concentrations is extremely important in order to develop better catalysts. Due to the complexity of the catalyst surface and the extreme working conditions of some industrial catalytic systems, it is no small task to characterize the catalysts *in situ.* Traditionally, techniques such as X-ray diffraction, X-ray photoelectron spectroscopy, and Fornier-transfer infrared have been used to probe the structure of solid catalysts and to develop structure-activity relationships. However, most of these techniques have been carried out under atmospheric conditions or under vacuum. Very few studies have focussed on the characterization of the catalysts in the actual reaction conditions where high temperature and high pressure are present. The conditions experienced by the catalyst during actual reactions are very different from those under which it is usually characterized. The catalyst can undergo changes during the reaction in the form of structural reorganization and changes in the active-site concentrations. This can have a direct impact on the structure-activity relationships of the catalyst. Therefore, *in situ* studies are of immense importance, because the information obtained about the structure can be directly correlated with the performance of the catalyst under reaction conditions. As a consequence, the development of new catalysts, their optimization, and the localization of their optimum working conditions can be predicted accurately, rather than through trial and error.

In situ FTIR has made an important contribution toward catalyst characterization. However, almost all the studies have been performed under ambient conditions. Some high-temperature, high-pressure studies have been described in the literature [89-94]. However, most of these studies are based either on transmission cells or on diffuse-reflectance techniques (DRIFTS). A major problem with such systems is that there is very strong absorption in the same region due to gas-phase molecules. This problem is even greater at high pressures since the high gas concentrations and the long path lengths lead to intense gas-phase absorption, which makes the study of adsorbed species difficult and unreliable, if not impossible [95]. Another important disadvantage is the fact that in transmission cells, the sample has to be pressed into a thin wafer by application of high pressure, which can collapse the catalyst structure leading to diffusional limitations of the probe molecules and reactants inside the catalyst pores. In order to counter these difficulties, the use of cylindrical internal reflectance (CIR) cells has been proposed [96, 97].

The primary objective of the work proposed in this subtask involves the fabrication of a stainless-steel, high-pressure, high-temperature IR cell and the assembly of an *in situ* FTIR probe for the characterization of catalysts and reaction intermediates under reaction conditions.

6.2 Experimental

Description of the High-Temperature, High-Pressure FTIR Cell

The *in situ* high-temperature, high-pressure FTIR cell is based on a design developed by Moser *et al.* [96], and comprises a high-pressure plug-flow microreactor fabricated from 316 stainless steel, capable of reaching temperatures as high as 500 ^{O}C and pressures as high as 1000 psi. The cell has a ZnSe optical rod embedded in the reactor, which is 0.25 inch in diameter and 3.25 inches in length. This crystal is polished at an angle of 45° at the two ends and has the mechanical strength to withstand the extreme high-pressure, high-temperature conditions present in the proposed experimental studies. Graphite O-rings capable of withstanding high temperatures are used to seal off the reactor and the crystal rod. Since graphite absorbs very strongly in the mid-IR region, the O-rings are coated with a very thin layer of gold to prevent interference with the absorbance from the surface-adsorbed species and intermediates. The catalyst sample is introduced around the crystal rod after sealing off one end of the reactor. The quality of the spectra depends upon the extent of contact between the catalyst sample and the crystal surface. The smaller the catalyst particle, the better is the contact, and hence, the better the quality of the spectra. Moser *et al.* [96] have suggested a particle size of 10-40 µm as optimum for good catalyst-crystal contact. Better contact between the catalyst sample and the crystal rod is also obtained by gently tapping down the catalyst with a hollow cylinder so as to pack the catalyst as tightly around the crystal as possible.

6.2.2 Layout of the Analytical Setup

Figure 25 shows a schematic of the analytical setup of the FTIR instrument. The high-temperature, high-pressure cylindrical internal reflectance cell is heated by a cubical, aluminum heating jacket containing four 100-watt Omega cartridge heaters. A K-type thermocouple (Omega), attached to the body of the stainless-steel cell, is used to measure the reactor temperature, which is controlled by an Eurotherm temperature-controller unit. The FTIR cell, encapsulated within the heating jacket, is mounted on a CIRCLE optical accessory (obtained from Spectra-Tech) within the Nexus 470 FTIR spectrometer (obtained from Nicolet). The high-pressure inlet and outlet lines consist of 1/16 inch 316 stainless steel. The inlet lines will be used to introduce various gases (H_2, He, CO/He, N_2), which will be used as both purge and probe gases. An ISCO 500D high-pressure, liquid-feed pump will also be used for circulation of liquid feeds during the study of *in situ* hydrodesulfurization and hydrogenation reactions. A TESCOM downstream back pressure regulator is used to control accurately the pressure within the cell. A stainless-steel high-pressure by-pass line will be used to fill up the whole unit with the reactant mixture before sending it through the CIR cell. The experimental data obtained will be processed and manipulated using Nicolet OMNIC E.S.P. software.

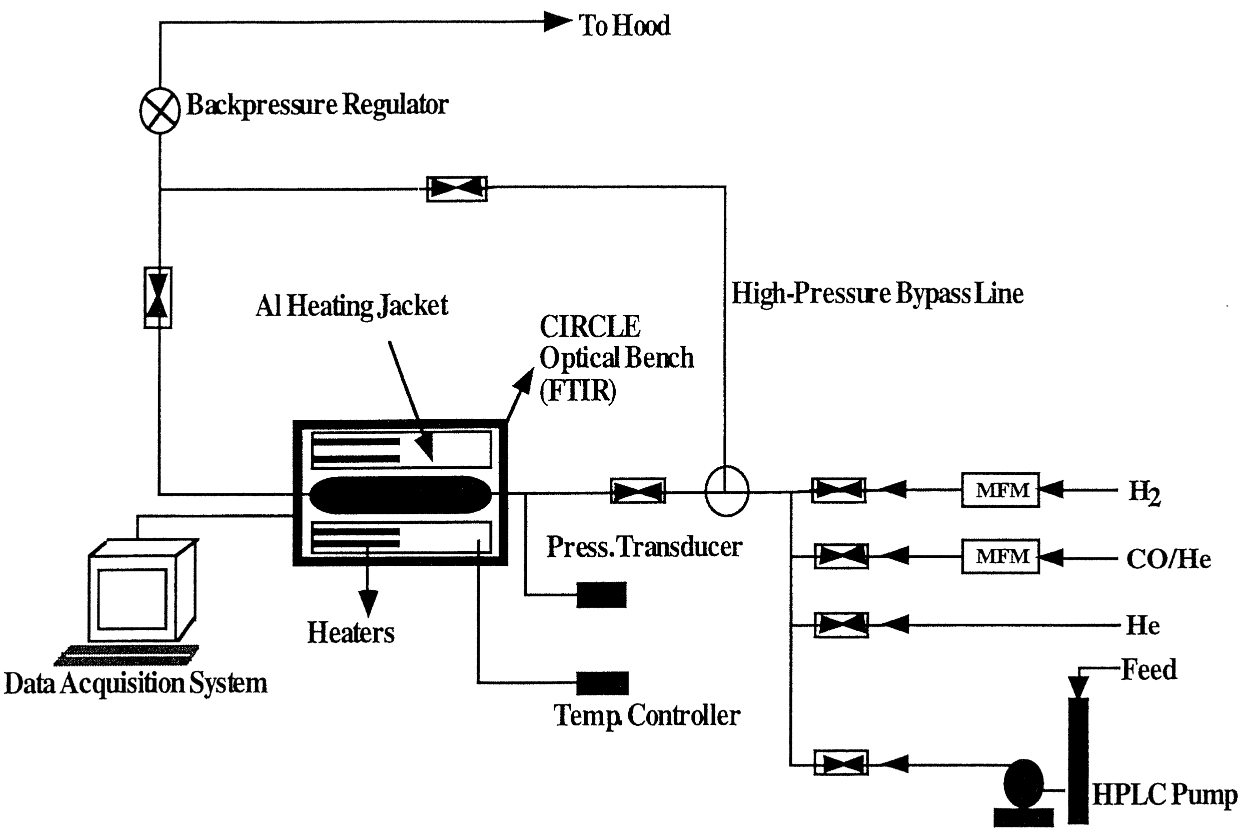
To Hood
Backpressure Regulator
Al Heating Jacket
CIRCLE Optical Bench (FTIR)
High-Pressure Bypass Line
MFM
H2
MFM
CO/He
He
Feed
Press. Transducer
Heaters
Data Acquisition System
Temp. Controller
HPLC Pump

Schematic of the Experimental Setup

Figure 25. Schematic of the Analytical Setup of the FTIR

6.2.3 Alignment Procedures of the FTIR Cell

The FTIR cell was successfully fabricated and installed in the Nicolet Nexus 470 FTIR instrument; Figure 26 shows the design of the cell. The alignment of both the FTIR and the cell is crucial in order to ensure the proper functioning of the instrument and the accessory, as well as the quality of the spectra obtained. Figure 27 shows the spectrum of the crystal, as provided by SpectraTech, while Figure 28 shows the spectrum of the crystal using the fabricated FTIR cell, at 32 scans and 4 cm^{-1} resolution. The spectrum of the empty cell, which will be used as a background spectrum, was correlated with that provided by SpectraTech. Comparisons were made so as to ensure the proper alignment of the instrument and accessory as well as the quality of the spectra obtained. The spectrum of the empty cell without purge (Figure 28) and that of the cell with an N_2 purge (Figure 29) are similar in their general appearance indicating the proper alignment of the instrument and the cell. However, there is interference due to CO_2 and H_2O, as can be seen from Figure 28. The C-O and O-H stretching frequencies in CO_2 and H_2O have very strong signals and so interfere with the spectra of the catalysts. In order to eliminate this problem, the sample chamber of the FTIR is purged with N_2 continuously during the experiments. Purging allows the elimination of these gases from the sample chamber, thus removing the stretching frequencies from the spectrum. Figure 29 shows the spectrum of the empty cell while the sample chamber in the FTIR is continuously being purged with a mixture of

N_2 and He. As can be seen from a comparison of Figures 28 and 29, the elimination of CO_2 and H_2O from the sample chamber improves the quality of the spectrum obtained. Also, the FTIR instrument and the cell were successfully aligned and calibrated.

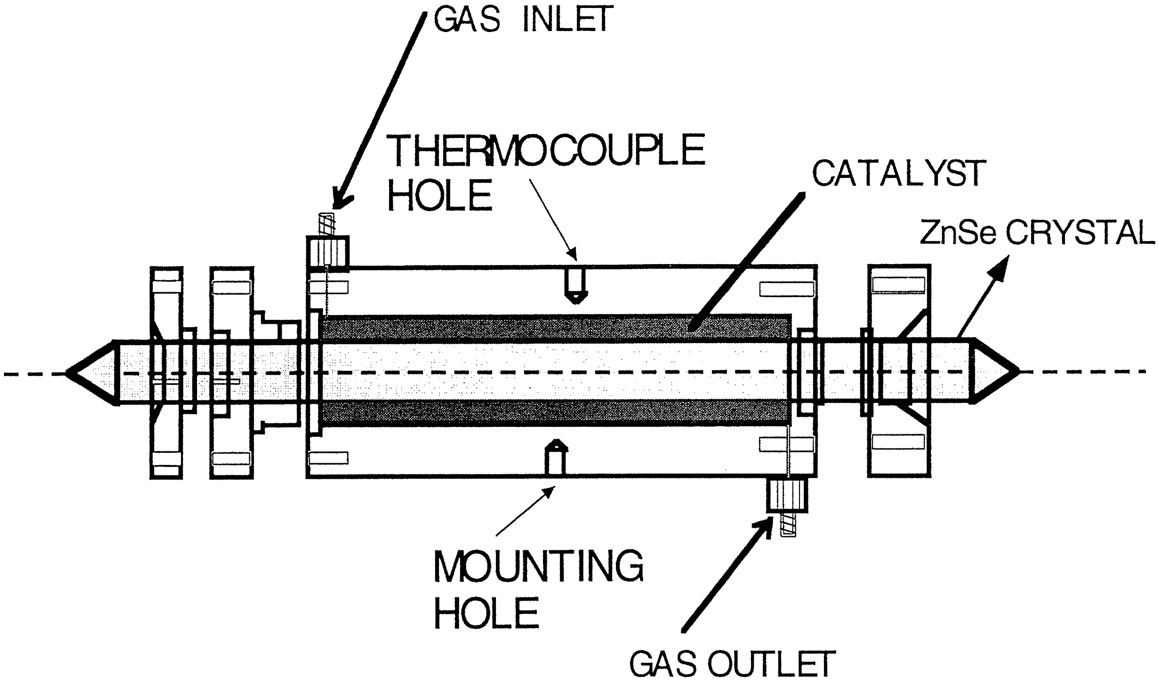
GAS INLET
THERMOCOUPLE HOLE
CATALYST
ZnSe CRYSTAL
MOUNTING HOLE
GAS OUTLET

Figure 26. Design of the High-Pressure, High-Temperature FTIR Cell

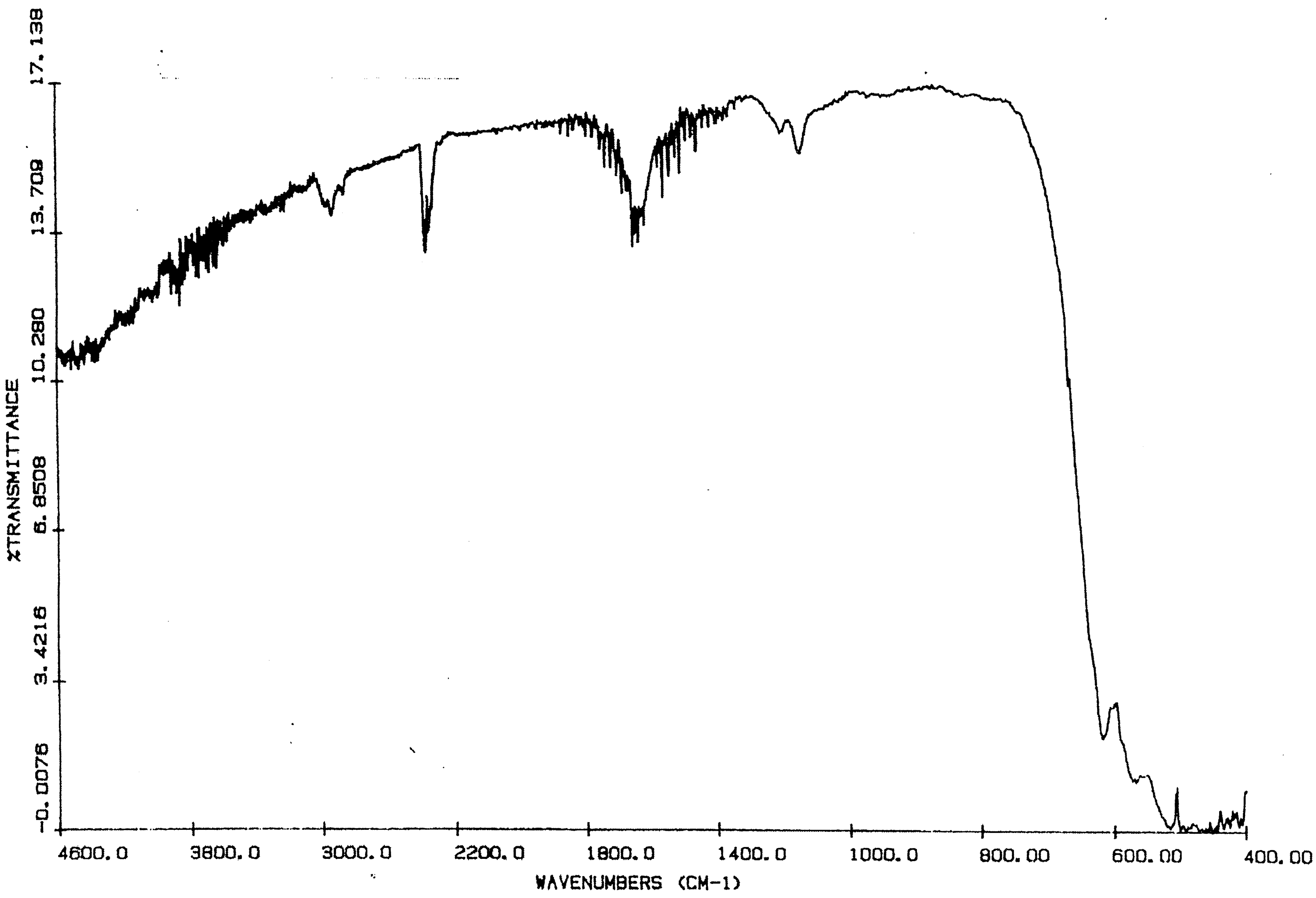

Figure 27. Spectrum of Crystal as Provided by SpectraTech

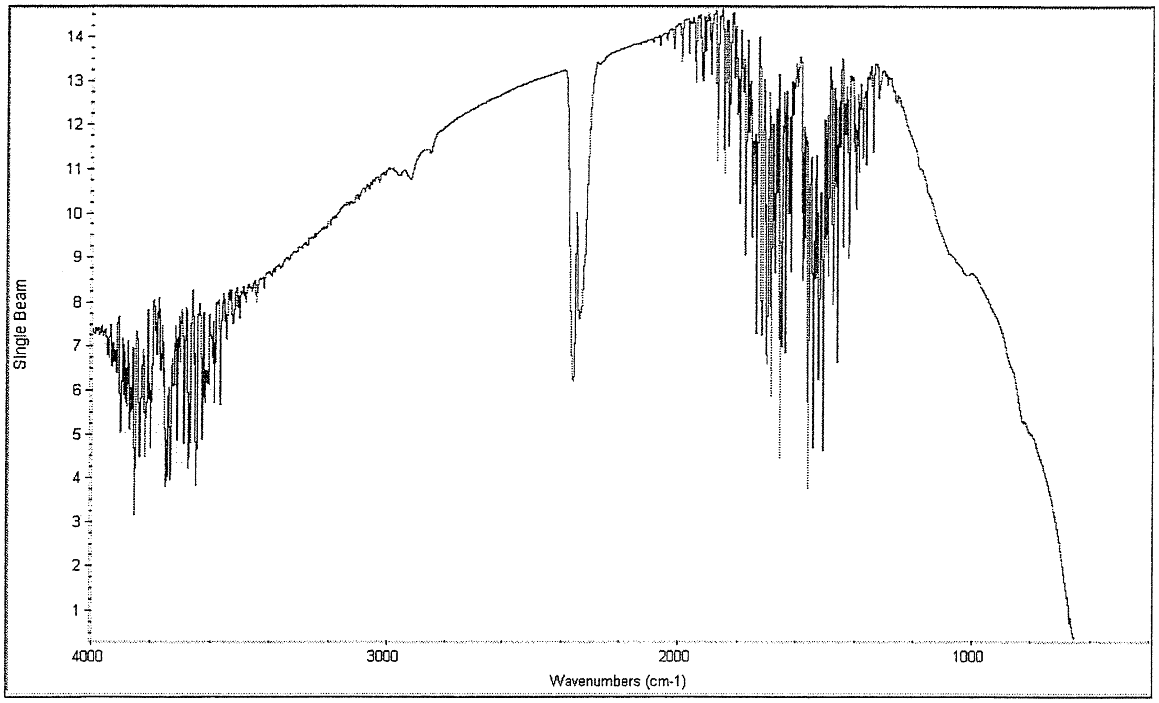

Figure 28. Spectrum of the Crystal in the Empty Cell (without purge)

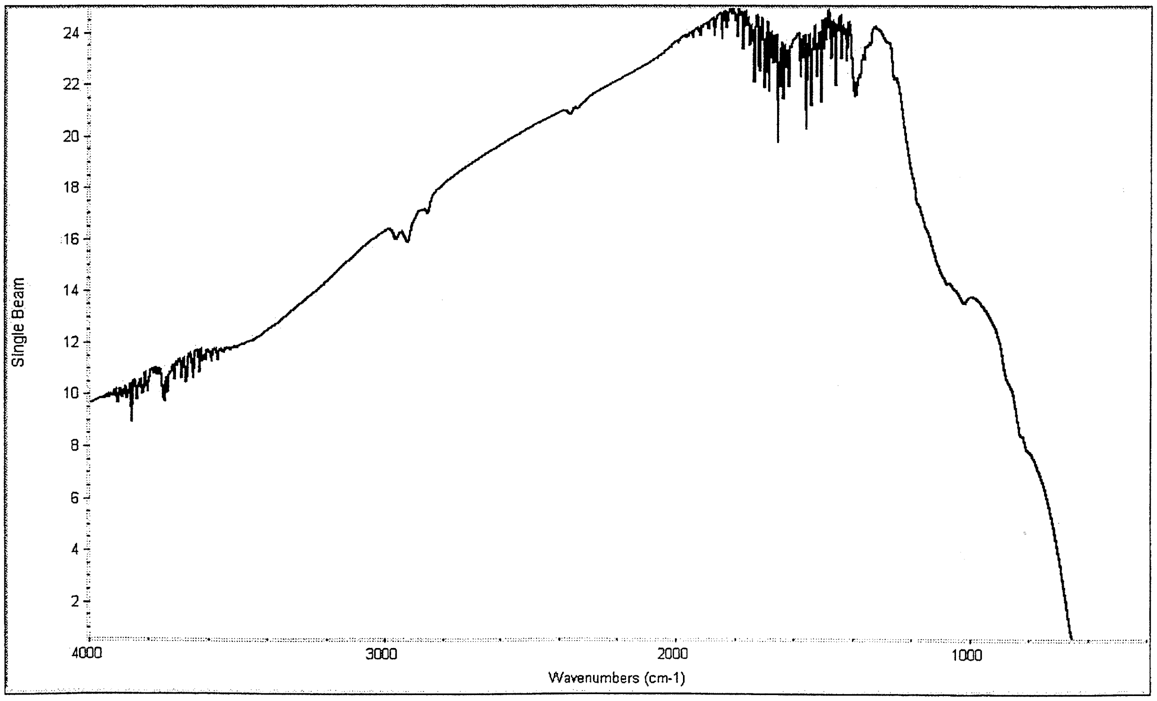

Figure 29. Spectrum of the Empty Cell in the Presence of N_2 Purge

6.3 Results and Discussion

Two types of *in situ* studies will be carried out using the high-temperature, high-pressure FTIR cell. Noble-metal based supported catalysts are used for hydrogenating naphthalene at temperatures of about 200 ^{o}C to produce tetralin and decalin, the former being an important jet-fuel stabilizer (hydrogen donor). In addition, deep hydrodesulfurization is a very important process for obtaining high-performance, low-sulfur, clean-burning jet fuels. Important commercial catalysts used for these processes are subjected to high pressures and temperatures. Therefore, it is important to characterize these catalysts under the actual reaction conditions so that direct correlation can be established between the structural and chemical features and the performance of the catalysts under different processing conditions.

6.3.1 Supported Noble-Metal Hydrogenation Catalysts

Supported noble-metal hydrogenation catalysts are typically Pt and Pd supported on TiO_2, SiO_2, and Al_2O_3. These catalysts are used for the hydrogenation of naphthalene to produce tetralin, which acts as a very good H-donor thereby terminating free radicals that are involved in the thermal decomposition of jet fuel, and decalin, which increases the thermal stability of the jet fuel in the pyrolitic regime [98, 99]. Since the electronic state of the noble metal is important, it is essential to characterize the nature of the active hydrogenation sites generated by these metals. The adsorption of CO is typically used to characterize supported-metal catalysts. In general, the CO adsorption depends on the metals themselves, their dispersion, and their oxidation state, as well as the support. The C-O stretching frequency depends on the amount of electron density transferred from CO to the metal. Therefore, the stronger the C-Metal interaction, the weaker the C-O bond, resulting in a decrease in the C-O stretching frequency. Since the electron density on the metal particle is also an indication of the extent of the metal-support interaction, the C-O stretching frequency reflects the electronic environment of the metal particle. Two principal IR bands are observed and correspond to (1) linearly adsorbed CO (high-frequency band), and (2) bridged-bonded CO (low frequency band). In Pt, the high-frequency band occurs between 2040 and 2075 cm^{-1}, while the low-frequency band lies between 1800 and 1865 cm^{-1}. For Pd, the respective frequencies are ~2075 and ~1900 cm^{-1} [100-103].

Since the electron density of the metal particle depends on the extent of metal-support interaction, which in turn depends on the acidity of the support, a change in the acidic nature of the catalyst brought about by the reaction conditions can induce a corresponding change in the electronic structure of the metal particle. This can further affect the activity of the metal toward hydrogenation as well as its sulfur tolerance. Therefore, it becomes necessary to study the effect of reaction conditions on the catalyst.

Future work will include the development of experimental methods for the study of several commercially available catalysts by TPR using FTIR, as well as TPD of hydrogen using pulse chemisorption methods. Experiments will also be designed for the study of metal-support interactions using CO adsorption. As stated earlier, the C-O stretching frequency is very sensitive to the electronic structure of the noble-metal particle, and therefore, can help determine the extent of metal-support interactions in the catalysts. If the metal-support interaction is strong, the noble metal has a slight positive charge resulting in a weaker C-O bond, thereby causing a decrease in the stretching frequency [104]. Some studies will also be done on the nature of the H^+ on the acidic supports and the effect of pressure and temperature.

6.3.2 Hydrodesulfurization Catalysts

The HDS is a very important process for obtaining low-sulfur jet fuels. Keeping current and future environmental regulations in mind, deep hydrodesulfurization will be a key aspect in hydrotreating jet fuels. New catalysts will, therefore, have to be developed to remove even the most stable sulfur compounds from the fuel. A detailed understanding of the nature of the active sites and the reaction mechanism will play a major role in the improvement of existing commercially available HDS catalysts. Present commercially available HDS catalysts are usually sulfided Co-Mo/Al_2O_3, Ni-Mo/Al_2O_3, and Ni-W/Al_2O_3, where Co and Ni act as promoters. Though a vast amount of work has been carried out on the characterization of these catalysts, it is only recently that the nature of the active sites in these catalysts has been elucidated [105]. Many structural models have been put forward to elucidate the active state of Co-Mo/Al_2O_3 and related HDS catalysts, the most widely accepted model being the Co-Mo-S phase proposed by Topsoe *et al.* [106] . According to this model, the Co-Mo-S phase consists of MoS_2-like structures with the promoter atoms located at the MoS_2 edges in the Mo plane. Although many characterization studies have been carried out on the various HDS catalysts, the surface structure of the catalyst in its working state is not known, especially concerning the nature of the active sites that are actually involved in the hydrodesulfurization reactions. One of the reasons for this lack of insight is the fact that HDS reactions are performed at pressures between 1 and 200 bar in the temperature region of 600 to 670 K [107]. These extreme temperatures and pressures make *in situ* characterization of the catalysts extremely difficult.

6.3.3 *In Situ* FTIR Studies of HDS Catalysts

Infrared spectroscopy has been a very valuable characterization tool for studying *in situ* the nature of the active sites and the surface structure of Cobalt-Mo/Al_2O_3 and related catalysts, since the interaction between the active sites and suitably selected probe molecules leads to modifications in the characteristic stretching frequencies of these probe molecules. Nitric oxide is one of the most extensively used probes to characterize the active sites of HDS catalysts, because it gives valuable information regarding the dispersion, oxidation state, and extent of unsaturation of the active-phase metal [108-113]. Another important feature of NO is that it adsorbs only on the supported active phase and not the support itself, thus giving important information only about the active sites [114-117]. The Infra-red spectrum of adsorbed NO consists of a characteristic doublet caused by two NO molecules adsorbing on each site resulting in symmetric (higher frequency) and anti-symmetric (lower frequency) stretching vibrations, although it is still not clear whether the NO molecules are present as a dimer or as a dinitrosyl [117]. Freshly calcined oxidic Mo/Al_2O_3 does not show any NO adsorption due to the (+VI) oxidation state of Mo (d^0 configuration), which results in a lack of electron back-donation from Mo to NO and hence weak NO adsorption [118]. However, upon reduction of the Mo phase by heating in a vacuum, in hydrogen, or in mixtures of hydrogen/hydrogen sulfide, the characteristic doublet is observed at about 1800-1815 cm^{-1} (symmetric stretching) and 1700-1715 cm^{-1} (anti-symmetric stretching). For the sulfided catalysts, these bands shift toward lower wavenumbers by a maximum of 40 cm^{-1}, due to the lower electronegativity of sulfur in comparison with oxygen [110, 119, 120]. The Co/Al_2O_3 gives similar bands, although in this case the bands are at higher frequencies where the two bands are 1860-1880 cm^{-1} (symmetric) and 1780-1800 cm^{-1} (anti-symmetric). The NO bands shift to lower wavenumbers as the catalyst is reduced (10 cm^{-1}) or sulfided (33 cm^{-1}). In the case of reduced Co-Mo/Al_2O_3, a triplet is observed due to the partial overlap of the two doublets corresponding to Co and Mo, respectively. The positions of the three bands are 1880-1895 cm^{-1} (symmetric for Co), 1700-1705 cm^{-1} (anti-symmetric for Mo), and 1795-1800 cm^{-1} (overlap of the anti-symmetric mode of Co and symmetric mode of Mo). Sulfidation of these catalysts results in the bands shifting to the lower-frequency region [121].

6.3.4 Probe Molecules for High-Temperature *In Situ* HDS Characterization

Although (NO) has been extensively used for the characterization of HDS active sites, a serious drawback associated with its use is that NO is not entirely unreactive, even at temperatures below 300 K. This results in dissociative chemisorption, leading to oxidation of the catalyst surface [106, 120, 122]. Therefore, NO cannot be used as a probe molecule for high-temperature studies. Carbon monoxide has been proposed as an alternative, although it has recieved much less attention due to its weak IR signal, resulting from its low heat of adsorption. The carbonyl stretching frequency is sensitive to the nature, oxidation state, and coordinative environment of the catalyst. Apart from this, the extinction coefficient of CO is relatively high, so that reasonable sensitivities can be achieved [123]. Knozinger *et al.* first demonstrated that CO adsorption at 273 K correlated linearly with HDS activity for thiophene [124]. Peri reported the appearance of a carbonyl infrared band at 2100 cm^{-1} when CO was adsorbed on a sulfided Mo/Al_2O_3 catalyst at room temperature, and this band was assigned to Mo(vi) sites [108]. A band similar to this was observed by Bachelier at 2105 cm^{-1} [125]. They also observed a shoulder at 2070 cm^{-1} which was assigned to a CO molecule coordinated to a Mo center in a still lower oxidation state. In the case of sulfided Co-Mo/Al_2O_3, the two bands were observed at 2110 cm^{-1} and 2065 cm^{-1}. Delgado [126] studied the adsorption of CO on sulfided Mo/Al_2O_3 at 77 K and observed bands in the 2100 to 2120 cm^{-1} range which were attributed to Mo^{2+} - CO adsorption complexes, the Mo^{+2} sites presumably being located at the edges of the MoS_2 platelets.

Even though infrared adsorption studies of CO and NO have provided vital information regarding the nature of active sites, their use has been largely restricted to low temperatures and pressures. Hydrotreating catalysts typically operate at pressures up to 200 bar in the temperature region 600 to 670 K. It is therefore important that the catalysts are characterized *in situ* at these conditions. It has been shown that the nature of coordinatively unsaturated sites depends on the reduction and sulfidation temperatures and pressures [127-129]. Sulfidation at higher pressure resulted in the coordinatively unsaturated sites (cus) being formed selectively on the Co site of Co-Mo/Al_2O_3, and the selectivity also increased by high-pressure sulfiding. It has also been shown that at higher reduction temperatures (773 K), corner sites dissapear due to morphological changes and changes in the Mo dispersions [130]. It is very likely that similar structural reorganizations can occur while the catalyst is operating at high temperatures and pressures, leading to the changes in the concentrations of various active sites. Topsoe proposed that the edge sites are responsible for hydrogenation activity while the corner sites are responsible for direct sulfur extraction [121]. For the highly substituted dibenzothiophenes, ring hydrogenation prior to sulfur extraction is the major route. Therefore, such changes in the concentration of edge and corner sites will have a direct bearing on the catalytic activity of the HDS catalysts toward deep hydrodesulfurization of 4-MDBT and 4, 6-DMDBT. Therefore, the study of these hydrotreating catalysts at high temperatures and pressures is important in order to develop better catalysts.

As part of future work, NO and CO adsorptions on commercially available hydrodesulfurization catalysts will be carried out at high temperatures and pressures for CO, and only high pressures for NO, in order to determine the changes in the catalyst properties brought about by the extreme operating conditions. Since the activity depends strongly on the degree of dispersion of the active components and the interaction between the Co^{2+} and $Mo^{\delta+}$, studies will be carried out to observe the changes in these properties as well as the concentration of the active sites. *In situ* infrared studies of the hydrodesulfurization of 4-MDBT and 4, 6-DMDBT will be done to correlate the data obtained from the above studies.

6.4 Conclusion

The fabrication of the high-pressure, high-temperature FTIR cell was successfully completed and the experimental setup was fully installed. The alignment procedures were carried out on the cell and the Nicolet Nexus 470 FTIR instrument in order to calibrate properly the instrument and ensure the proper functioning of the setup and the reliability of the data obtained.

7.0 CO-COKING COAL AND PETROLEUM RESIDUES

7.1 Goals

In this task we set out to achieve the following goals:

- The exploration of reaction conditions, which actively promote the desired liquid-hydrocarbon production
- The utilization of clean coals supplied by PrepTech
- The quantitative and qualitative analyses of the liquid products and comparisons with similar liquefaction and coprocessing studies
- Preliminary work on the batch hydrotreatment of selected liquid products
- Interfacing with BP on possible scale-up to pilot-plant runs

Most of these goals were met to some degree during the execution of this delivery-order period

7.2 Summary

The work performed in this study is a continuation of work performed in Delivery Order 3, Task 4. Significant improvements have been made during this study on the work previously reported. Among these was the development of a vented reactor system, which simulated the conditions found in a delayed coker better than the sealed reactor had previously. The use of decant oil as a feedstock led to an increase in the quality and yield of the liquid products from the co-coking reactions when compared with the products from reactions involving coker-feed vacuum resid.

7.3 Introduction

Delayed coking is a process used in many petroleum refineries throughout the world for the conversion of heavy petroleum residua (vacuum resid and decant oil) into a light distillate fraction and coke. This is achieved by the pyrolysis and thermal degradation of the feedstock in a semi-continuous process, at temperatures between 450 and 500 °C in an inert atmosphere, and at pressures around 10 psig. The volatiles produced during the thermal degradation of the feedstock are vented during the operation and transferred to a distillation tower where they are fractionated into the appropriate distillates. The coke product builds up in the reaction vessel over a period of 18 hours, at which point the feed is pumped into a parallel reaction vessel. The coke is then removed from the full vessel. The coke produced has varying qualities that depend on the feedstock and reaction conditions. A typical product distribution for a delayed coking operation is 70 percent liquid, 20 percent coke, and 10 percent gas.

With the introduction of coal to the process stream, it is assumed that the volatile constituents of coal may be produced along with the volatiles from the petroleum feedstock, and subsequently fractionated. The integrity of the coal-derived structures should be maintained.

During the processing, aromatic-ring systems are produced, which could be upgraded into a thermally stable jet fuel during hydrotreatment with the petroleum-derived compounds.

7.4 Experimental

7.4.1 Feedstocks Used

The vacuum resid used was obtained from BP. The decant oil was supplied by the Marathon Oil Company

A search of the Penn State Database and a survey of some of the coal companies supplying metallurgical-grade coals to the cokemaking industry revealed that most of the naturally high thermoplastic coals are located in western Pennsylvania, southeastern Kentucky, and southwestern Virginia. From the survey, a 9-kg car-top composite sample of 2.4-mm coal was obtained from A.T. Massey for both the Powellton- and Eagle-seam coals from Virginia. As shown in Table 11, these coals were selected because of their comparative rank with the Upper Banner– and Pittsburgh-seam coals already employed in a previous study as well as their high fluidity, relatively low-ash yield, and high content of reactive macerals. Furthermore, the fluid properties of Massey's coals are reported to be well out of the range of measurement by the ASTM method.

Table 11. Characteristics of Project Coals

	Pittsburgh	**Powellton**	**Eagle**
Rank	**hvAb**	**hvAb**	**hvAb**
Vitrinite Reflectance, %	0.87	1.03	1.01
% Reactive Macerals	89.1	80.9	78.8
Moisture	2.4	6.75	6.75
% Ash Yield	10.0	5.0	5.5
%Volatile Matter	43.5	33.5	34.5
%C	83.3	87.6	87.3
%H	5.7	5.8	5.6
%N	1.4	1.6	1.6
%S	1.3	0.9	-
%O	8.4	3.9	-
Max. Fluid. Ddpm	20,002	>30,000	>30,000
Max. Fluid. T°C	438	448	437
Softening T°C	390	387	401
Resolidification T°C	476	490	493

7.4.2 Co-Coking Studies

Co-coking experiments were performed using 25-ml stainless-steeltubing bomb-type reactors and a vented reactor system (see Figure 30). Feedstock ratios ranged from 4:1 to 2:1 (resid to coal), with approximately 10 g of combined feedstock used in each experiment. The length of each run ranged from 0.5 to 4 hours. Temperatures of 450, 465, 475, and 500 °C were used during these experiments. Heating was achieved by immersion of the loaded reactor in a preheated fluidized sandbath. Prior to heating, the coals had been dried at 110 °C for 1 hour to remove any excess moisture. Once the reactor was loaded, it was purged with nitrogen to obtain an inert atmosphere and left at ambient pressure.

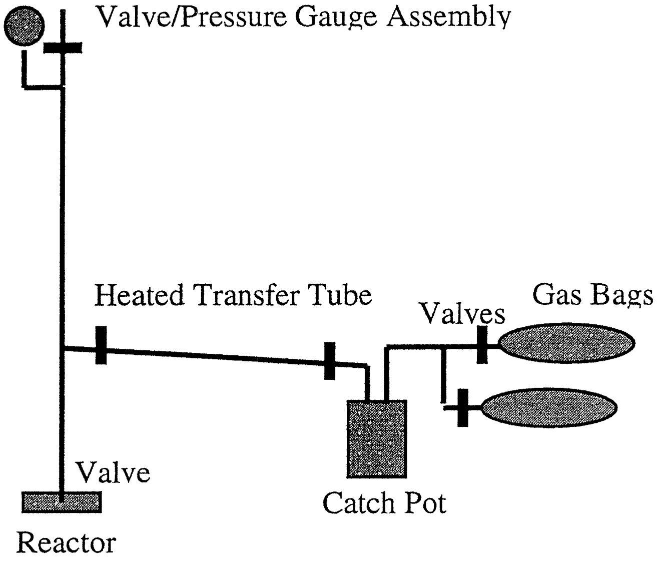

Figure 30. Schematic Representation of Vented Reactor System

After the run the reactor was allowed to cool to room temperature. At this point, the products of the reaction were removed from the reactor and subjected to exhaustive solvent extraction using a soxhlet extractor. The products were separated into oils, asphaltenes, pre-asphaltenes, and coke fractions using hexane, toluene, toluene, and Tetrahydrofuran, respectively.

7.4.3 Analysis

Ultimate analysis of carbon, hydrogen, and nitrogen composition and sulfur analysis was obtained using CHN-600 and SC-132 sulfur-determination analyzers (LECO). Proximate analysis (moisture and ash) was performed using an LECO MAC 400 proximate analyzer. The liquid feedstocks and products were analyzed by high-temperature simulated distillation gas chromatography (SimDist GC) using a HP 5890 Series II Plus fitted with a FID detector and a Restek MXT-500 Sim Dist column. The boiling-point distribution and the cut point of the 180 to 330 °C fraction were observed in order to monitor the yield in the jet-fuel range. Quantitative and chemical speciation were performed on the feeds and samples using a GC-17A gas chromatograph and QP-5000, a compact, high-performance quadrupole mass spectrometer, from

Shimadzu. The column used was a XTi-5 from Restek with dimensions of 30 m; 0.25 mm ID, and 0.25 μm df (5 percent phenyl film thickness). Optical microscopy was performed on the solid (THF insoluble) samples using a Zeiss Microphot reflected-light microscope.

7.5 Results and Discussion

7.5.1 Effect of Reactor Type on Product Yield

The typical product distribution from a delayed-coking process is 10 percent gas, 70 percent liquids, and 20 percent coke. Previous work at Penn State (see Final Report Delivery Order 3, Task 4) considered simulating the delayed-coking process within sealed reactors. Table 12 shows examples of the product distributions obtained from experiments performed in the sealed reactor system using 2-hour runs at 465 °C.

Table 12. Overall Product Distribution (in percent yield) for Sealed Co-Coking Reactions at 465 °C for 2 Hours

COAL	RESID	LIQUID	SOLIDS	GAS
Eagle	Coker feed	20.56	50.39	22.31
None	Coker feed	57.46	14.49	16.07
None	Decant	66.08	26.06	16.19

The sealed-reactor results show that we have not quite achieved the desired product distribution of a delayed-coking operation. To try and achieve this goal, a vented reactor system was designed (Figure 30). The overall product distributions that are being obtained from the vented reactor system are displayed in Table 13.

Table 13. The Overall Product Distribution for the Various Vented Reactions (in percent yields) at 465 °C for 2 Hours

		PERCENT YIELDS (%)				
COAL	RESID	GAS	CATCHPOT LIQUID	PIPING LIQUID	TUBE BOMB LIQUID	COKE
None	Coker	0.00	44.06	13.60	6.60	13.62
None	Decant	0.00	53.35	3.56	19.37	12.30
Powellton	Decant	0.11	44.87	3.75	6.85	37.67
Eagle	Decant	6.94	35.28	4.12	4.90	30.22
Eagle	Coker	0.00	42.52	5.18	7.49	33.82
Eagle	None	0.00	0.99	6.57	24.91	60.65
Powellton	None	0.33	0.22	2.68	3.39	77.04

When compared with the sealed system, the results show that the vented reactor system produces product distributions closer to those of the delayed-coking operation (see Table 13).

We are obtaining liquid yields of around 60 percent and coke yields around 15 percent. The results from the vented-product distribution also show that the reactions involving the resids alone produce product yields that are close to those of a full-scale delayed-coking operation (70 percent liquids and 20 percent coke). The lack of gaseous products indicates a problem in containing the gases being evolved. The current method of containing the evolved gases in a gasbag, in series with the condenser, may not be adequate. It may be necessary to put a liquid-nitrogen trap in series to condense the gases evolved, and then determine their mass.

From the vented-reactor-system results in Table 13, we see that the majority of our product is being obtained within the catchpot, or condenser portion of the reactor system. Essentially the vented system is a flash-distillation process. The samples that are over undergo relatively little change compared with the sealed-reactor operation. Therefore, we expect to see different product distributions and different compounds being produced.

7.5.2 Time and Temperature Effects

Table 14 shows the product yields for two different feed ratios, 1:2 and 1:4 (coal to resid), as well as three different run times for reactions performed at 465 °C. We know from previous research that the product distribution from these vented co-coking reactions was unaffected by temperature effects [131]. As the reaction time was increased for a particular feed ratio, the overall liquid yield decreased, while the solid-product yield increased. As reaction time increased, there was a decrease in overall liquid-product yield. This was mainly a result of the decrease in the liquid products obtained by THF extraction from the bomb. This occurred because the liquids were exposed to further cracking reactions. However, the catchpot liquids were relatively unaffected by the length of reaction time, since most of these liquids were flashed off very early in the reaction and condensed in the piping or catchpot.

Table 14. Feed Ratio and Reaction-Length Effects on Product Yields from Co-Coking Reactions with Powellton Coal and the Two Petroleum Resids at 465 °C

		Feed Ratio 1:2			Feed Ratio 1:4		
		% Yield			% Yield		
Resid	Time	Condensed	Bomb	Coke	Condensed	Bomb	Coke
Coker	30 minutes	58.83	24.78	24.78	52.05	16.94	26.71
Coker	2 hours	36.96	1.89	40.74	59.97	1.57	30.98
Coker	4 hours	48.08	0.63	38.87	54.57	1.21	28.20
Decant	30 minutes	39.12	33.97	28.57	57.53	20.70	13.78
Decant	2 hours	48.62	6.85	37.67	45.36	11.52	34.03
Decant	4 hours	37.65	2.02	43.12	43.40	5.84	49.24
Decant/Coker	30 minutes	43.58	10.28	30.50	*	*	*
Decant/Coker	2 hours	42.08	2.56	39.88	55.88	4.71	26.50
Decant/Coker	4 hours	49.87	3.10	40.49	60.96	1.05	26.53

* Data incomplete

Table 14 also shows the effect of feed ratio on the product distribution of co-coking reactions at 465 °C. As the concentration of petroleum resid was increased for a particular reaction time, the overall liquid products increased while the overall solid products decreased. The reactor system did not have an adequate gas-collection device. However, mass-balance calculations indicate that the amount of gas produced from these co-coking reactions would have been minimal.

Ultimate analysis was performed on the hexane-soluble fractions produced from co-coking reactions at 465 °C. Table 15 shows the H/C ratio for the hexane-soluble products. The results indicate that the liquid H/C ratio obtained from the catchpot for reactions with a 1:2 feed ratio (coal:resid) is relatively unaffected by length of reaction time. These results show that the liquids obtained in the catchpot had undergone flash pyrolysis early in the reactions. Table 15 also shows that as the feedstock ratio was increased to 1:4 (coal:resid) there was no significant effect on the H/C ratio of the liquids condensed in the catchpot. Conversely, the liquid H/C ratios from the bomb portion showed a decrease in H/C ratio as the reaction length was increased. This probably occurred due to the increased decomposition of the liquid in the bomb portion of the reactor during longer co-coking reactions.

Table 15. Feed Ratio and Reaction Length Effects on Hexane-Soluble Product H/C Ratios from Co-Coking Reactions with Powellton Coal and Various Petroleum Resids at 465 °C

			HEXANE SOLUBLE H/C RATIOS			
			Feed Ratio (1:2)		Feed Ratio (1:4)	
COAL	RESID	TIME	CATCHPOT	BOMB	CATCHPOT	BOMB
Powellton	Coker	30 minutes	2.30	1.64	2.49	2.01
Powellton	Coker	2 hours	1.86	1.36	2.30	1.36
Powellton	Coker	4 hours	2.30	0.87	2.47	1.03
Powellton	Decant	30 minutes	1.30	1.05	1.23	0.90
Powellton	Decant	2 hours	1.40	0.70	1.45	0.82
Powellton	Decant	4 hours	*	0.90	1.59	0.76
Powellton	Decant/Coker	30 minutes	1.60	0.98	*	*
Powellton	Decant/Coker	2 hours	1.51	1.16	1.74	1.46
Powellton	Decant/Coker	4 hours	1.67	1.82	1.78	1.04

* Data missing

When the feedstock ratio was increased to 1:4 (coal:resid), a higher bomb H/C ratio occurred possibly as a result of the increased concentration of paraffinic and/or alkyl-substituted aromatic compounds.

Ultimate analysis was performed on the THF-insoluble products to give an indication of the quality of the coke produced. Figure 31 illustrates that as the reaction length was increased, the H/C ratio of the coke product decreased, indicating a more carbon-rich product. This trend was a result of cracking and polymerization reactions occurring in the co-coking experiments. The effect of feed ratio was negligible on the solid-H/C ratio.

7.5.3 Effect of Processing Conditions on Boiling-Point Distribution

The jet-fuel range for these analyses is defined as the boiling range 180 to 330 °C (JP-8 distillation range). Simulated distillation analysis was performed on the hexane-soluble (GC-amenable) fraction of our liquid products. The majority of the liquid product was obtained in the catchpot of our reactor system. In the sealed reactor system, the hexane solubles were extracted using Soxhlet extraction of the products retrieved from the bomb.

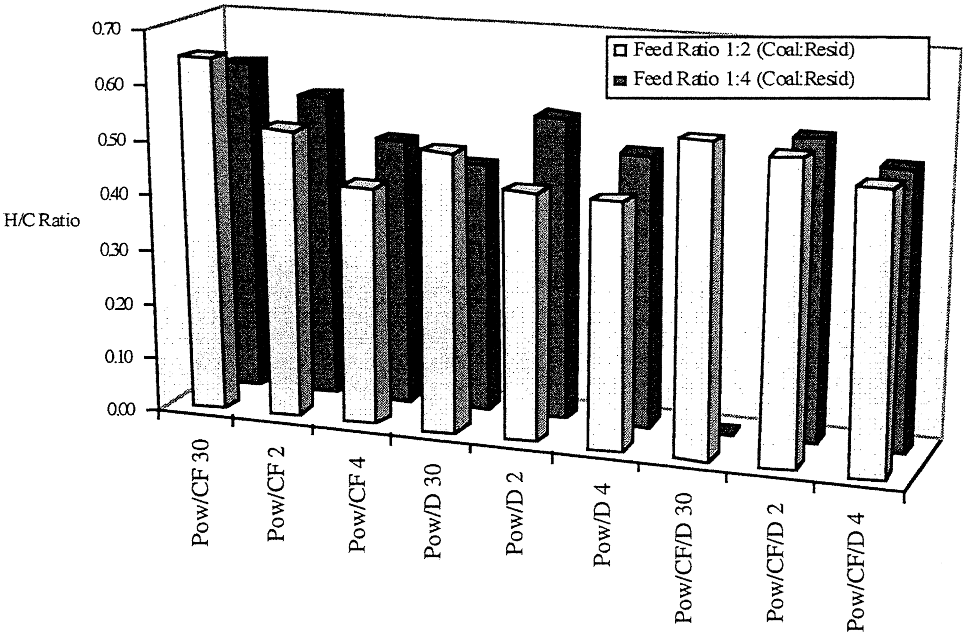

Pow/CF 30 mins Pow/CF 2 hours Pow/CF 4 hours	Pow/DO 30 mins Pow/DO 2 hours Pow/DO 4 hours	Pow/CF/DO 30 mins Pow/CF/DO 2 hours Pow/CF/DO 4 hours

Figure 31. Reaction Length and Feed-Ratio Effects on the Solid Coke Products Formed from Co-Coking Reactions at 465 °C with Powellton (Pow) Coal and the Two Petroleum Resids
(D = decant oil, Cf = coker feed)

Figure 32 shows the boiling-point distributions of the products from the heat treatment of coker feed and decant oil in both reactor systems. In both the sealed and vented reactors there is little change in the fraction eluted in the jet-fuel range for either the coker-feed or decant-oil experiments. However, the fractions boiling in the other distillation ranges change significantly between feedstocks and reactors.

The evolution of gaseous products leads to an increase in pressure in the sealed reactor during co-coking reactions. The buildup of pressure results in an increase in the decomposition of the liquids present into coke and gas, which in turn leads to higher pressures and further decomposition of the liquids [132]. Figure 32 also shows that the products from the vented system are concentrated in the high boiling-point range and, thus, they are not subjected to reaction conditions that increase decomposition.

It appears that in experiments using coker feed, significant quantities of liquids are produced, especially in the jet-fuel range; however, these liquids are of low quality. The liquid products from co-coking reactions with coker feed have a high aliphatic content, which may not be a good feedstock for the production of thermally stable jet fuel. Thermally stable jet fuel must contain hydroaromatic and cycloalkene compounds, which are derived from aromatic precursors. Such compounds are found in abundance in the products from co-coking experiments using decant oil.

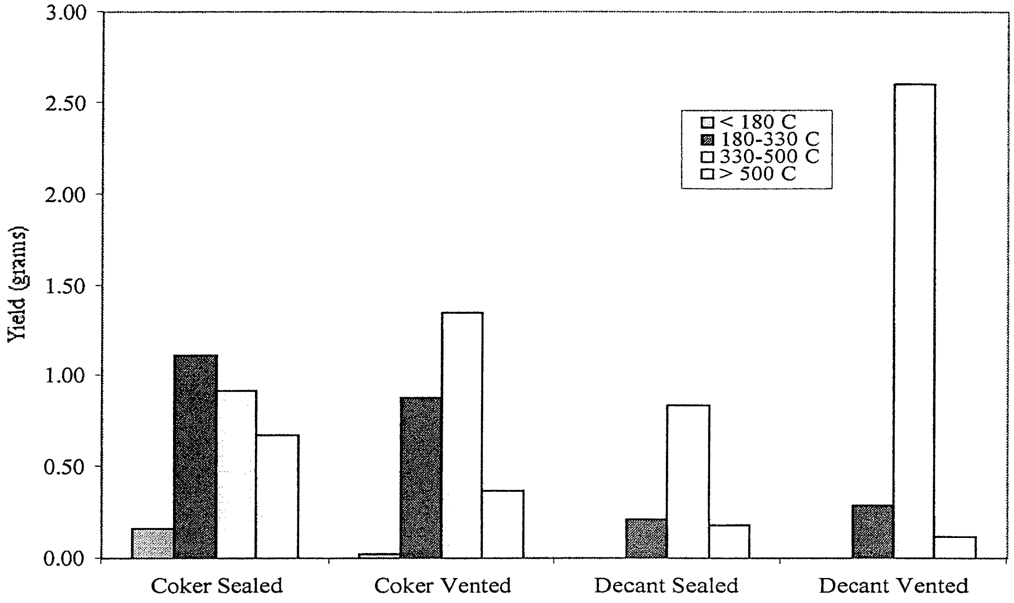

Figure 32. Boiling-Point Distributions of Heated Treated Resids at 465 °C

Figure 33 examines the effects of co-coking the resids both alone and with the addition of coal in the sealed reactor system at 465 °C. It is evident that the jet-fuel yield from the decant oil in the sealed reactor system was relatively unaffected by the addition of coal. However, with the decant oil, we note an increase in the amount of product in the 330 to 500 °C distillation range in the co-coking reactions performed at 465 °C. We believe this is due to the inclusion of high-molecular weight, coal-derived compounds. Conversely, Figure 33 also shows that the fraction boiling within the jet-fuel range from reactions with coker feed in the sealed reactor system at 465 °C was reduced by over 75 percent when the coal was added. Similar results were also observed in the other boiling fractions. This phenomenon may be due to a coal-induced mechanism that increases gas and coke formation from the coker feed relative to liquid products.

Figure 34 shows the various effects of co-coking resids and coal in the vented reactor system. When coal was added to the coker feed in the vented reactor system at 465 °C, there was a dramatic increase (five times the yield of the sealed reactor system – see Figure 33) in the amount of sample boiling in the jet-fuel range. The increase of product in this range can be attributed to the decrease in the decomposition of the liquids to gaseous and coke products. The results show that with the addition of coal to the decant oil at 465 °C, there is little change in the jet-fuel range yield. However, there are slight increases in the higher-boiling fractions. We believe again, this is due to the increase in coal-derived material.

Figure 35 shows the effect of different temperatures on the boiling-point distributions for co-coking reactions in both reactor systems. In the vented reactor one of the major trends observed for the co-coking reactions using decant oil and Powellton coal was, that with an increase in reaction temperature, there was little change in the boiling-point distributions. We attribute this to flash distillation of the liquid products in the vented reactor system.

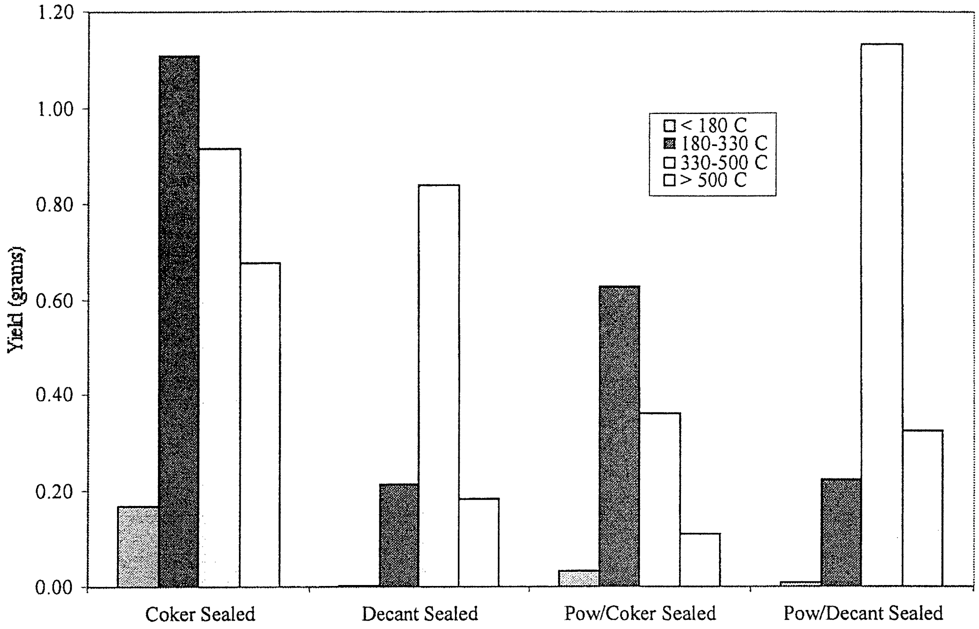

Figure 33. Boiling-Point Distributions of Co-Coking Reactions in Sealed Reactor at 465 °C Pow= Powellton Coal

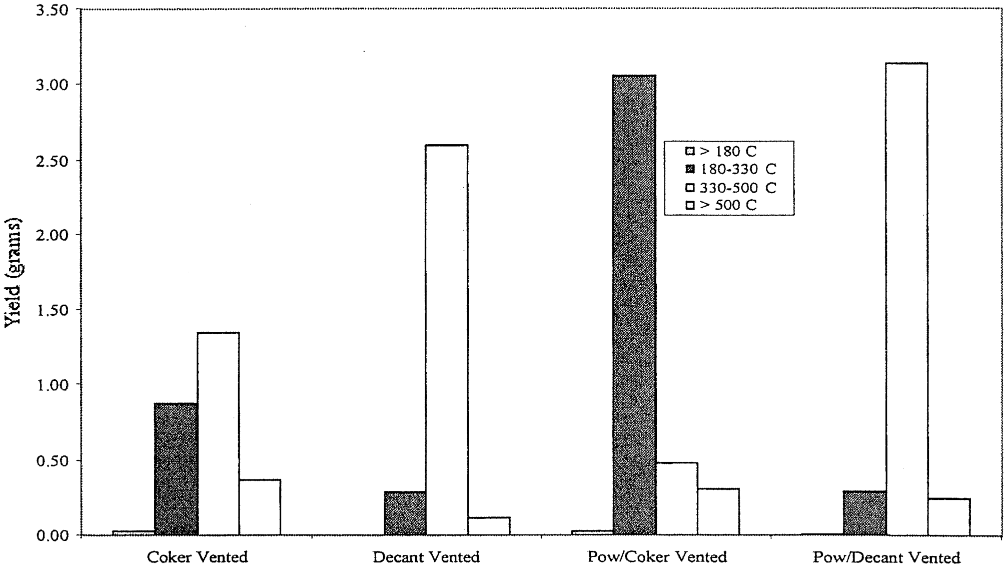

Figure 34. Boiling-Point Distributions of Co-Coking Reactions in Vented Reactor at 465 °C. Pow= Powellton Coal

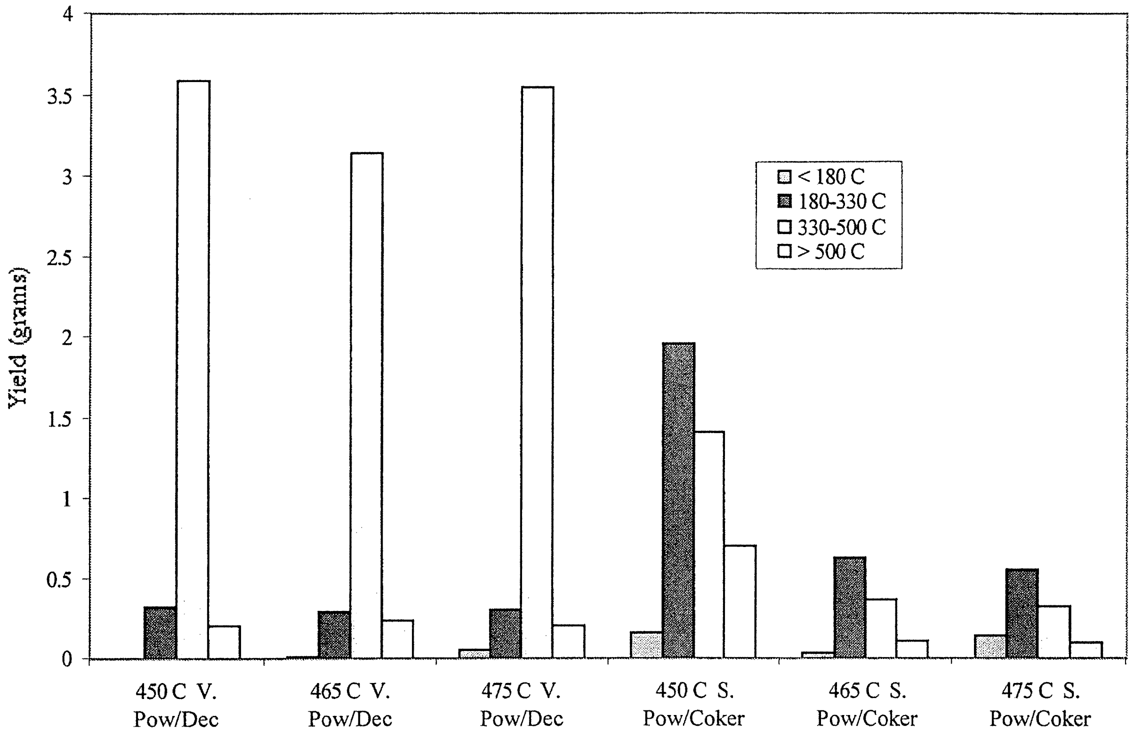

Figure 35. Boiling-Point Distributions from Co-Coking Reactions at Different Temperatures V= Vented Reactor System; S= Sealed Reactor System; Pow= Powellton Coal; Dec= Decant Oil; Coker= Coker Feed

Decant oil is an atmospheric resid from the fluidized catalytic cracking process. It has an initial boiling point of around 350 °C. Therefore, when the reactor is placed in a heated sandbath at 465 °C, flash distillation of a significant quantity of the sample occurs.

Temperature effects for co-coking reactions with coker feed and coal in the sealed reactor system were observed. As the temperature was increased, the yield of liquids in all fractions decreased. This was due to the increase in cracking reactions that occur as the reactants are subjected to higher temperatures and pressures.

7.5.4 Qualitative Analysis of Liquid Products

Figures 36 and 37 show GC traces comparing vented and sealed reactor systems. The GC analyses shows that in the vented system we are producing an overabundance of aliphatic coker feed–derived compounds. The aromatic coal-derived material is still there, but it has essentially been diluted. This suggests a need to assess the use of decant oil – a predominantly aromatic feedstock – for use in co-coking studies.

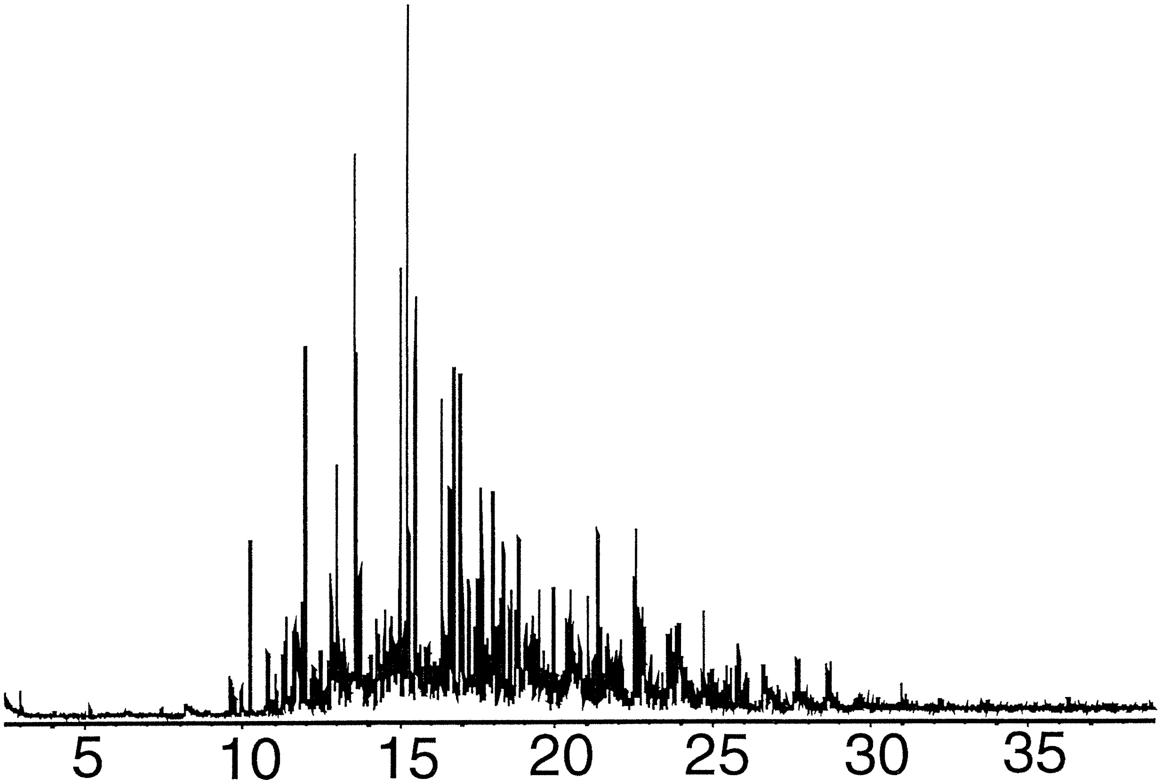

Figure 36. Chromatogram of Hexane-Soluble Fraction from a Co-Coking Run at 465 °C in a Sealed Reactor

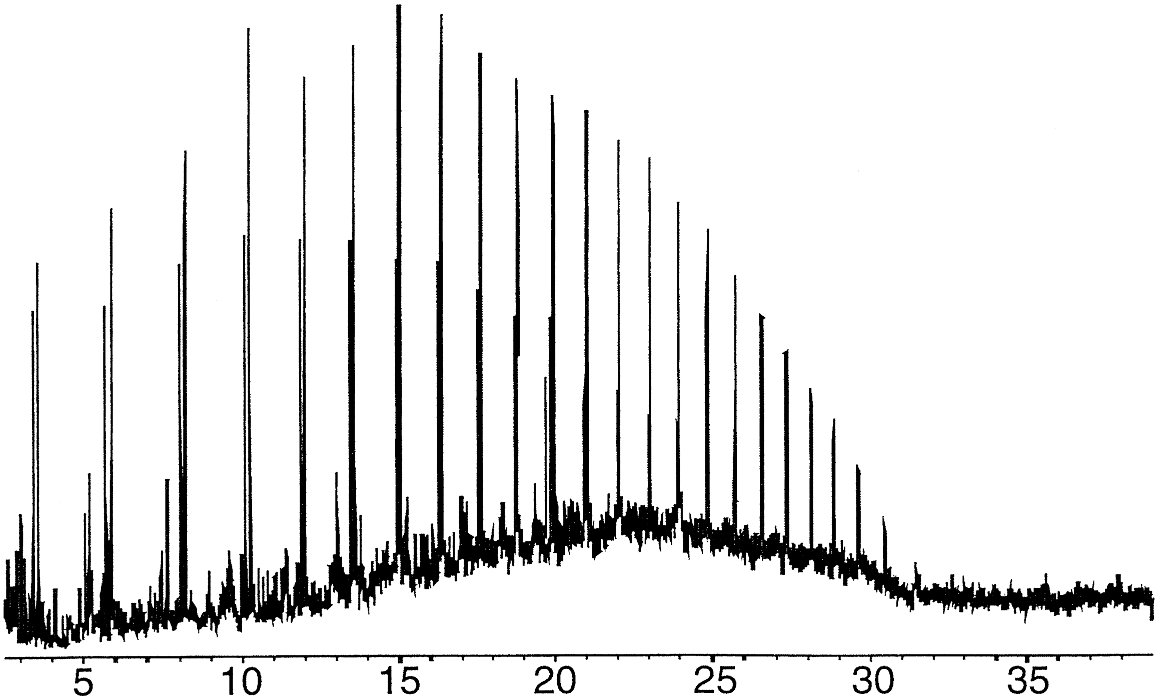

Figure 37. Chromatogram of Hexane-Soluble Fraction from a Co-Coking Run at 465 °C in a Vented Reactor

Semi-quantitative analysis was performed using GC-MS techniques. This method allowed us to identify positively all of the major components in the chromatograms and express them as a percentage of the total area for the whole chromatogram. Table 16 shows the percentage of identified compounds that fall into various compound classes, from the analysis of liquid products from co-coking with coker feed in a sealed reactor.

Table 16. Compound Distribution of Co-Coking Products

REACTION	Benzenes	Phenols	Alkanes	Naphthenes	Fluorenes	Anthracenes/ Phenanthrenes	Pyrenes	Total **
Powellton 450	8.68	5.52	11.92	0.81	4.88	-	-	31.81
Eagle 450	-	6.79	6.92	12.10	-	3.90	-	29.71
Coker 465	-	-	38.32	2.04	-	-	-	40.36
Co-Eagle 465	1.44	1.19	9.85	22.61	1.45	5.68	0.58	42.81
Co-Pitts 465	-	-	12.20	11.19	-	2.07	27.41	52.87
Co-Pow 450	-	-	35.25	-	-	-	-	35.25
Co-Pow 465	0.89	-	3.32	18.57	0.75	6.89	1.26	31.67
Co-Pow 475	4.09	-	-	23.76	1.36	9.93	1.66	40.80
Co-Pow 500	-	-	-	22.93	1.70	13.70	4.31	42.63

** This column indicates the total percent of identified major peaks; the remaining percent are the unidentified minor peaks. The values above are absolute values and not those from just the identified peaks. Reactions preceded by a Co- indicates co-coking experiments.

As the temperature of the reaction increased, the presence of aromatic compounds increased. This would indicate that the coal conversion and the inclusion of coal-derived material in the products increased. Conversely the coker feed consisted of mainly saturated alkanes, which contributed to the high content of alkanes in the co-coking reactions at lower temperatures. It is also worth noting that different coals produced different coal-derived compounds at similar reaction temperatures. For example, co-coking experiments performed at 465 °C with Eagle produced high quantities of naphthenes; Pittsburgh produced high quantities of pyrenes; and Powellton had compounds that averaged out across the range of those identified. In addition, we can see that in the products identified from co-coking, with the exception of Eagle at 465 °C, no phenols were identified. This suggests that their numbers have been sufficiently reduced under the reaction conditions, possibly due to their inclusion in the propagation reactions that lead to coke formation, and thus, to their removal from liquid products.

Table 17 shows the compound distribution for the total percent yielded in the hexane-soluble fractions of these co-coking reactions based on the total oil yield. The values give some indication of the levels of the individual compounds within the oil samples. These values are ratios of those in Table 16 but corrected for the oil yield produced during the reactions.

Tables 18 and 19 show the percentage yields of methyl-substituted compounds that were identified in the oil fraction from co-coking experiments. The C1, C2, C3, etc., correspond to mono-, di-, and tri-substituted compounds, respectively. It is clear that heat-treated coker feed does not contribute any significant quantities of substituted aromatic compounds to the oil fraction. Therefore, all the aromatics identified come from coal-derived material.

Table 17. Compound-Distribution Yield in the Hexane-Soluble Fraction

FEED	Oil Yield	Benzenes	Phenols	Alkanes	Napthenes	Fluorenes	Anthracenes/ Phenanthrenes	Pyrenes
Eagle 450	4.4	-	0.30	0.31	0.53	-	0.17	-
Pow 450	2.3	0.20	0.13	0.27	0.02	0.11	-	-
Coker 465	47.7	-	-	18.28	0.97	-	-	-
Co-Eagle 465	13.2	0.19	0.16	1.30	2.99	0.19	0.75	0.08
Co-Pitts 465	16.9	-	-	2.06	1.89	-	0.35	4.63
Co-Pow 450	32.2	-	-	11.34	-	-	-	-
Co-Pow 465	14.1	0.13	-	0.47	2.62	0.11	0.97	0.18
Co-Pow 475	7.7	0.32	-	-	1.84	0.11	0.77	0.13
Co-Pow 500	6.7	-	-	-	1.52	0.11	0.91	0.29

Table 18. Substituted-Compound Distribution and Yield for the Hexane-Soluble Fraction

REACTION	OIL YIELD	Benzene			Phenols			Naphthenes		
		C1	C3	C4	C1	C2	C3	C1	C2	C3
Pow 450	2.30	-	-	-	0.07	0.09	0.04	0.08	0.14	0.06
Eagle 450	4.41	-	-	-	-	0.21	0.09	0.21	0.25	-
Coker 465	47.71	-	-	-	-	-	-	0.97	-	-
Co-Eagle 465	13.22	-	-	0.15	0.05	0.11	-	0.76	1.21	0.88
Co-Pitts 465	16.90	-	-	-	-	-	-	0.56	0.98	0.35
Co-Pow 450	32.18	-	-	-	-	-	-	-	-	-
Co-Pow 465	14.11	0.11	-	-	-	-	-	0.78	1.17	0.48
Co-Pow 475	7.74	-	0.04	0.27	-	-	-	0.61	0.74	0.29
Co-Pow 500	6.65	-	-	-	-	-	-	0.59	0.60	0.15

Once again, it is apparent that different coals produce compounds with differing levels of substitution, thus indicating differences in the molecular composition of the coals, even though they are of the same rank classification. The effect of an increase in temperature is exemplified in the series of tests performed on Powellton coal between 450 and 500 °C. The general trend shown is that with an increase in temperature, there is a decrease in the amount of substitution. This is due to the increased cleavage of the methyl groups from the ring at elevated temperatures, with formation of gaseous products.

7.5.5 The Effect of Blending Coker Feed and Decant Oil

We reported earlier that the vacuum resid used in our experiments produced liquid products in the desired middle-distillate range, but they were mainly aliphatic in nature. Being aliphatic, they would not be able to produce significant quantities of hydroaromatics and cycloalkanes

Table 19. Substituted-Compound Distribution and Yield for the Hexane-Soluble Fraction

REACTION	OIL YIELD	Fluorene	Anthracene/ Phenanthrene		Pyrene
		C1	C1	C2	C1
Pow 450	2.30	0.02	0.09	-	-
Eagle 450	4.41	-	0.11	-	-
Coker 465	47.71	-	-	-	-
Co-Eagle 465	13.22	0.19	0.53	0.09	0.04
Co-Pitts 465	16.90	-	0.20	-	-
Co-Pow 450	32.18	-	-	-	-
Co-Pow 465	14.11	0.11	0.49	0.30	-
Co-Pow 475	7.74	0.11	0.45	0.15	0.05
Co-Pow 500	6.65	0.05	0.50	0.12	0.08

when hydrogenated. Hydroaromatics and cycloalkanes are required for increased thermal stability in advanced jet fuels. Conversely, the decant-oil feedstock we have been using produces aromatic-ring compounds that can be upgraded to hydroaromatics and cycloalkanes. However, the liquid products from the decant-oil co-coking do not undergo cracking reactions as does the vacuum resid. This in turn leads to a product with a high boiling–point distribution, which would need to undergo severe hydrotreating in order to produce hydroaromatics and cycloalkanes in the jet-fuel boiling range.

In order to try and produce a mainly aromatic liquid product in the correct boiling range, we decided to blend the vacuum resid (coker feed) and decant oil, and study the effect that this may have on the products from co-coking in a vented reactor system.

The solid products were analyzed by elemental analysis; it was found that the blends of decant oil, coal, and vacuum resid lowered the H/C ratio significantly. Table 20 shows the solid H/C ratios obtained from the various co-coking reactions in the vented reactor system.

This occurred as a result of the timing of the gas evolution during the co-coking reactions. The lower H/C ratio indicates that the gas was released quite some time before solidification of the final coke product occurred. When gas evolves during solidification, it gets trapped in the coke product, producing a porous and fragile coke. This gas evolution is a function of the initial feedstock. Vacuum resid has a higher paraffinic content with longer side chains, which creates a delayed gas evolution that occurs during solidification. On the other hand, decant oil has a more aromatic nature, which produces smaller amounts of gases prior to solidification. By creating a mixture of the two resids, a more optimal situation is created. This phenomenon has also been noted by other researchers working on the coking of blends of different oil feedstocks in the absence of coal [133, 134].

Table 20. Solid H/C Ratios for Co-coking Reactions at 465 °C in the Vented Reactor System

Coal	Resid	Ratio	CORRECTED C%	H%	N%	H/C
POW	DEC/CF	4 g/4g/4g	97.9	2.1	0.6	0.26
POW	CF	3 g/ 6 g	91.5	3.7	1.4	0.49
POW	DEC	3 g/ 6 g	93.3	3.4	1.2	0.44
NONE	CF	3 g/ 6 g	92.2	4.2	1.3	0.54
NONE	DEC	6 g	88.7	3.5	0.1	0.47
POW	NONE	3 g	89.1	3.2	1.8	0.43

POW= Powellton Coal
CF= Coker Feed
DEC=Decant Oil

The H/C ratios of the liquid products are shown in Table 21. The values for the blend experiment indicate an average of the results for co-coking experiments using coker feed and decant oil with the coal. This suggests that there is no significant detrimental effect on the products produced by blending the resids. This is also true for the yield of liquid and solid products (see Table 22).

Table 21. Liquid H/C Ratios for Co-Coking Reactions at 465 °C in the Vented Reactor System

		LIQUID H/C RATIO	
FEED	RATIO	CATCHPOT	BOMB
POW/CF/DEC	4g/4g/4g	1.51	1.16
CF/POW	6g/3g	1.63	2.01
DEC/POW	6 g/3g	1.00	0.70
DEC	6g	1.30	0.90
CF	6g	1.79	1.14
POW	3 g	*	1.45

Table 22. Product Distribution for Co-Coking Reactions at 465 °C in the Vented Reactor System

COAL	RESID	RATIO	TOTAL % LIQUID	TOTAL % SOLIDS
POW	DEC/CF	4g/4g/4g	44.64	39.86
POW	CF	3g/6g	38.84	40.74
POW	DEC	3g/6g	55.47	37.67
NONE	CF	6 g	64.26	13.62
NONE	DEC	6g	76.28	12.30
POW	NONE	3g	6.29	77.04

Figure38 shows the boiling-point distributions of the hexane-soluble products taken from the catchpot after the coking experiments.

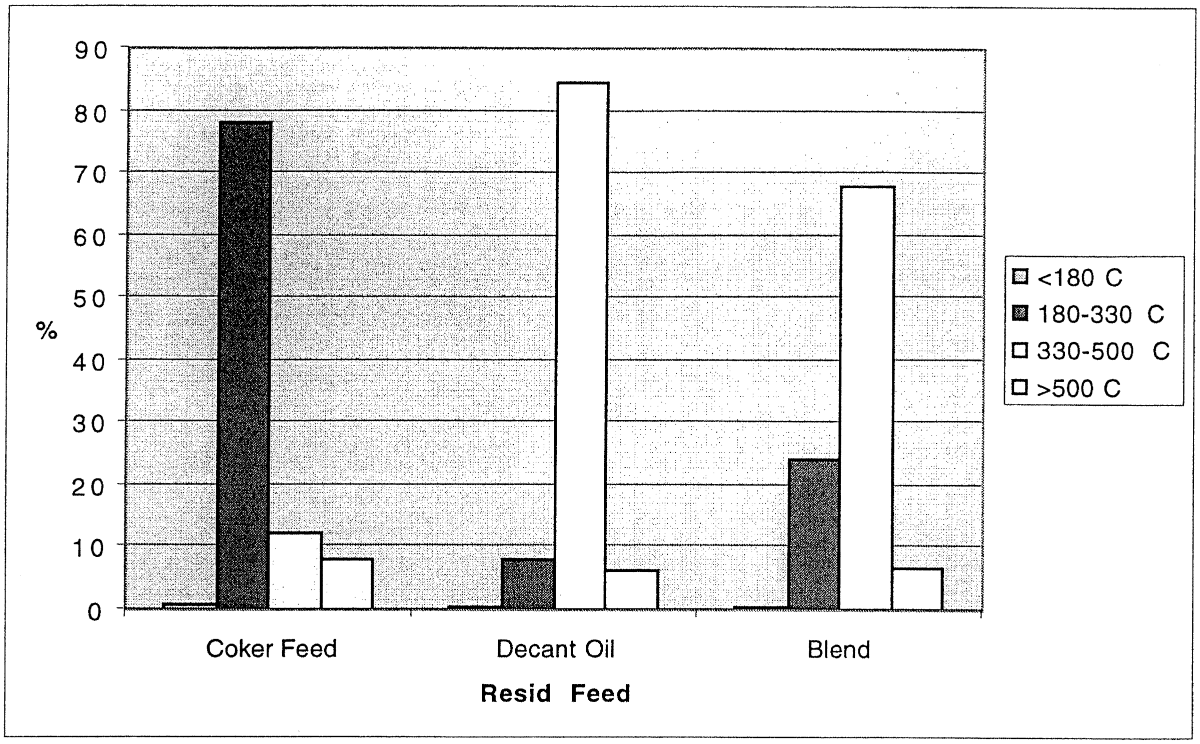

Figure 38. Boiling-Point Distributions of Hexane-Soluble Fractions form Co-Coking Experiments Using Different Resid Feeds

7.5.6 Optical Microscopy of Coke Products

Residues from co-coking experiments using coker feed and decant oil with the Eagle- and Powellton-seam coals at 465 °C were characterized to evaluate the influence of the closed and vented reactor systems. Two parts of coker feed or decant oil to one part coal used in each run generated a variable amount of coke residue. Carbon materials produced from the coker feed have a distinctive texture compared with those derived from high-volatile bituminous coals. In general, the vitrinite portion of the coals employed in this study develops a fine anisotropic texture having isochromatic units from 0.5 to 2.0 μm. Trapped within this matrix are particles of recognizable and carbonized inertinite macerals and mineral matter. The carbon textures generated by decant oil are similar in many respects to those of the coker-feed material, except that the textures tend to be larger and more elongated. Easy recognition of the carbon forms derived from coal and petroleum-residua material permits quantification by point-count analysis.

Solvent-extracted and insoluble residues from co-coking experiments were embedded in a cold-setting epoxy resin and, after hardening, were polished for reflected-light microscopy. The carbon material was evaluated in white light using air and oil-immersion objectives at a total magnification of 500 X in polarized or cross-polarized light. Point-count analysis was performed at 625-X magnification in oil immersion by traversing the sample based upon a 0.4 by 0.4-mm grid and identifying the textural element under a crosshair held in the microscope eyepiece. A total of 1000 counts was accumulated, 500 from each of two polished mounts.

Eight different textural elements were identified in the co-coking residues:

Isotropic – a relatively low-reflecting, dark-gray carbon material derived from coker feed or decant oil, displaying little or no optical activity under polarized light.

Mosaic – a higher-reflecting carbon textural element identified from coker-feed or decant- oil materials, displaying optical anisotropy and characterized by isochromatic units of less than 10 µm.

Small Domain – an anisotropic carbon form identified from coker-feed or decant-oil materials, exhibiting isochromatic units of between 10 and 60 µm.

Domain – an anisotropic carbon form identified from coker-feed or decant-oil materials, having much larger isochromatic units of greater than 60 µm.

Flow Domain – an anisotropic texture exhibiting elongated isochromatic areas of greater than 60 µm in length and less than or equal to 10 µm in width and identified from coker-feed or decant-oil materials.

Vitrinite-Derived Mosaic – the characteristic 0.5-2.0 µm diameter isochromatic units typically generated during the carbonization of vitrinite of high-volatile bituminous coals.

Inertinite-Derived Texture – angular- and irregular-shaped particles trapped in the vitrinite or petroleum-residua matrix, which may or may not display remnant cell structures; particles are typically isotropic.

Mineral Matter – remnant particles of coal-derived mineral matter that usually include clays, pyrite, quartz, and carbonate minerals.

The distribution of carbon textures recognized from the coker feed changes very little with respect to the system being sealed or vented. Between 60 and 70 percent of the residues (by volume) are derived from coal, Eagle or Powellton seam. However, when decant oil was employed in the vented system (only) an apparent decrease in the amount of carbon derived from coal was observed, i.e., 35-40 vol percent. This observation may have more to do with the influence of decant oil on the coals than it does with the venting of the system. Figure 39A shows a photomicrograph of the characteristic micron-sized optical texture derived from the vitrinite of Powellton coal (with included angular inertinite particles and mineral matter). Figure 39B shows an interface between carbonized vitrinite of this same coal with carbon material (small domain texture) derived from the coker feed. The apparent inactivity and immiscibility of the two components is fairly characteristic of the whole sample. Figure 39C exhibits the optical texture of vitrinite from the Powellton coal after being co-coked in the presence of decant oil. The optical texture has increased from that shown in Figure 39A, from 0.5-2.0 µm to 5-8 µm in Figure 39C. Furthermore, the interface between decant oil–derived carbon and the coal material shown in the upper part of Figure 39D is now indistinct, showing clearly a greater interaction between the two materials as a result of co-coking. Because of this co-mingling, it is now more difficult to distinguish between coal-derived and petroleum-derived carbon textures.

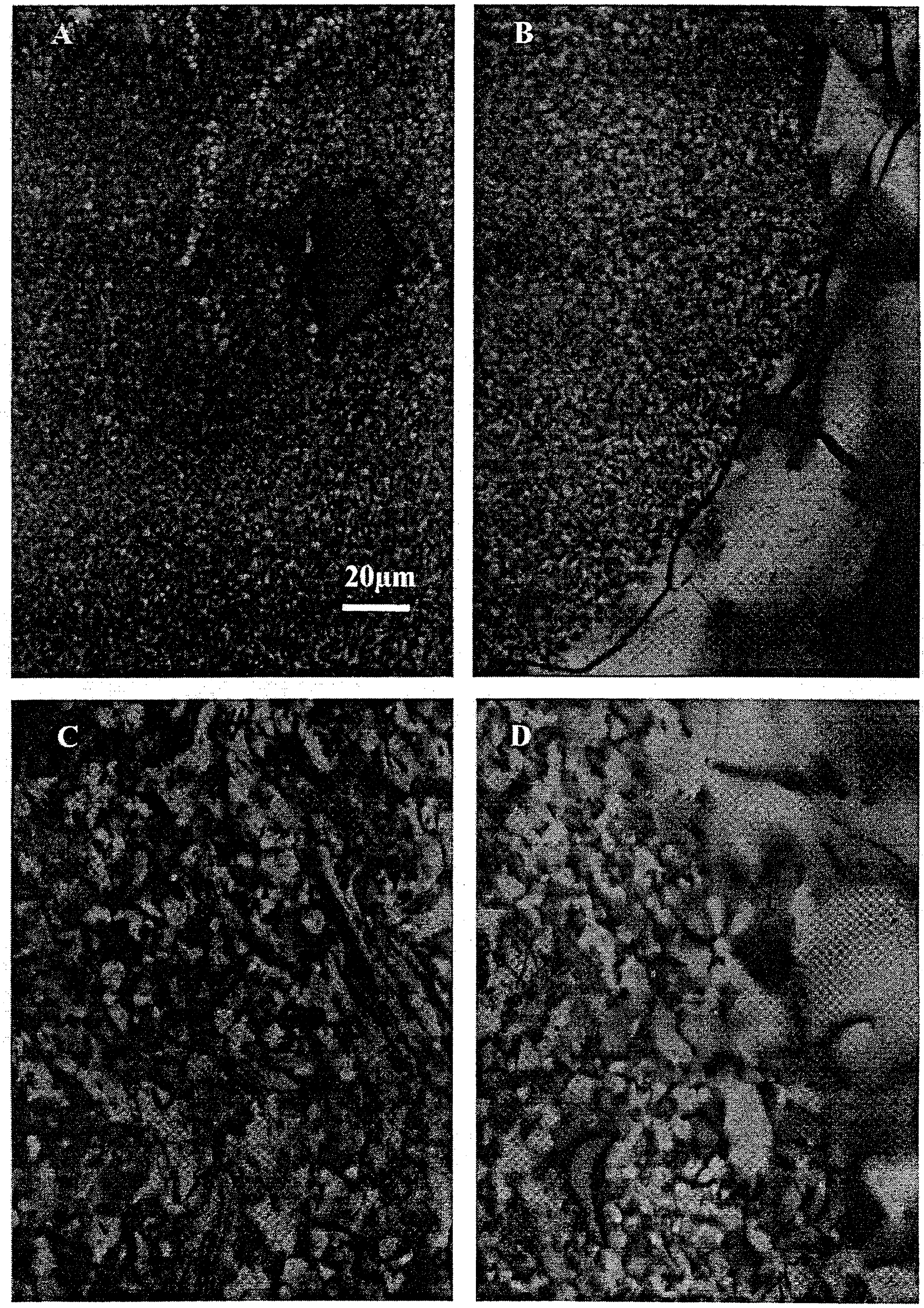

Figure 39. Photomicrographs of Solid Residues from Various Coking Experiments

Carbon textures generated from coking of decant oil are generally larger than those derived from coker feed. Although the small-domain (10-60 μm) textures are dominant, the isochromatic units tend to be larger in this range, and the number of flow-domain and domain (>60 μm) textures is about twice that for coker feed. Also, there is evidence that decant oil has a greater fluid temperature range that completely involves that of the coal material. The apparent interaction of the carbon materials produced from decant oil suggests that volatile materials generated from the decant oil represent an effective solvent for fluid coal.

The concentration of petroleum- and coal-derived components for the residues evaluated are shown in Figure 40

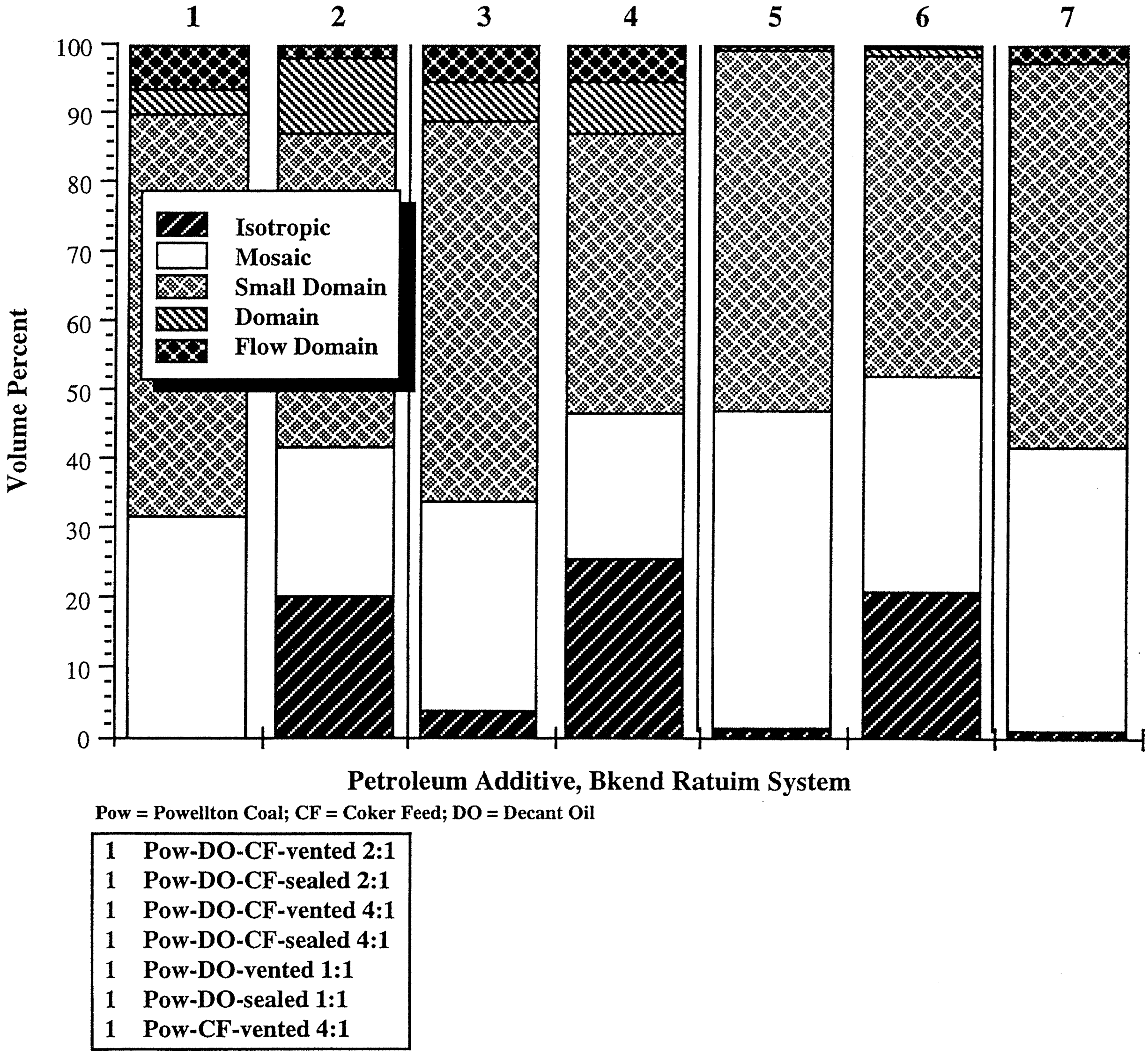

Figure 40. Distribution of Petroleum-Derived Carbon Textures in Residues from Petroleum-Fraction/Coal Blends Following Carbonization at 465 °C

When the Powellton coal was co-coked with decant oil at a 2:1 ratio in a vented reactor system, nearly all of the thermoplastic components of coal showed significant enhancement of the size of the isochromatic anisotropic textures. Although the carbon forms obtained from the individual blend components are distinctive, interfaces between the materials are quite indistinct as coal textures were increased 2 to 4 times. When the proportions of coal were increased to equal that of the decant oil (1:1) in the vented system, there was ample opportunity to observe co-mingling of the two components of the blend on a micron scale. Many remnant coal particles can be observed with an open porosity containing mesophase-derived spheres from the decant oil. However, the open structure suggests that there are insufficient amounts of decant oil to complete the interaction.

When a higher concentration of coal (1:1) is co-carbonized with decant oil in the sealed system, much less influence is observed on the coal-derived textures, as they remain small 2-5 µm. This may have less to do with the blend ratio than it does with the conditions of carbonization that develop in the sealed reactor. As shown in Figure 41, when decant oil is co-coked with coal in a sealed system, it results in a fairly large volume of isotropic carbon, which implies that under the sealed conditions there is incomplete development of a mesophase from the decant oil.

Regarding the influence of coker feed on the Powellton coal, there appears to be little interaction between the two components, whether the system is vented or sealed. Previous investigations using a 2:1 coker feed–to-coal ratio demonstrated that the carbon textures derived from the coker feed form distinct contacts with those of the coal, with only minor near-surface interactions. When the ratio of coker feed was increased to 4:1 in the vented system, there was little influence on the coal textures. In general, a higher concentration of coker feed resulted in a greater amount of larger carbon textures in the residue as shown in Figure 41.

The co-coking of equal amounts of decant oil and coker feed with the Powellton coal under different concentrations (2:1 and 4:1) in the vented and sealed systems exhibited variable results. As discussed previously, decant oil permits a high concentration of larger-size anisotropic textures to be formed. However, in the sealed system there is an incomplete development of the mesophase as is evident from the relatively high concentration of isotropic carbon shown in Figure 41. Isotropic carbon is present despite the initial concentration of petroleum-derived components. Furthermore, the influence of decant oil on the enhancement of coal carbon textures is diminished and quite variable among different particles, i.e., while some are fully enhanced, others are not influenced, and the majority lies between the two extremes. This variability may result from the initial contact of coker-feed materials with coal particles that serves to act as a barrier to further contact with the decant oil. In those areas where there is partial or complete contact with the decant oil, some enhancement of the coal-derived textures is achieved. With this in mind, future experimentation should include preparing a slurry of coal and decant oil, with perhaps some preheating before blending with the coker feed, as a means of ensuring the interaction and maximum benefit to carbon texture distribution.

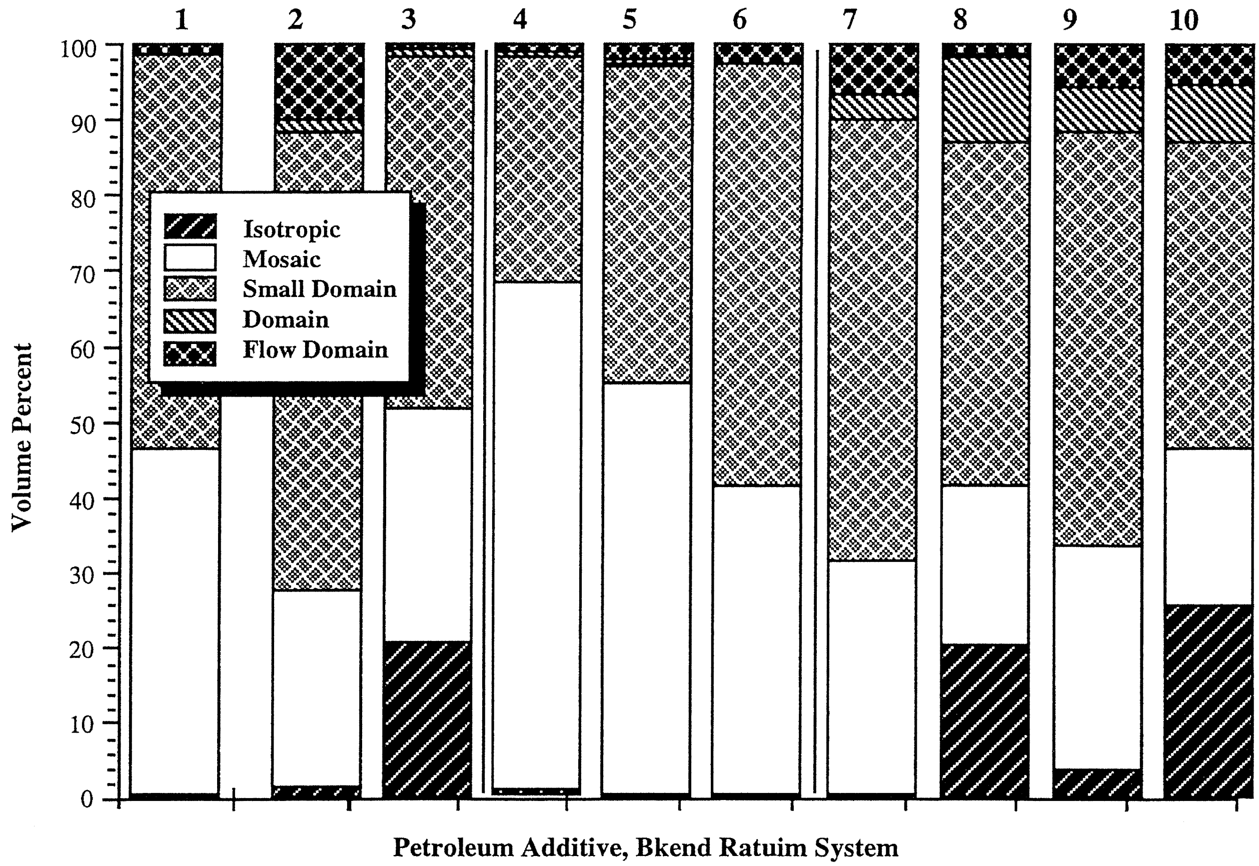

Pow = Powellton Coal; CF = Coker Feed; DO = Decant Oil

1	Pow-DO-CF-vented 2:1
1	Pow-DO-CF-sealed 2:1
1	Pow-DO-CF-vented 4:1
1	Pow-DO-CF-sealed 4:1
1	Pow-DO-vented 1:1
1	Pow-DO-sealed 1:1
1	Pow-CF-vented 4:1

Figure 41. Distribution of Petroleum-Derived Carbon Textures in Residues from Petroleum-Fraction/Powellton Coal Blends after Carbonization at 465 °C

7.6 Conclusions

As a conceptual process, the work conducted in this study has shown that co-coking can be applied as a method for producing coal-based liquid feedstocks, which may be used in the production of a coal-based thermally stable jet fuel.

The introduction of a vented reactor system, which mimicked the conditions in a full-scale delayed coker, enabled us to enhance product yield and quality. The use of decant oil created better physical and chemical interactions with the coal. This lead to an increase in the amount of coal-derived material in the liquid products and a more homogeneous coke, which may ultimately be refined into a premium carbon product.

7.7 Future Work

Work is continuing in the study of co-coking. The optimization of process parameters to obtain a superior product with high yields is our main goal. To this end, we are in the process of designing a small pilot-scale delayed coker, which will allow us to perform experiments on a larger scale, more closely resembling those of a conventional delayed-coker unit used in industry.

We also intend to focus on the quality of the solid product, whose improvement would allow us to produce a commodity with a competitive market value. This would ultimately offset the cost of producing the jet fuel. We will assess coke as a fuel and its ability to be upgraded to a premium carbon product. To this end, the use of quality, cleaned coals produced by PrepTech will become imperative. This will ensure the minimization of impurities (ash) in the coke.

8.0 COAL-BASED FUEL FORMULATION AND ENGINEERING

8.1 Introduction

Preparation of coal feedstocks for the co-coking process has continued to be scrutinized with emphasis on:

138. Coal selection to cover a range in coal rank

139. Production of laboratory quantities of coal covering a range in ash content

Efforts to produce larger quantities of low-ash coal were postponed so that a better evaluation, of the products including a maceral analysis, could be obtained prior to larger-scale investigations. In addition, the pilot-scale delayed coker will be available during Phase III of the project. It is best to produce the larger quantities of low-ash coal just prior to testing in the delayed coker to maintain their characteristics, especially moisture content, and to prevent oxidation.

The work conducted during this second phase included:

- A review of current low-ash coal production as it compares with production statistics given in Phase I [139]
- The evaluation of additional coals for their cleaning potential
- The development of capital, operating, and maintenance cost estimates for two specific cases for producing low-ash coal at the coal cleaning-plant sites where two of the study samples were obtained

This report documents this information.

8.2 Sources of Ultralow-Ash Coal

As in Phase I of the project, Federal Energy Regulatory Commission data (from the Energy Information Administration at www.eia.gov) on coal delivered to utility power plants was searched to determine the quantity and quality of coal used in the United States. While this does not represent all coal use, electric power generation does constitute the major use of coal in the United States.

As shown in Table 23, coal containing less than 4-percent ash was produced in 1996 in three states: Virginia, Illinois, and Kentucky. This differed in 1998, with a significant quantity of this very low-ash coal coming from off-shore sources. Significantly more coal (approximately 3-million tons) was produced in the range of 4-5 percent ash. If the specification is relaxed to 6-percent ash, then close to 10-million additional tons are produced that meet the low-ash criterion. This gives a good indication of the potential sources and quantities of relatively low-ash coal already produced in the United States.

Table 23. Summary of Low-Ash Bituminous-Coal Production in the United States in 1996 and 1998 as Shipped to Power Stations (Energy Information Agency)

1996		**1998**	
States	**Total Tons**	**States**	**Total Tons**
Coal Less Than 4% Ash			
VA, IL, KY	33,360	CO, KY, PA, VA	23,769*
Coal Between 4 and 5% Ash			
IL, KY, MT, OH, VA, WY	2,965,995	CO, IL, IN, KY, VA, WY	3,217,759**
Coal Between 5 and 6% Ash			
CO, IL, IN, KS, KY, NM, OH, OK, PA, VA, WV, WY	11,315,651	AL, CO, IL, IN, KY, PA, VA, WV, WY	9,117,017***

* An additional 683,369 tons of coal (less than 4 percent ash) was delivered to utility power plants from foreign sources.

**An additional 361,772 tons of 4 - 5 percent ash coal was delivered to utility power plants from foreign sources.

***An additional 1,120,605 tons of 5 - 6 percent ash coal was delivered to utility power plants from foreign sources.

8.3 Flowsheet Selection for Production of Ultralow-Ash Coal

To select a coal cleaning-plant flowsheet for producing the low-ash feedstock for co-coking, it was first necessary to understand the following requirements for the feedstock: particle size, rank, and desired ash content, for example.

8.3.1 Requirements for Co-Coking Feedstock

Based on laboratory work at Penn State University, it was determined that finer sizes of coal are better for use in this process. A higher content of the vitrinite maceral may also be desirable, and the rank of the coal is also likely to be important, with a higher high-volatile A bituminous coal being the most desirable based on present test results. And, of course, coal with the lowest possible ash content is also desirable.

It is desirable, then, to focus on obtaining the co-coking feedstock from the fine-coal stream at existing cleaning plants. This will limit or remove any requirement for grinding coal-that greatly increases costs. Moreover, it can help to alleviate a problem that many current coal-cleaning plants have: too much moisture in the fine coal that leads to problems in meeting their customers' moisture specifications and handling requirements.

8.3.2 Flowsheet

The flowsheet that will be used to evaluate the economics of producing feedstocks for the co-coking process is represented schematically in Figure 42. Clean coal from the froth-flotation circuit of an existing cleaning plant will be recleaned in column froth-flotation cells to obtain the lowest ash content possible. Froth flotation also has an advantage in that it tends to concentrate vitrinite macerals.

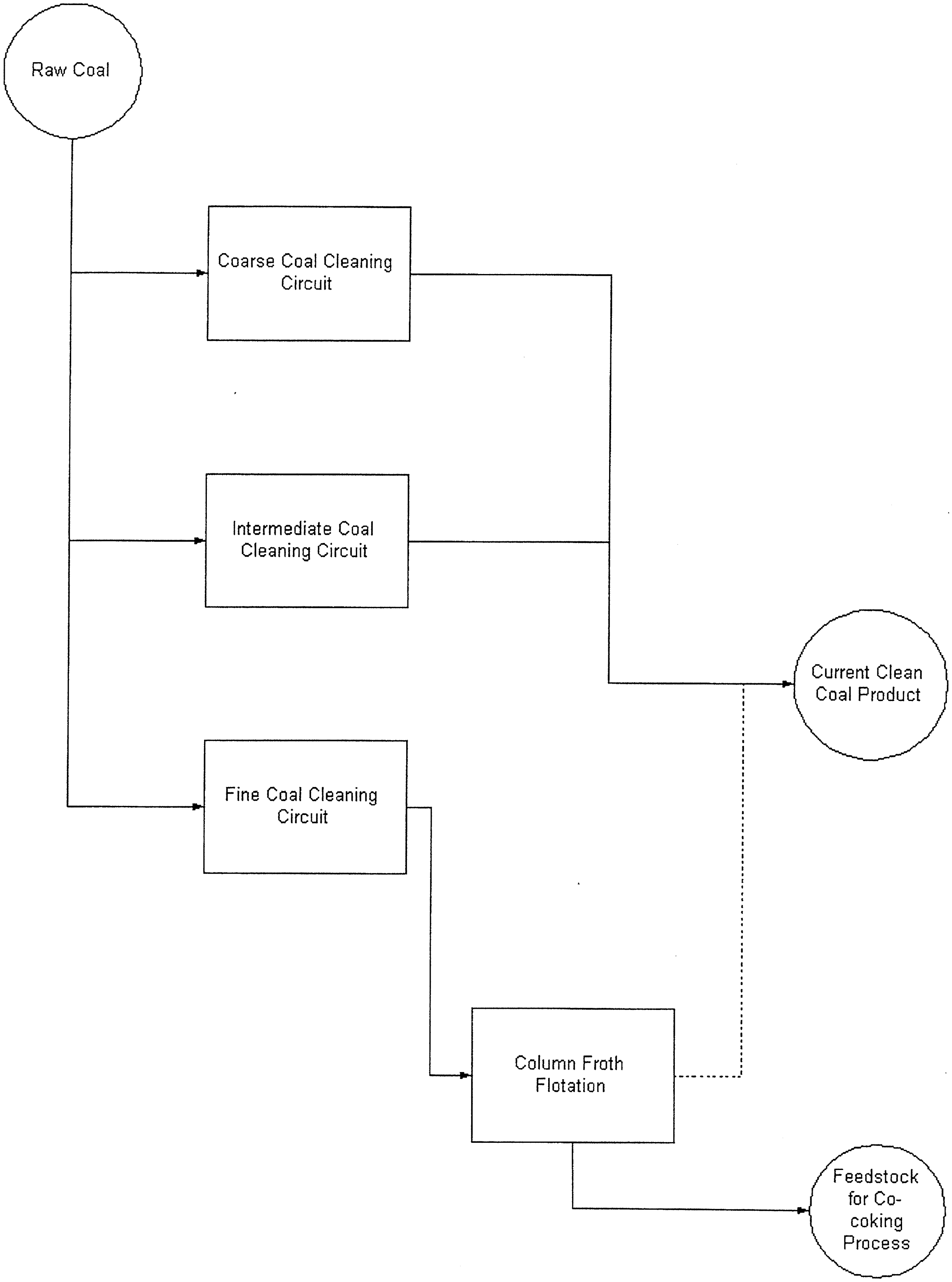
Raw Coal
Coarse Coal Cleaning Circuit
Intermediate Coal Cleaning Circuit
Current Clean Coal Product
Fine Coal Cleaning Circuit
Column Froth Flotation
Feedstock for Co-coking Process

Figure 42. Flowsheet Schematic for Low-Ash Coal Production

This low-ash, froth-flotation product will then be dewatered at the cleaning plant for shipment to the refinery. It will be dried at the refinery, taking advantage of the excess heat and steam available at that location. This flowsheet will be used to develop the economics in the case studies in this report.

8.4 Evaluation of Co-Coking Test Coals (Phase II)

With the selection of an appropriate flowsheet (as given above), additional coal sources were evaluated at laboratory-scale for their cleanability using froth-flotation testing. Froth-flotation testing was used more extensively in this phase since froth flotation is the major flowsheet unit operation. In addition, since the feed to the froth-flotation unit will be a froth-flotation concentrate from an existing cleaning plant, attempts were made to obtain such concentrates for further testing.

Samples obtained for testing included:

- Pittsburgh-seam froth-flotation concentrate from Greene County, PA (Two samples were obtained from two different coal-cleaning plants. These will be designated Pitt 1 and Pitt 2)
- Powellton-seam froth concentrate from central WV
- Lower Kittanning-seam minus 100-mesh material (designated LK 1) from Somerset County, PA (This is actually a low-volatile bituminous coal being used for coal-rank comparisons. No froth-flotation circuit was used at this cleaning plant. This sample would represent the feed to froth flotation)
- Lower Kittanning–seam froth-flotation concentrate (designated LK 2) from Armstrong County, PA (This is a high-volatile A bituminous coal)

The results from these froth-flotation tests are given in Table 24, showing the trade-off between yield and ash content. Table 24 shows the cumulative-yield versus cumulative-ash results from release analysis tests. Individual froth concentrate and tailings sample analyses are composited to give these cumulative values.

A release analysis test is conducted to determine the theoretical limit for froth flotation of a coal. This is analogous to a washability analysis for density separations. In a release analysis test, care is taken to clean and reclean the froth in subsequent steps to remove effectively all entrained fine minerals. In a final stage of flotation, starvation amounts of air (induced by low impeller speed) and reagents are used to cream off the cleanest coal fractions. This type of test is often used for column froth-flotation predictions. The test conditions and sample analyses are on file with PrepTech, Inc.

The results show that care must be taken in coal selection if a very low-ash content is critical for co-coking operation. Only the Pitt 1 sample was reduced to an ash content below 3 – 2.63 percent ash. This was at a relatively low yield of 39.35 percent. However, if an ash content of about 4 percent is acceptable for the co-coking process, then most of these coals could be reduced in ash to that level at a relatively good yield.

Table 24. Froth-Flotation Yield Versus Ash Results for Project Coal Samples

	Pitt 1		Pitt 2		Powellton		LK 1		LK 2	
	wt %	Ash %	wt %	Ash %	wt %	Ash %	wt %	Ash %	wt %	Ash %
Final Clean Coal	9.03	2.12	55.93	3.82	48.99	3.07	23.29	3.81	37.95	4.16
Intermediate Product 2	19.13	2.34	68.64	3.94	78.64	2.97	32.53	4.03	54.65	4.30
Intermediate Product 3	39.35	2.63	70.84	4.00	89.17	3.19	53.42	4.91	60.02	4.43
Intermediate Product 4	53.07	3.09	71.51	4.08	90.52	3.27	83.90	7.28	78.68	5.30
Intermediate Product 5	92.06	5.38	--	--	92.38	3.47	--	--	80.70	5.41
Reconstituted Feed Analysis	100.00	9.56	100.00	11.66	100.00	7.81	100.00	12.01	100.00	12.16

8.5 Case Studies: Cost of Production of Ultralow-Ash Coal for Co-Coking Feedstock

The economics of two specific cases for low-ash coal production were investigated. These cases used the results from the Powellton-seam coal and Pittsburgh-seam coal (Pitt 2) to produce low-ash coal. For both cases, it was assumed that a portion of the froth-flotation concentrate, about 50 tph, would be diverted to a new column froth-flotation plant that would be constructed on the coal cleaning-plant site. In this manner, the new plant would tie in to the existing cleaning plant for tailings disposal (which may actually be a saleable clean-coal product for the existing plant). It would share the water and electrical supply with the existing plant.

However, this plant will simply dewater the coal. It will provide a centrifuge cake at approximately 20 – 25 percent moisture for transport to the delayed-coking facility. Any drying of this material would be conducted at the delayed-coking facility to avoid transportation of potentially explosive dry coal powder. As such, dewatering and transportation costs are not included in the following case studies. All costs are given free on board cleaning-plant site. These costs include the coal-feedstock cost (mining and pre-cleaning), capital-cost recovery, and operating costs.

8.5.1 Case Study 1: Powellton-Seam Coal

Powellton-seam coal is mined and cleaned in central West Virginia. The existing cleaning plant's froth-flotation circuit produces approximately 60 tph of 7 – 8 percent ash clean coal. As shown in Table 24 above, this coal can be reduced further in ash to approximately 3 percent, at a theoretical yield of about 78 percent. For the flowsheet and cost calculations, we have discounted this yield to about 70 percent to account for inefficiencies in operation.

Figure 43 gives a balanced flowsheet with equipment sizes to produce this 3-percent ash product. It consists of column froth-flotation cells for cleaning and screen bowl centrifuges for dewatering.

8.5.1.1 *Operating Cost Estimate*

The operating cost for producing the 3-percent ash clean-coal product using the flowsheet in Figure 43 was calculated.

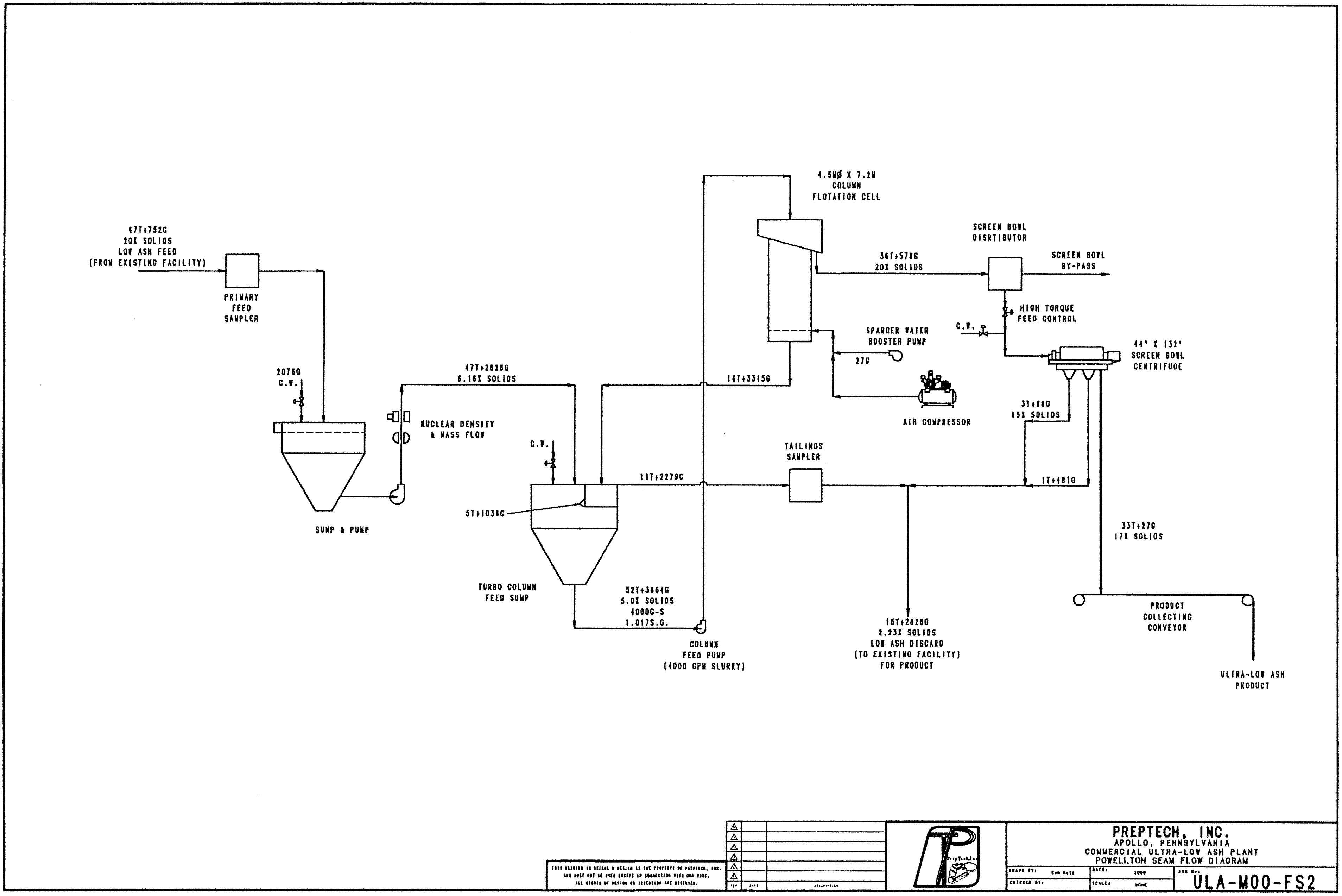
47T+752G
20% SOLIDS
LOW ASH FEED
(FROM EXISTING FACILITY)
PRIMARY
FEED
SAMPLER
2076G
C.W.
SUMP & PUMP
NUCLEAR DENSITY
& MASS FLOW
47T+2828G
6.16% SOLIDS
C.W.
5T+1036G
TURBO COLUMN
FEED SUMP
52T+3864G
5.0% SOLIDS
4000G-S
1.017S.G.
COLUMN
FEED PUMP
(4000 GPM SLURRY)
11T+2279G
16T+3315G
4.5MØ X 7.2M
COLUMN
FLOTATION CELL
36T+578G
20% SOLIDS
SPARGER WATER
BOOSTER PUMP
27G
AIR COMPRESSOR
TAILINGS
SAMPLER
15T+2828G
2.23% SOLIDS
LOW ASH DISCARD
(TO EXISTING FACILITY)
FOR PRODUCT
SCREEN BOWL
DISRTIBUTOR
SCREEN BOWL
BY-PASS
C.W.
HIGH TORQUE
FEED CONTROL
44" X 132"
SCREEN BOWL
CENTRIFUGE
3T+68G
15% SOLIDS
1T+481G
33T+27G
17% SOLIDS
PRODUCT
COLLECTING
CONVEYOR
ULTRA-LOW ASH
PRODUCT
PREPTECH, INC.
APOLLO, PENNSYLVANIA
COMMERCIAL ULTRA-LOW ASH PLANT
POWELLTON SEAM FLOW DIAGRAM
DATE:
SCALE:
NONE
ULA-M00-FS2

Figure 43. Balanced Flowsheet for Producing 3-Percent Ash Powellton-Seam Coal

Table 25 Estimated Operating Conditions for Producing 3-Percent Ash Powellton-Seam Coal

	Annual	**Monthly**		
Average Capacity (tph)	47			
Scheduled Operating Hours	6,240	520		
Availability	80 %			
Raw Tons Processed	234,624	19,552		
Yield	70 %			
Clean Tons Produced	164,736	13,728		
Reject Tons	69,888	5,824		
DIRECT COSTS	**$ Per Raw Ton**	**$ Per Clean Ton**	**Monthly Dollars**	**Annual Dollars**
Fixed Costs				
Labor*	0.598	0.852	11,700.00	140,400.00
Property & Liability Insurance	0.064	0.091	1,250.00	15,000.00
Total Fixed Costs	0.662	0.943	12,950.00	155,400.00
VARIABLE COSTS				
Operating Supplies				
Electricity	0.200	0.285	3,910.40	46,924.80
Chemical & Flocculants	0.250	0.356	4,888.00	58,656.22
Lubricants	0.001	0.001	19.55	234.62
Safety & Compliance	0.001	0.001	19.55	234.62
Tools	0.001	0.001	19.55	234.62
Water Treatment & Conditioning	0.005	0.007	97.76	1,173.12
Miscellaneous	0.005	0.007	97.76	1,173.12
Operating Supplies Total	**0.463**	0.659	9,052.58	108,630.91

* Labor is based on the process requiring 0.5/shift for operations, maintenance, & housekeeping.

Labor is also based on union rate.

8.5.1.2 *Capital Cost Estimate*

The capital cost of all equipment, a building to house this circuitry, and construction was estimated at $2.5 million for a turn-key project. This capital cost was then used to calculate the cost per ton of feed and per ton of low-ash clean-coal product.

The following parameters were used in the calculation:

Total capital cost:	$2,500,000
Years to recover capital:	7
Interest rate:	10 percent
Capital recovery factor:	0.20541
Annual payment:	$2,500,000 x 0.20541 = $513,525

Therefore, using the annual tonnages given in Table 26 for the operating costs, the capital cost is $2.19 per feed ton processed and $3.12 per clean ton processed.

Table 26. Estimated Operating Costs for Producing 3-Percent Ash Powellton-Seam Coal

DIRECT COSTS	$ Per Raw Ton	$ Per Clean Ton	Monthly Dollars	Annual Dollars
Maintenance Supplies				
Communication Systems	0.001	0.001	19.55	234.62
Pumps	0.020	0.028	391.04	4,692.48
Motors	0.015	0.021	293.28	3,519.36
Conveyors	0.002	0.003	39.10	469.25
Centrifuges	0.100	0.142	1,955.20	23,462.40
Piping	0.005	0.007	97.76	1,173.12
Flotation Devices	0.030	0.043	586.56	7,038.72
Electrical & Instrumentation	0.020	0.028	391.04	4,692.48
Plant Structures	0.010	0.014	195.52	2,346.24
Valves	0.008	0.011	156.42	1,876.99
Fire & Water Systems	0.001	0.001	19.55	234.62
Chutes, Hoppers & Sumps	0.001	0.001	19.55	234.62
Miscellaneous	0.005	0.007	97.76	1,173.12

Table 26. Continued

Maintenance Supplies Total	0.218	0.310	4,262.34	51,148.03
Variable Costs Total	0.681	0.970	13,314.91	159,778.94
Total Costs	1.343	1.913	26,264.91	315,178.94

* Labor is based on the process requiring 0.5/shift for operations, maintenance, & housekeeping.

Labor is also based on union rate.

8.5.1.3 *Powellton-Seam Low-Ash Coal Cost*

To estimate the cost to produce 3-percent ash content Powellton-seam coal (FOB cleaning-plant site), three cost components must be included:

- The cost of mining and preparing the feedstock to the column froth-flotation circuit plant. These costs can be estimated by the current selling price of this coal, which we will estimate at $30.00.
- The operating and maintenance cost for the column froth-flotation plant.
- The capital-recovery cost for the column froth-flotation plant.

The costs are summarized on a feed-ton and clean-ton basis and totaled in Table 27. This would reflect the cost of production of 3-percent ash Powellton-seam coal. Additional profit may be added to these costs to obtain a selling price for this material.

Table 27. Cost of Production of 3-Percent Ash Powellton-Seam Coal

Cost Component	**$ Per Feed Ton**	**$ Per Clean Ton**
Coal Feedstock	30.00	42.73
Operating	1.343	1.913
Capital Recovery	2.19	3.12
Total	33.533	47.763

(*Yield in Column Froth-Flotation Plant of 70.21 percent*)

8.5.2.1 Case Study 2: Pittsburgh-Seam Coal

The Pittsburgh-seam coal is mined and cleaned in southwestern Pennsylvania. The existing cleaning plant's froth-flotation circuit (Pitt 2) produces approximately 80 tph of 11 to 12 percent ash clean coal. As shown in Table 24, this coal can be reduced further in ash to approximately 4 percent, at a theoretical yield of about 71 percent. For the flowsheet and cost calculations, we have discounted this yield to about 65 percent to account for inefficiencies in operation.

Figure 44 gives a balanced flowsheet with equipment sizes to produce this 4-percent ash product. It consists of column froth-flotation cells for cleaning and screen bowl centrifuges for dewatering.

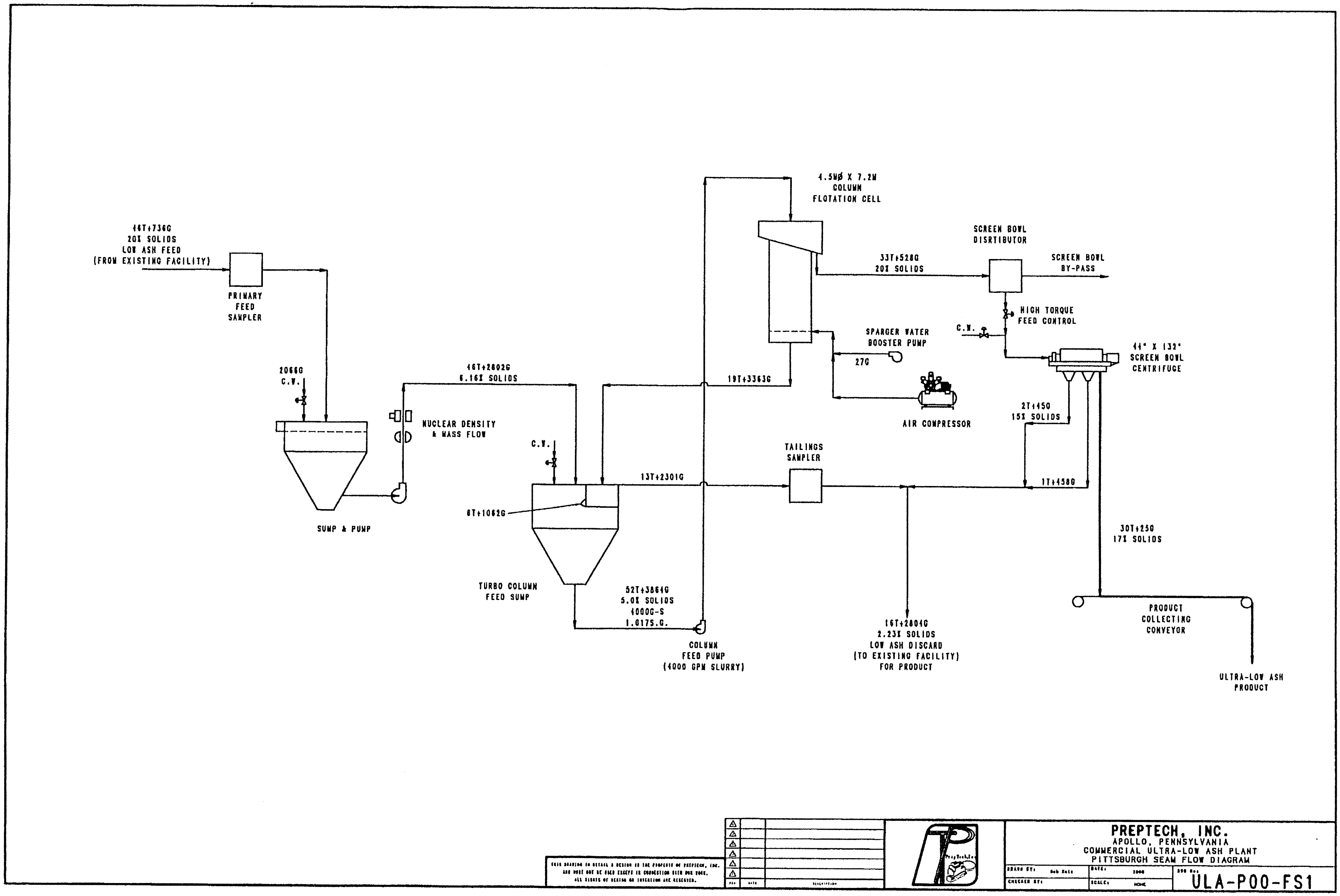
46T+736G
20% SOLIDS
LOW ASH FEED
(FROM EXISTING FACILITY)
PRIMARY
FEED
SAMPLER
2066G
C.W.
SUMP & PUMP
NUCLEAR DENSITY
& MASS FLOW
46T+2802G
6.16% SOLIDS
C.W.
6T+1062G
TURBO COLUMN
FEED SUMP
52T+3864G
5.0% SOLIDS
4000G-S
1.017S.G.
COLUMN
FEED PUMP
(4000 GPM SLURRY)
13T+2301G
19T+3363G
4.5MØ X 7.2M
COLUMN
FLOTATION CELL
33T+528G
20% SOLIDS
SPARGER WATER
BOOSTER PUMP
27G
AIR COMPRESSOR
TAILINGS
SAMPLER
16T+2804G
2.23% SOLIDS
LOW ASH DISCARD
(TO EXISTING FACILITY)
FOR PRODUCT
SCREEN BOWL
DISRTIBUTOR
SCREEN BOWL
BY-PASS
HIGH TORQUE
FEED CONTROL
C.W.
44" X 132"
SCREEN BOWL
CENTRIFUGE
2T+450
15% SOLIDS
1T+4580
30T+250
17% SOLIDS
PRODUCT
COLLECTING
CONVEYOR
ULTRA-LOW ASH
PRODUCT
PREPTECH, INC.
APOLLO, PENNSYLVANIA
COMMERCIAL ULTRA-LOW ASH PLANT
PITTSBURGH SEAM FLOW DIAGRAM
SCALE:
NONE
ULA-P00-FS1

Figure 44. Balanced Flowsheet for Producing 4-Percent Ash Pittsburgh-Seam Coal

Operating Cost Estimate

The operating cost for producing the 4-percent ash clean-coal product using the flowsheet in Figure 8.3 was calculated. Assumptions for fixed and variable costs are given in Table 28 on a raw- (or feed) ton and clean-ton basis. The operating and maintenance costs per feed ton were estimated at $1.358, which equates to $2.082 per clean ton.

Table 28. Estimated Pperating Costs for Producing 4-Percent Ash Pittsburgh-Seam Coal

	Annual	**Monthly**		
Average Capacity (tph)	46			
Scheduled Operating Hours	6,240	520		
Availability	80 %			
Raw Tons Processed	229,632	19,136		
Yield	65 %			
Clean Tons Produced	149,760	12,480		
Reject Tons	79,872	6,656		
DIRECT COSTS	**$ Per Raw Ton**	**$ Per Clean Ton**	**Monthly Dollars**	**Annual Dollars**
Fixed Costs				
Labor*	0.611	0.938	11,700.00	140,400.00
Property & Liability Insurance	0.065	0.100	1,250.00	15,000.00
Total Fixed Costs	0.677	1.038	12,950.00	155,400.00
Variable Costs				
Operating Supplies				
Electricity	0.200	0.307	3,827.20	45,926.40
Chemical & Flocculants	0.250	0.383	4,784.00	57,408.00
Lubricants	0.001	0.002	19.14	229.63
Safety & Compliance	0.001	0.002	19.14	229.63
Tools	0.001	0.002	19.14	229.63

Water Treatment & Conditioning	0.005	0.008	95.68	1,148.16
Miscellaneous	0.005	0.008	95.68	1,148.16
Operating Supplies Total	0.463	0.710	8,859.97	106,319.62

* Labor is based on the process requiring 0.5/shift for operations, maintenance, & housekeeping.

Labor is also based on union rate.

8.5.2.2 *Capital Cost Estimate*

The capital cost of all equipment, a building to house this circuitry, and construction was estimated at $2.5 million for a turn-key project. This capital cost was then used to calculate the cost per ton of feed and per ton of low-ash clean-coal product.

The following parameters were used in the calculation:

Total capital cost:	$2,500,000
Years to recover capital:	7
Interest rate:	10 percent
Capital recovery factor:	0.20541
Annual payment:	$2,500,000 x 0.20541 = $513,525

Therefore, using the annual tonnages given in Table 29 for the operating costs, the capital cost is $2.24 per feed ton processed and $3.43 per clean ton processed.

Table 29. Estimated Operating Costs for Producing 4-Percent Ash Pittsburgh-Seam Coal

DIRECT COSTS	$ Per Raw Ton	$ Per Clean Ton	Monthly Dollars	Annual Dollars
Maintenance Supplies				
Communication Systems	0.001	0.002	19.14	229.63
Pumps	0.020	0.031	382.72	4,592.64
Motors	0.015	0.023	287.04	3,444.48
Conveyors	0.002	0.003	38.27	459.26
Centrifuges	0.100	0.153	1,913.60	22,963.20
Piping	0.005	0.008	95.68	1,148.16
Flotation Devices	0.030	0.046	574.08	6,888.96
Electrical & Instrumentation	0.020	0.031	382.72	4,592.64
Plant Structures	0.010	0.015	191.36	2,296.32

Valves	0.008	0.012	153.09	1,837.06
Fire & Water Systems	0.001	0.002	19.14	229.63
Chutes, Hoppers & Sumps	0.001	0.002	19.14	229.63
Miscellaneous	0.005	0.008	95.68	1,148.16
Maintenance Supplies Total	0.218	0.334	4,171.65	50,059.78
Variable Costs Total	0.681	1.044	13,031.62	156,379.39
Total Costs	1.358	2.082	25,981.62	311,779.39

* Labor is based on the process requiring 0.5/shift for operations, maintenance, & housekeeping.

Labor is also based on union rate.

Pittsburgh-Seam Low-Ash Coal Cost

To estimate the cost to produce 4-percent ash content Pittsburgh-seam coal (FOB cleaning-plant site), the following three cost components must be included:

- The cost of mining and preparing the feedstock to the column froth-flotation circuit plant. These costs can be estimated by the current selling price of this coal, which we will estimate at $22.00.
- The operating and maintenance cost for the column froth-flotation plant.
- The capital recovery cost.

The costs are summarized on a feed-ton and clean-ton basis and totaled in Table 30. This would reflect the cost of production of 4-percent ash Pittsburgh-seam coal. Additional profit may be added to these costs to obtain a selling price for this material.

Table 30. Cost of Production of 4-Percent Ash Pittsburgh-Seam Coal

Cost Component	**$ Per Feed Ton**	**$ Per Clean Ton**
Coal Feedstock	22.00	33.73
Operating	1.358	2.082
Capital Recovery	2.24	3.43
Total	25.598	39.242

(Yield in Column Froth-Flotation Plant of 65.22 percent)

8.6 Summary and Conclusions

Coal sources are available in the United States to produce significant quantities of coals at ash levels between 4 and 6 percent. Only small quantities of coal that contain less than 4-percent ash are shipped to power plants in the United States.

Since the co-coking process will require coal fines (minus 100 mesh or minus 0.15 mm), the froth-flotation process was targeted as the technology to upgrade already cleaned coals at existing cleaning plants. In this phase, several froth concentrates from existing plants were obtained for additional froth-flotation testing. It was found that an ash level of 3 to 4 percent was obtainable at reasonable yields for the coals tested.

For two coals, detailed flowsheets and cost estimates were prepared. The cost of low-ash clean coal was estimated at $47.76 per ton for a 3-percent ash Powellton-seam coal and at $39.24 per ton for a 4-percent ash Pittsburgh-seam coal.

These costs include the cost of the column froth-flotation plant feedstock (mining and pre-cleaning), operating and maintenance costs, and capital costs for the new column froth-flotation plant. It is assumed that this new plant will be constructed at the existing cleaning-plant site to take advantage of existing facilities for water, tailings disposal, and electricity. These costs are FOB cleaning-plant site and do not include transportation or drying, which is assumed to occur at the delayed-coking site to avoid transportation of potentially explosive dry coal fines and to take advantage of the steam available at the refinery.

9.0 BLENDING OF COAL-TAR STREAMS WITH SUITABLE REFINERY STREAMS

9.1 Goals

In this task we set out to achieve the following goals:

- To expand the evaluation and selection of prototype feed mixtures to include hydrotreated tars, selected distillation cuts, and solvent-separated fractions.
- To perform preliminary work on the batch hydrotreatment mechanisms for upgrading gross products, including the evaluation of catalyst, time, temperature, and pressure regime.
- To examine the potential scale-up of the process.

All of the goals have been investigated and completed during the execution of this delivery order.

9.2 Summary

Our research has shown that under appropriate conditions thermally stable jet fuel can be produced from a hydrotreated blend of refinery feedstock and coal-tar distillate. It has also been shown that blends of dearomatized light cycle oil (DA/HT LCO) and refined chemical oil (RCO), in suitable catalytic hydrogenation reactions, can produce high quantities of tetralin. This indicates a potential for high thermal stability and an increase in the amount of material boiling in the jet-fuel range. The balance of jet fuel-fraction yield, tetralin conversion, and production of other potentially thermally stable cyclic structures can be controlled by blending composition and reaction conditions. The catalyst used plays an important role in tetralin conversion, desulfurization, and denitrogenation processes.

9.3 Introduction

As part of the development of processes for the production of coal-based thermally stable jet fuels, coal-tar pitch could become a potential source due to its adequate supply and cyclic-structure content. Cyclic structues can be upgraded into cycloalkanes and hydroaromatic compounds, which can contribute toward a high fuel stability at elevated temperatures.

Coal-tar pitch is a by-product from the metallurgical coke industry. It is made up of the volatile compounds evolved during coal carbonization. The predominant uses of coal-tar pitch currently include the manufacture of electrodes for arc furnaces and the production of fine chemicals through refining. Coal-tar pitch is distilled into various streams: High-quinoline insolubles (QI) and low-QI fractions are used in electrodes; carbon-black oil is used in carbon-black production; creosote oil is used for wood preservation; and naphthalene solvent residue (NSR), RCO, and light distillates are used for fine-chemical production. In addition, suitable petroleum-refinery streams have been selected for the coprocessing experiments.

9.4 Experimental

9.4.1 Analysis Performed

Ultimate analysis of carbon, hydrogen, and nitrogen composition and sulfur analysis were obtained using CHN-600 and SC-132 sulfur-determination analyzers (LECO). Proximate analysis (moisture and ash) was performed using a LECO MAC 400 proximate analyzer. The liquid feedstocks and products were analyzed by high-temperature simulated-distillation gas chromatography (SimDis GC) using a Hewlett-Packard 5890 Series II Plus fitted with a FID detector and a Restek MXT-500 Sim Dist column. The boiling-point distribution and the cut point of the 180 to 330 °C fraction were observed to monitor the yield in the jet-fuel range. Quantitative and chemical speciation were performed on the feeds and samples using a GC-17A gas chromatograph and a QP-5000, a compact, high-performance quadrupole mass spectrometer made by Shimadzu. The column used was a XTi-5 (Restek) with dimensions of 30 m, 0.25-mm ID, and 0.25-μm df (5 percent phenyl film thickness).

9.4.2 Catalyst Preparation [134]

The catalysts, which were manufactured by Criterion Catalysts, were sulfided before being used in this study.

The catalyst was crushed and passed through a sieve with a 60-mesh (0.25 mm) opening. Six g of dodecane, 1.2 g of carbon disulfide, and 1.6 g of catalyst were placed in a 25-ml tubing bomb reactor. The reactor was sealed, purged with hydrogen gas, and pressurized to 250 psig.

The sandbath was set to a temperature of 200 °C. The reactor was placed in the sand bath for 2.5 hours and agitated at 50 strokes per minute. After 2.5 hours, the temperature was raised to 350 °C over a 1-hour period and held there for 1.5 hours.

When the reaction was complete, the reactor was taken out of the sandbath and allowed to cool. The gases were released from the reactor in a fume hood, and the reactor's contents were removed and filtered. The catalyst was washed with hexane and then with acetone. Finally, the catalyst was placed into a sealed vial and dried in a vacuum oven at 110 °C for 2 hours to remove any remaining solvents.

9.4.3 Feedstocks Used.

The LCO, supplied by (BP), was processed into two additional products. First it was hydrogenated to produce a sample high in hydroaromatic content. This hydrogenated LCO went through a second deep-hydrogenation stage to yield a product (DA/HT LCO) rich in cycloalkanes. Koppers Industries supplied the RCO.

9.4.4 Hydrotreating Experiments

Hydrotreating experiments were performed in 25-ml tubing bomb reactors and in a 180-ml stirred-batch reactor. Experiments were conducted at temperatures ranging from 325 to 375 °C and hydrogen pressures ranging from 500 to 1500 psig for 1-2 hours under constant stirring or agitation.

9.5 Results and Discussion

9.5.1 Effects of Catalysts Used

We had previously reported (see final report Delivery Order 3, Task 4) that we had used both Ni/Mo and Co/Mo catalysts for the hydrotreating of blends of coal-tar distillates and petroleum-refinery streams. It was shown that neither of these catalysts demonstrated good overall performance. The Co/Mo was best for desulfurization, and Ni/Mo was best for hydrogenation. To this end, we contacted Criterion Catalysts to request an alternative catalyst that would provide good denitrogenation, desulfurization, and hydrogenation capabilities. Criterion Catalysts supplied us with a commercially available Ni-Mo-P/Al_2O_3 catalyst, which proved to be very effective in hydrogenation, hydrodesulfurization, and hydrodenitrogenation. Phosphorus in Ni-Mo-P was found to have a substantial effect on the hydrodenitrogenation but only a minor effect on the hydrodesulfurization.

9.5.2 Effects of Blending Types and Blending Composition

The types of feedstock from petroleum and coal tar are the key factors in the production of thermally stable jet fuel. In Delivery Order 3, we had shown that the most promising feedstocks for the coal-tar blending work were DA/HT LCO and RCO. The work performed in this delivery order concentrated on blends of DA/HT LCO and RCO, which have shown the best results in producing tetralin. In addition, an exploratory study was conducted in the use of a coal-derived liquid produced from SGI's En-Coal process; this product had a very high level of oxygen-containing species. These oxygenates were removed via solvent extraction, and the neutral fraction remaining was hydrotreated with DA/HT LCO; however, the results were poor in comparison with those from experiments involving RCO.

For blends of DA/HT LCO and RCO, we see a reduction in sulfur and nitrogen content, as well as an increase in the hydrogen-to-carbon ratio (see Figures 45-47). Adding DA/HT LCO, which has a low sulfur and nitrogen content, to the blend provided products low in sulfur and nitrogen content that did not require significant attention to desulfurization and denitrogenation. However, through hydrotreating RCO is also a good source of tetralin. To achieve optimum quality and thermal stability in jet fuel, finding the suitable blending ratio for DA/HT LCO and RCO is another important factor. The blend composition greatly affected the jet-fuel yield and conversion of naphthalene to tetralin (see Figure 48).

An increase of DA/HT LCO in the blends provided an increase in the number of hydrogen-shuttling reactions and yielded hydrogenated products with a high hydrogen-to-carbon ratio and low sulfur and nitrogen content. However, increasing RCO with its high-naphthalene content resulted in a higher tetralin yield. Figure 49 shows that the highest tetralin yield can be provided from the hydrogenation of RCO only. However, the thermal-stability testing showed that hydrogenated products from RCO, after stressing, gave undesirable naphthalene solids. After stressing, the hydrogenated products from the blend DA/HT LCO:RCO 1:3 resulted in very low gas and solid yields. From this consideration, it can be postulated that the blend DA/HT LCO:RCO 1:3 produces a fuel of highest thermal stability.

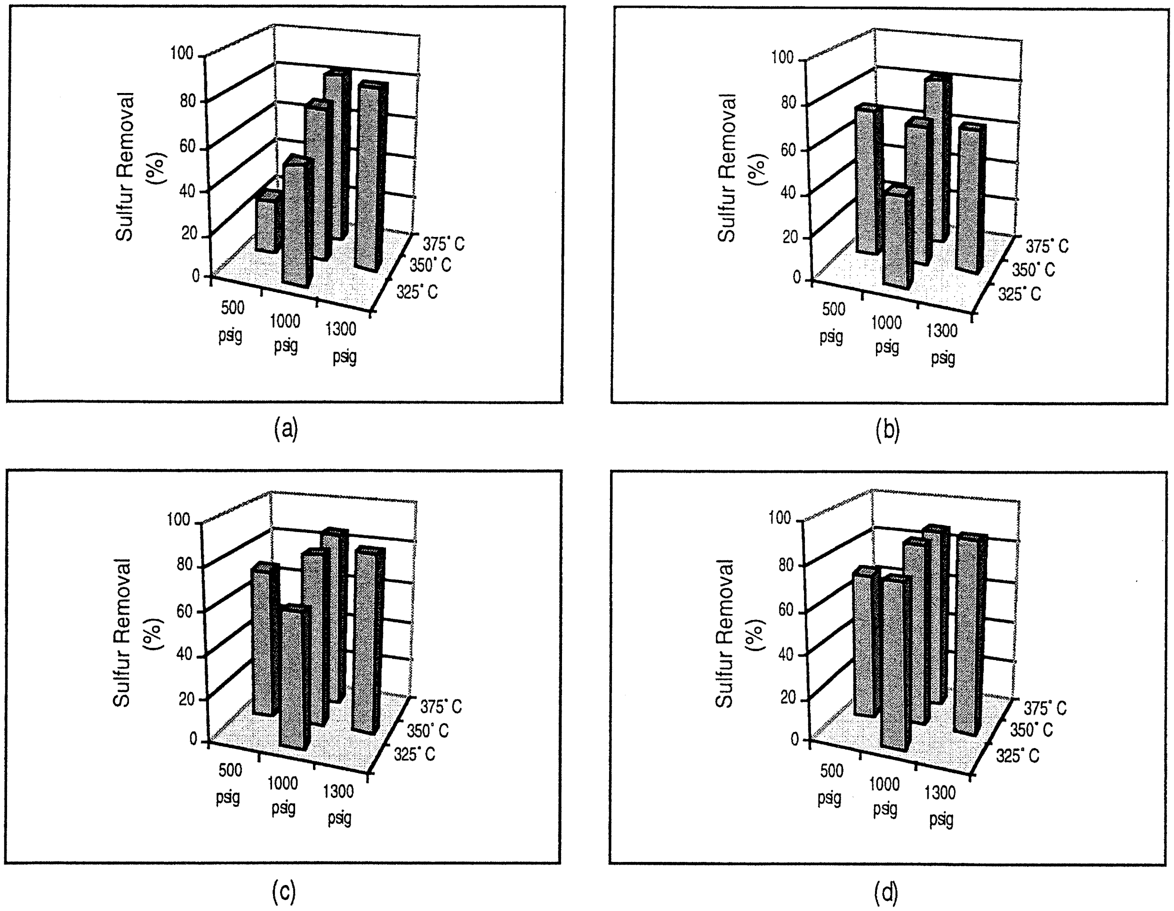

(a) (b) (c) (d)

Figure 45. The Sulfur Removal after Hydrogenation of Different Blends at Varying Temperature and Pressure in a Micro-Reactor
(a) DA/HT LCO:RCO 3:1; (b) DA/HT LCO:RCO 1:1; (c) DA/HT LCO:RCO 1:3; and
(d) DA/HT LCO:RCO 0:1

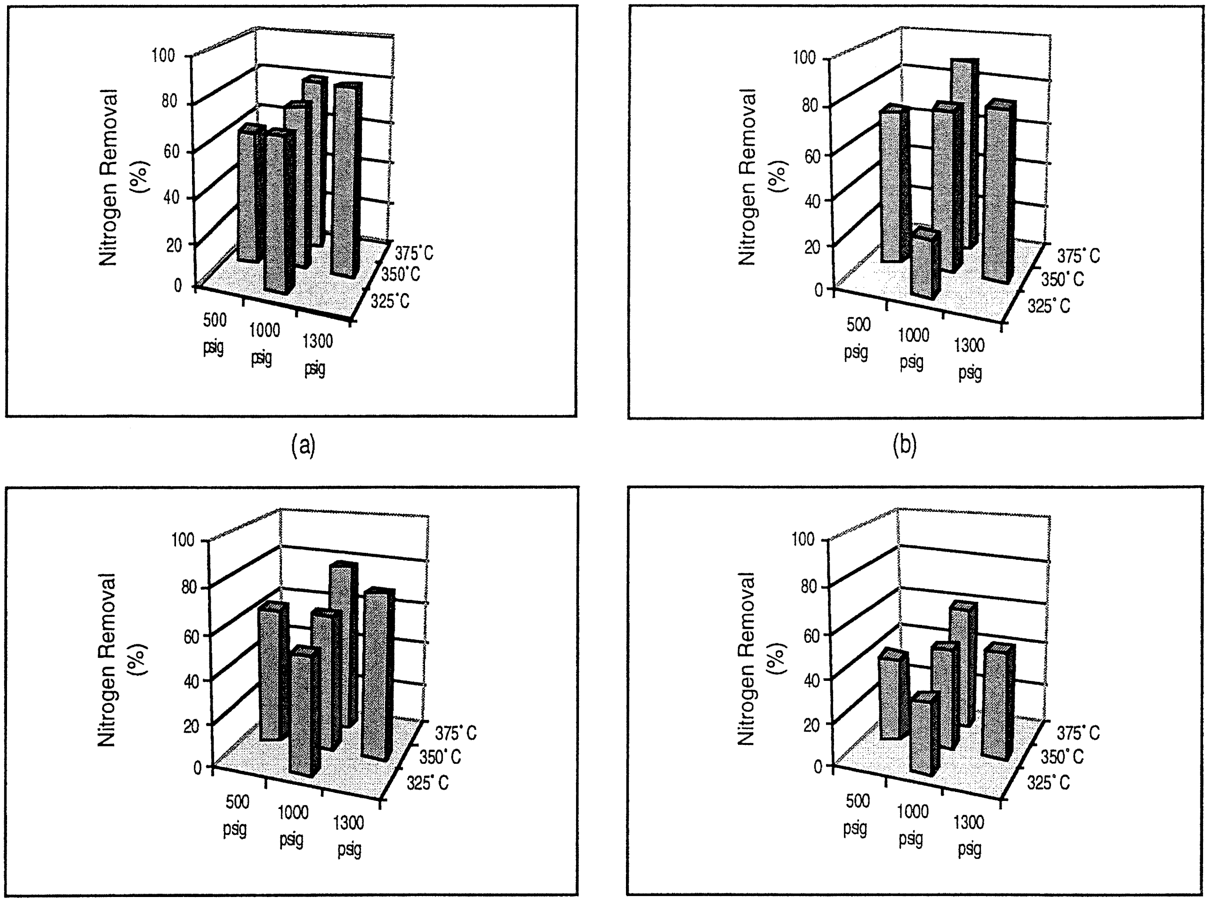

(a) (b) (c) (d)

Figure 46 The nitrogen removal after hydrogenation of different blends at varying temperature and pressure in a micro-reactor
(a) DA/HT LCO:RCO 3:1; (b) DA/HT LCO:RCO 1:1; (c) DA/HT LCO:RCO 1:3; and
(d) DA/HT LCO:RCO 0:1

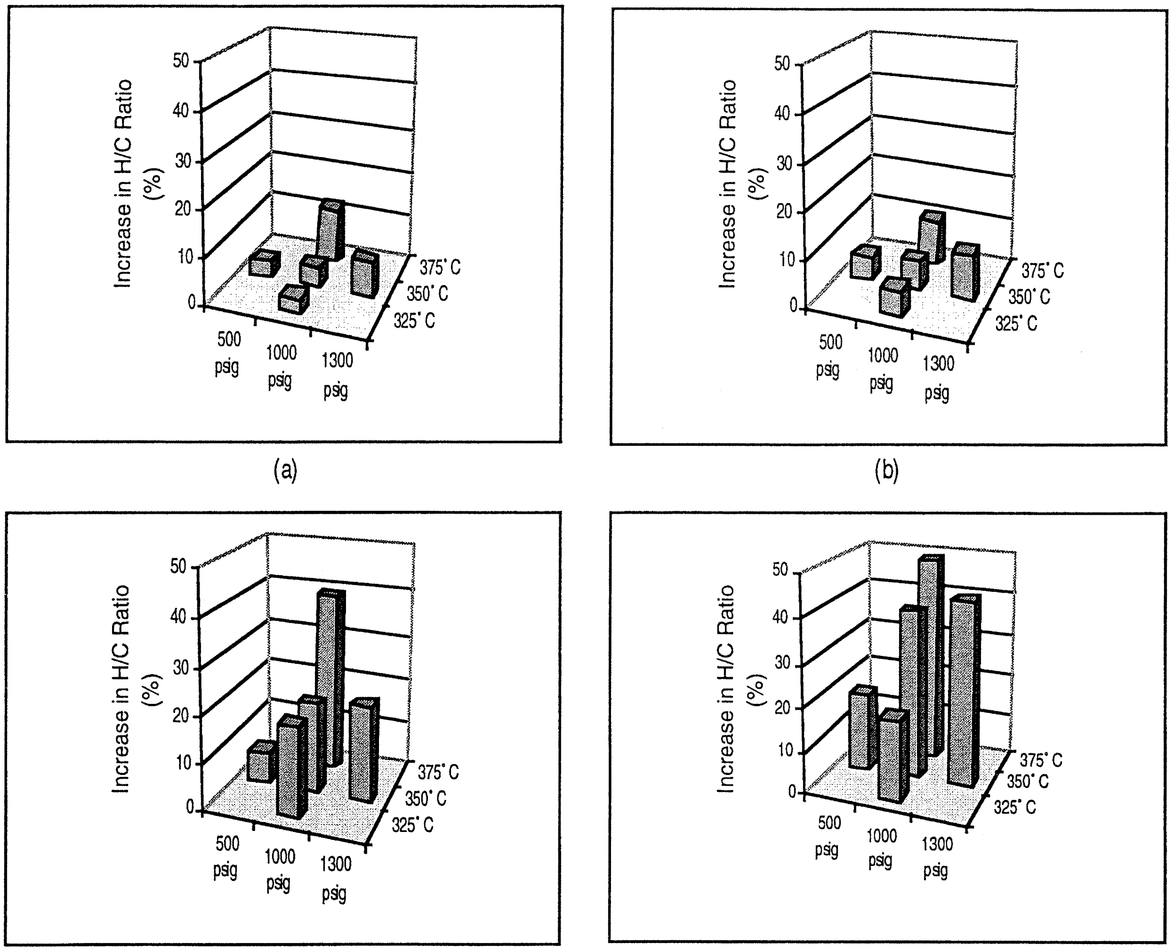

(a) (b) (c) (d)

Figure 47. The Increase in Hydrogen-to-Carbon Ratio of Hydrogenated Products from Different Blends at Varying Temperature and Pressure in a Micro-Reactor
(a) DA/HT LCO:RCO 3:1; (b) DA/HT LCO:RCO 1:1; (c) DA/HT LCO:RCO 1:3; and
(d) DA/HT LCO:RCO 0:1

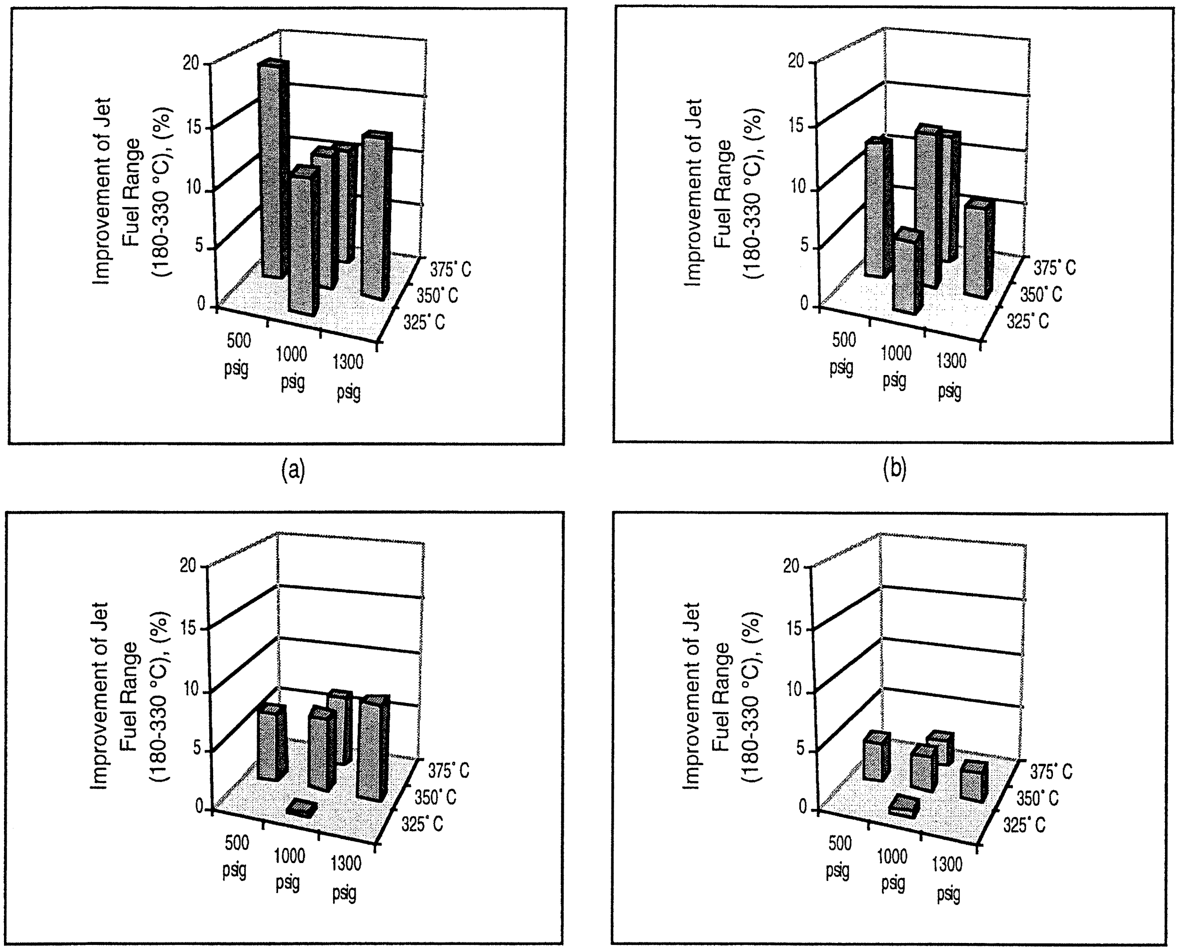

(a) (b)

(c) (d)

Figure 48. The Improvement in the Jet Fuel Range (180-330°C) of Hydrogenated Products from Different Blends at Varying Temperature and Pressure in a Micro-Reactor
(a) DA/HT LCO:RCO 3:1; (b) DA/HT LCO:RCO 1:1; (c) DA/HT LCO:RCO 1:3; and
(d) DA/HT LCO:RCO 0:1

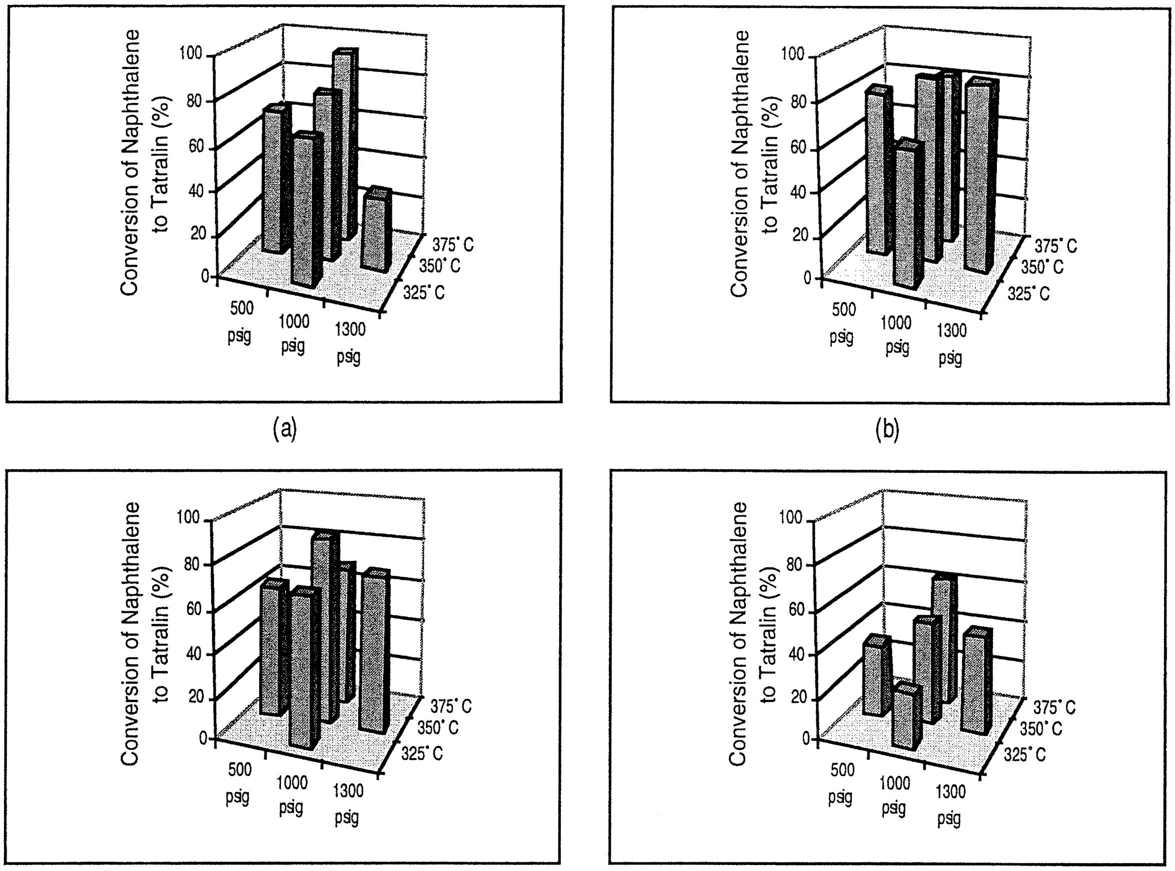

Figure 49. The Conversion of Naphthalene to Tetralin in Hydrogenated Products from Different Blends at Varying Temperature and Pressure in a Micro-Reactor
(a) DA/HT LCO:RCO 3:1; (b) DA/HT LCO:RCO 1:1; (c) DA/HT LCO:RCO 1:3; and
(d) DA/HT LCO:RCO 0:1

9.5.3 Effects of Reaction Conditions

In Figure 47 we see that the temperature greatly affected the hydrogen-to-carbon ratio, as an increase in temperature resulted in cracking to lighter fractions. This led to an increased yield of lower-boiling components (<180 °C), which resulted in a lower jet-fuel yield (180 to 330°C). The sulfur (Figure 45) and nitrogen (Figure 46) contents decreased due to the cracking of heteroatomic compounds to produce H_2S and NH_3, respectively. A temperature of 325 °C was not sufficient for the hydrogenation of RCO, because solid naphthalene precipitated out after the reaction was complete. The reaction of some blends at 375 °C led to products which had boiling points below 180 °C. Changes in temperature did not show any trends or effect on tetralin production. In fact, the hydrogenation of naphthalene in DA/HT LCO:RCO to produce tetralin requires additional study.

Pressure played an important role in the hydrogenation of DA/HT LCO:RCO blends. Most reactions that occurred at 1500 psig showed a significant improvement in tetralin yield, hydrogen-to-carbon ratio, and reduction of sulfur and nitrogen content. For reactions in the micro-reactor, a high initial pressure of 1300 psig (which was closer to 2000 psig when the reactor reached reaction temperature) did not produce results different from those produced when the reactions were performed at initial pressures of 500 and 1000 psig.

Both temperature and pressure greatly affected the properties of jet fuel, e.g., sulfur and nitrogen content, hydrogen-to-carbon ratio, jet-fuel yield, and conversion of naphthalene to tetralin. High pressure and temperature help reduce sulfur and nitrogen content and improve hydrogenation. However, pressure does not have a significant effect on jet-fuel yield.

9.5.4 Scale-Up

A comparison of hydrogenation experiments performed in a 25-mL micro-reactor and in a 180-mL stirred batch reactor showed no significant difference in sulfur and nitrogen removal, in jet-fuel yield, or in the conversion of naphthalene to tetralin (compare Figures 45-49 with Figures 50-54). The results show that the trends in product properties obtained from both reactors are the same. The stirred batch reactor did not improve elemental properties (sulfur and nitrogen removal, hydrogen-to-carbon ratio, and material boiling in jet-fuel range); however, it provided us with an adequate amount of sample (up to 40 ml) and allowed us to calculate hydrogen consumption values. This was very useful as it enabled us to conduct thermal stability tests and observe the hydrogenation ability of the blends.

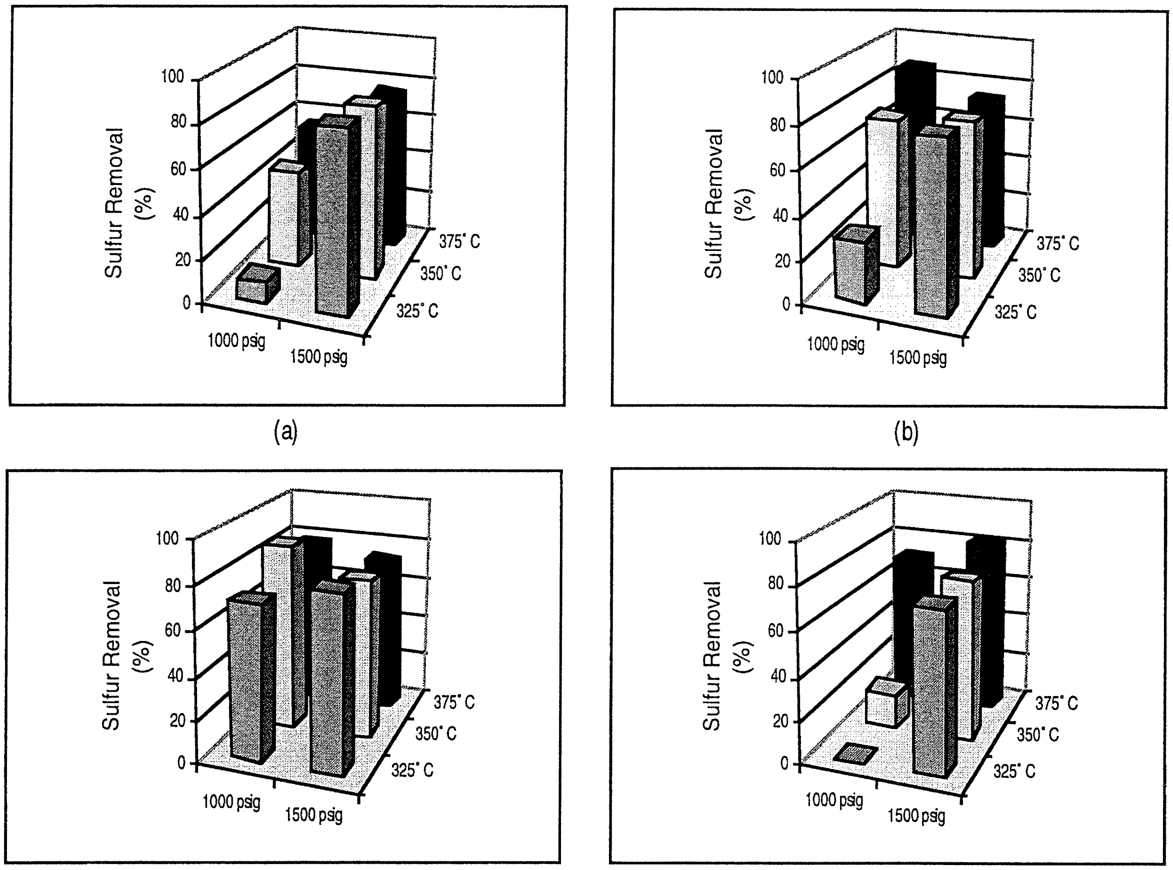

(a) (b)

(c) (d)

Figure 50. The Sulfur Removal after Hydrogenation of Different Blends at Varying Temperature and Pressure in a Stirred Batch Reactor
(a) DA/HT LCO:RCO 3:1; (b) DA/HT LCO:RCO 1:1; (c) DA/HT LCO:RCO 1:3; and
(d) DA/HT LCO:RCO 0:1

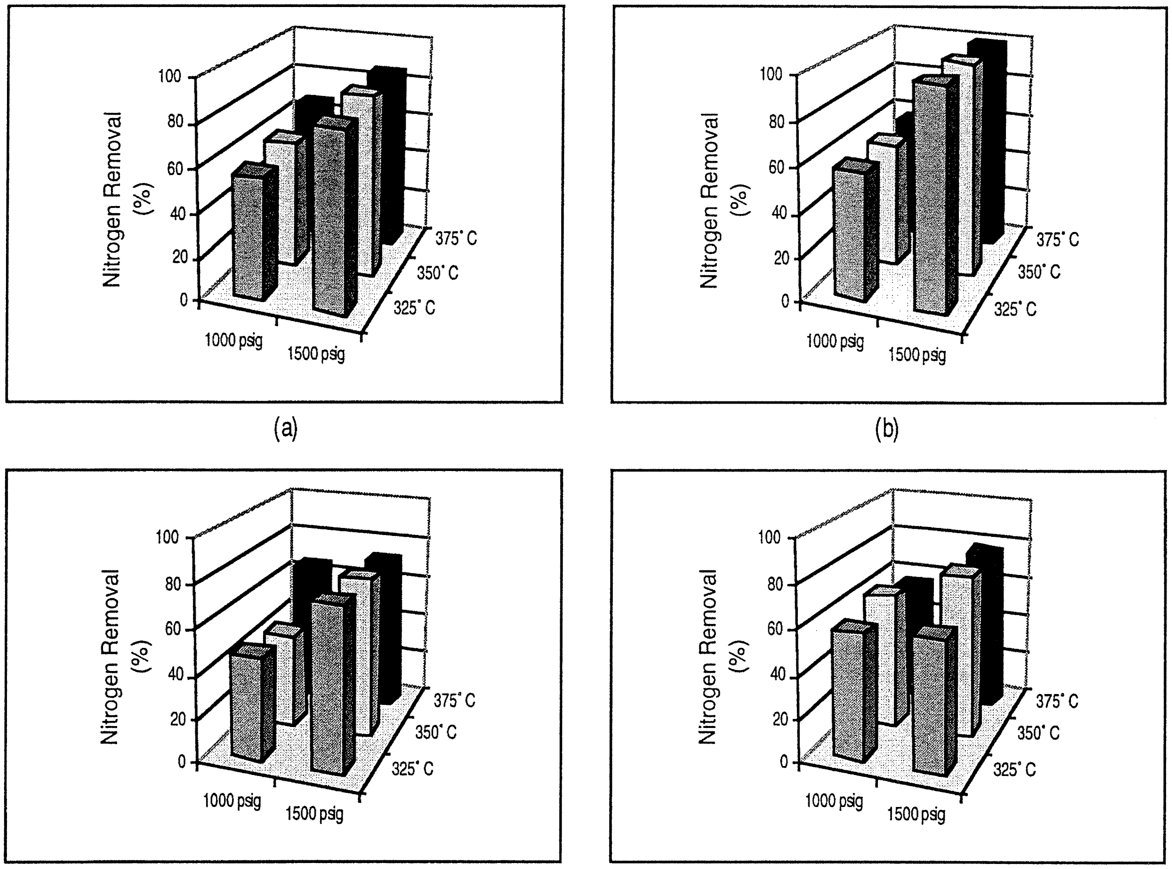

(a) (b) (c) (d)

Figure 51. The Nitrogen Removal after Hydrogenation of Different Blends at Varying Temperature and Pressure in a Stirred Batch Reactor
(a) DA/HT LCO:RCO 3:1; (b) DA/HT LCO:RCO 1:1; (c) DA/HT LCO:RCO 1:3; and (d) DA/HT LCO:RCO 0:1

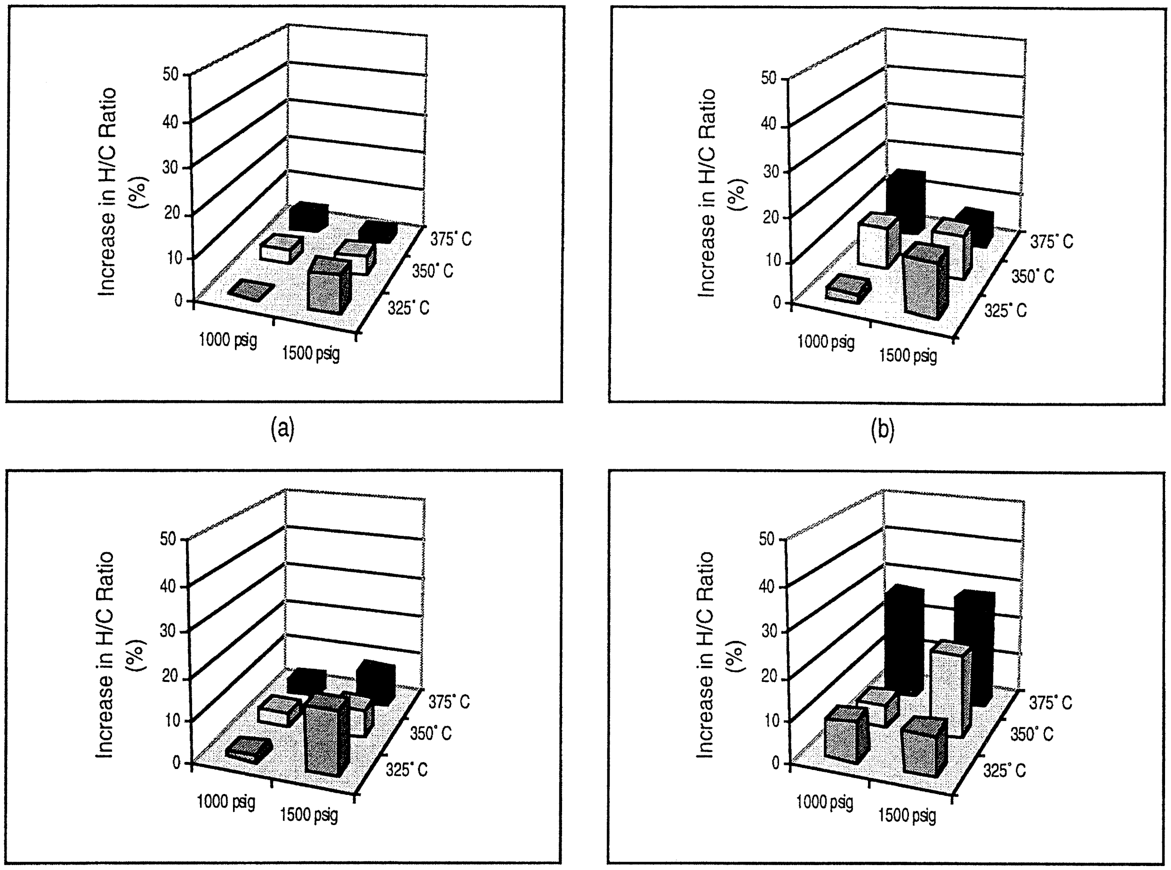

(a) (b) (c) (d)

Figure 52. The Increase in Hydrogen-to-Carbon Ratio of Hydrogenated Products from Different Blends at Varying Temperature and Pressure in a Stirred Batch Reactor
(a) DA/HT LCO:RCO 3:1; (b) DA/HT LCO:RCO 1:1; (c) DA/HT LCO:RCO 1:3; and
(d) DA/HT LCO:RCO 0:1

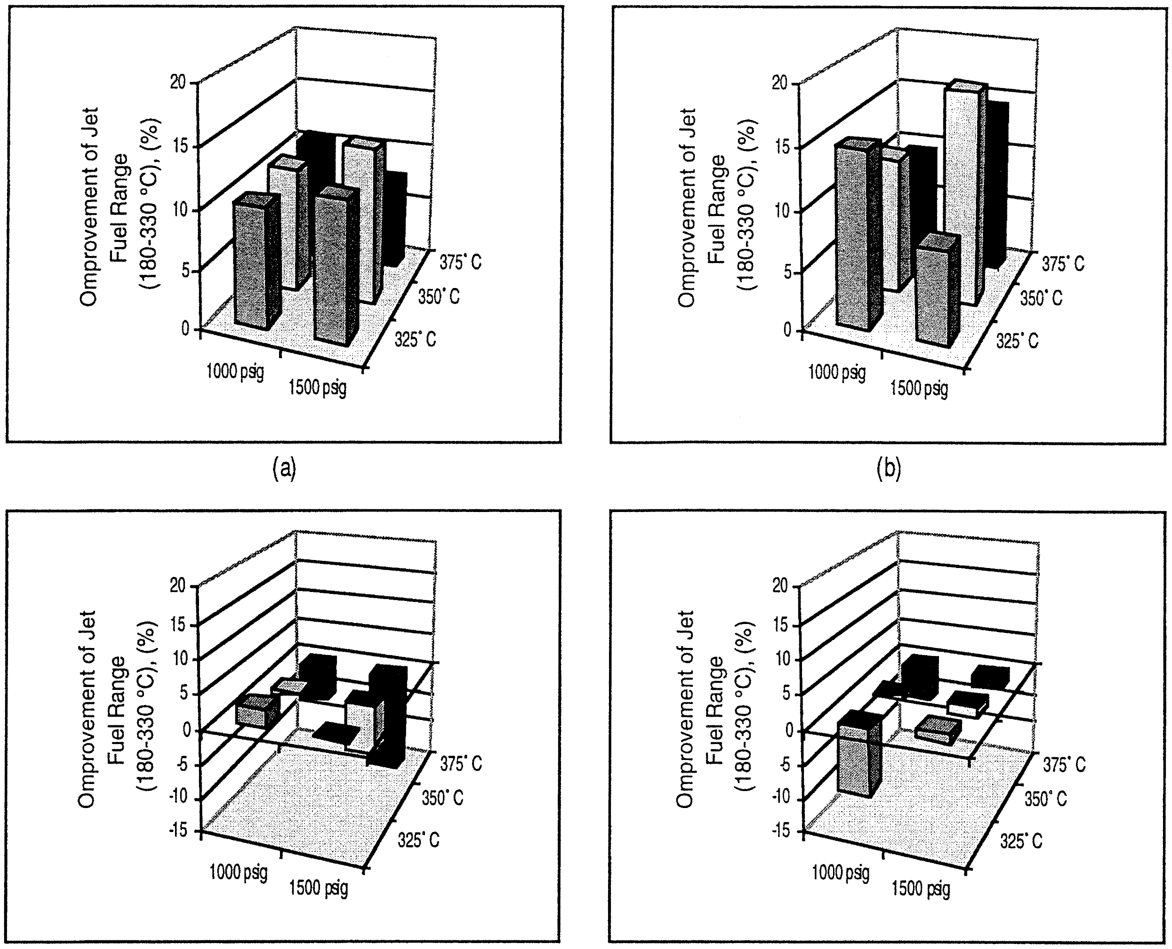

(a) (b)

(c) (d)

Figure 53. The Improvement in the Jet-Fuel Range (180 to 330°C) of Hydrogenated Products from Different Blends at Varying Temperature and Pressure in a Stirred Batch Reactor (a) DA/HT LCO:RCO 3:1; (b) DA/HT LCO:RCO 1:1; (c) DA/HT LCO:RCO 1:3; and (d) DA/HT LCO:RCO 0:1

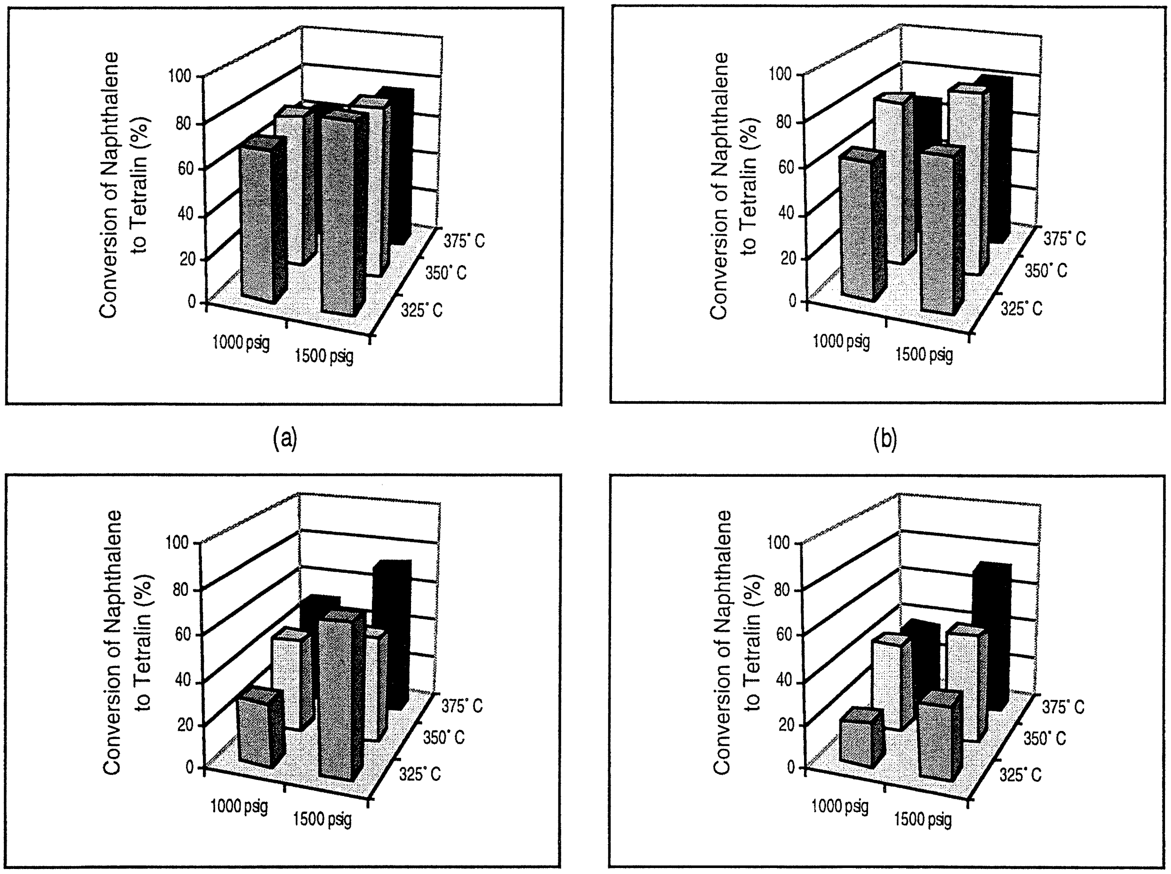

(a) (b)

(c) (d)

Figure 54. The Conversion of Naphthalene to Tetralin in Hydrogenated Products from Different Blends at Varyin9.5.5 g Temperature and Pressure in a Stirred Batch Reactor
(a) DA/HT LCO:RCO 3:1; (b) DA/HT LCO:RCO 1:1; (c) DA/HT LCO:RCO 1:3; and
(d) DA/HT LCO:RCO 0:1.

Thermal-Stability Tests

The thermal-stability test was performed using a 25 mL vertical microautoclave reactor [135, 136]; and a 5-mL volume of liquids. To remove entrapped air, the system was degassed six times with 1000-psig, ultrahigh purity N_2 (99.999 percent). Under an initial pressure of 100-psig N_2, the products were stressed for 2 hours at 480 °C with continuous agitation. When cooled to ambient temperature, the gas phase and liquid fraction were removed for analysis. The tube and stem of the microautoclave were washed in hexane until the hexane remained clear and then dried. Solid deposition was determined through weight gain. The GC-MS was used to determine the composition of liquid products whereas the gas analysis was done by headspace GC.

Figures 55 and 56 show the results from thermal-stressing tests. The DA/HT LCO, containing 32-mole percent cyclohexanes, 32-mole percent decalins, 15-mole percent other cycloalkanes and larger-cycloalkane systems, and 21-mole percent other compounds such as monoaromatics, linear and branched alkanes [135, 136], produced about 37-wt percent gas and 6-wt percent solids. The JP8C, which contains about 22 percent hydroaromatics consisting primarily of alkylated tetralins [136], produced 23-wt percent gas and 4-wt percent solids after 2 hours of stressing. It seems clear that the high gas yield from DA/HT LCO is due to linear alkanes being cracked during stressing. These results agree with the findings of Strohm *et al.* [136].

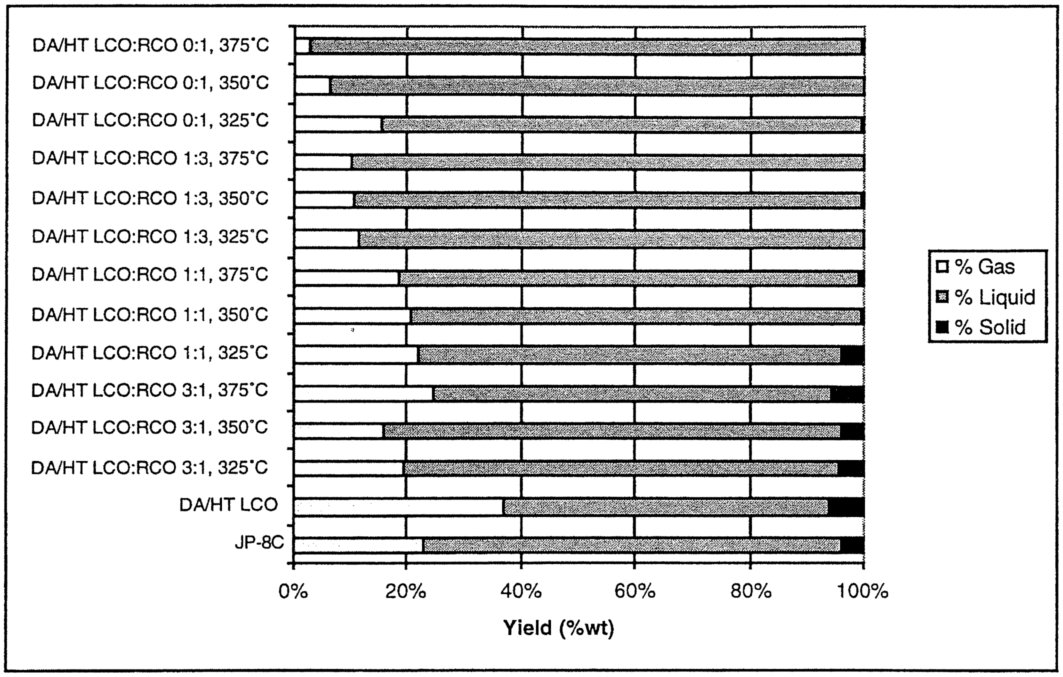

Figure 55. Yields of Conventional Fuels and Hydrogenated Fuels from Reaction at 1000 psig in a Stirred Batch Reactor after Thermal Stressing at 480 °C

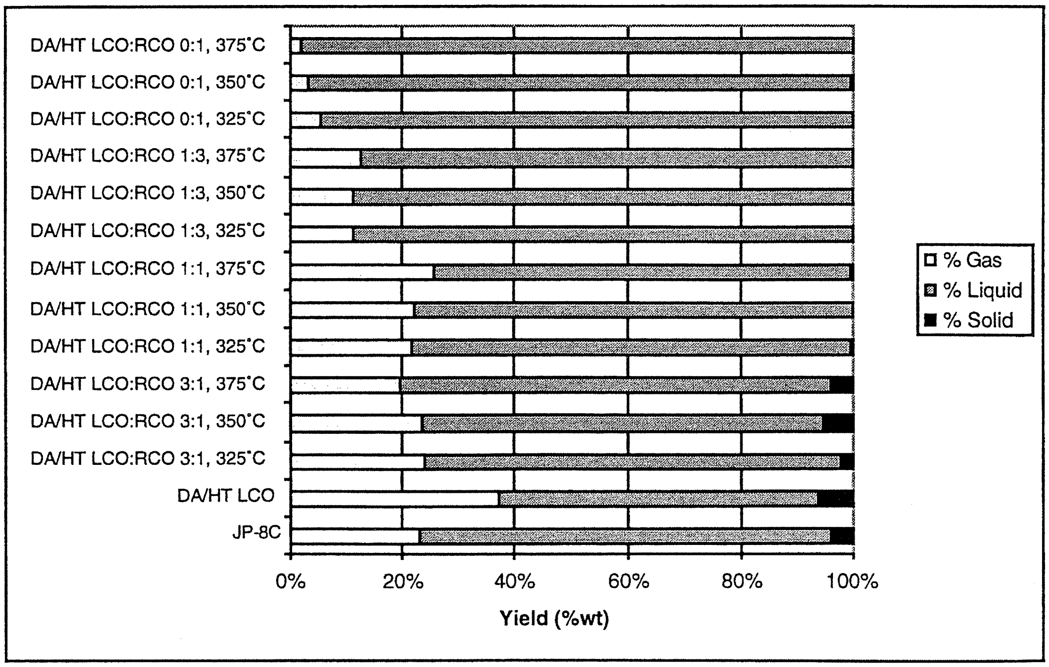

Figure 56. Yields of Conventional Fuels and Hydrogenated Fuels from Reaction at 1500 psig in a Stirred Batch Reactor after Thermal Stressing at 480 °C

Stressing fuels from the hydrogenation of DA/HT LCO:RCO blend yielded less gas and solids than those derived from DA/HT LCO and JP-8C. This was due to tetralin, which is the main component in hydrogenated fuels, acting as a hydrogen donor. Hydrogenated fuels derived from RCO yielded very little gas and coke. However, most of the liquid became a naphthalene-rich solid after thermal stressing for 2 hours. As a result of the conversion of tetralin to naphthalene, there was no coke on the reactor wall, only a naphthalene solid at the bottom of the reactor. This result agrees with the findings of Dutta [137] and Song *et al.* [138] that dehydrogenation is the major reaction at high temperatures (>450 °C). Tetralin is relatively stable to decomposition and dehydrogenation, up to a temperature of 450 °C.

Figures 57 and 58 are GC-MS traces of hydrogenated fuels from the 1:1 blend before and after stressing. It is clear that the main component of the fuel before stressing was tetralin, whereas naphthalene was a minor component. After stressing, the tetralin peak disappeared and the naphthalene peak became predominant.

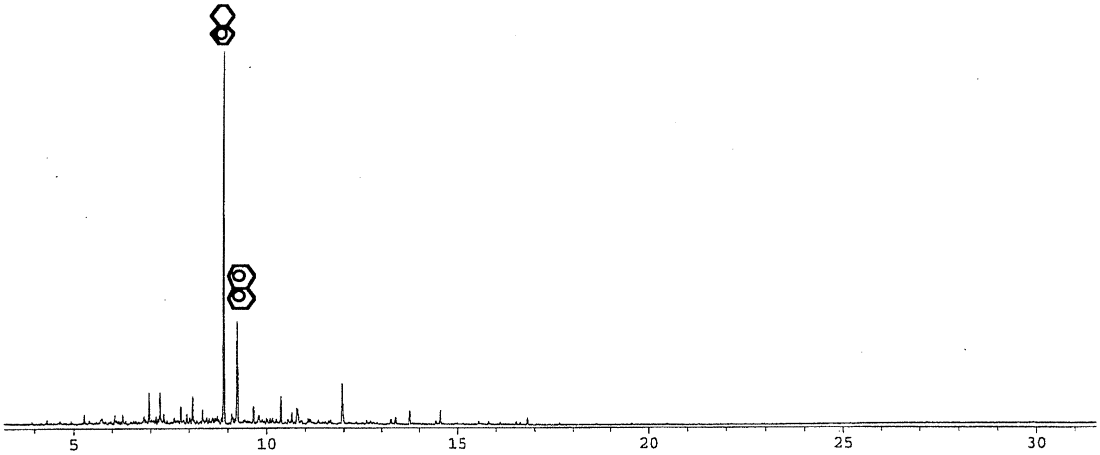

Figure 57. GC-MS Trace of Hydrogenated Product of DA/HT LCO:RCO 1:1 (under 1000 psig and 350°C) before Stressing

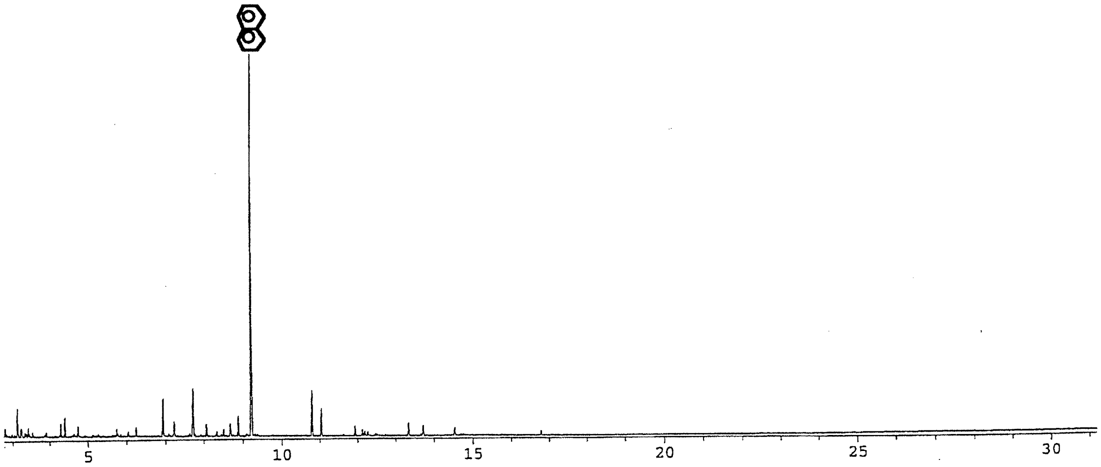

Figure 58. GC-MS Trace of Hydrogenated Product of DA/HT LCO:RCO 1:1 (under 1000 psig and 350°C) after Stressing

Tables 31 and 32 list examples of the components of hydrogenated fuels (from reaction at 1000 psig and 1500 psig) before and after stressing. The three main components before stressing were tetralin, naphthalene, and decalin. After thermal decomposition tetralin yielded toluene, alkylbenzenes, indane and alkylindanes, and naphthalene. In most instances, decalins were found to be present in the products in smaller amounts after stressing, whereas tetralins were still present in significant quantities in stressed fuels derived from the hydrogenation of DA/HT LCO:RCO 0:1. Naphthalene and alkylnaphthalene were the main components in all stressed fuels, followed by indane and alkylindanes, benzene and alkylbenzenes, and toluene.

Hydrogenated fuel from DA/HT LCO:RCO 1:3 possesses the most desirable thermal stability. Both parameters obtained from the stressing of the 1:3 blend are very low compared with those from other blends. This is a result of the 1:3 blend containing a large amount of tetralin. Both gas and solids were formed in proportion to the decrease in tetralin yield. This means that the hydrogenated fuels from the blend rich in RCO yielded a large amount of tetralin, resulting in a higher thermal stability.

Figure 56 shows that fuels from blends of DA/HT LCO:RCO 1:3 at 1500 psig (325 and 375 °C) resulted in the lowest gas formation and solid deposition. Therefore, the 1:3 blend appear to have the most desirable ratio for thermally stable jet-fuel production. Even though the fuels derived from the hydrogenation of only RCO produced less gas and coke, the naphthalene solid appearing at the bottom of reactor is undesirable. Naphthalene is a precursor to solid deposition, and the presence of its solid phase at room temperature may cause combustion problems.

Table 31. Examples of Composition Analysis of Hydrogenated Fuels from Reaction at 1000 psig and 350°C in a Stirred Batch Reactor before and after Stressing

		DA/HT LCO:RCO			
Condition	Composition	3:1	1:1	1:3	0:1
Before Stressing	Decalin (%)	4.4	3.0	0.7	< 0.2
	Tetralin (%)	20.2	31.4	31.3	31.0
	Naphthalene (%)	7.8	8.9	39.4	42.7
After Stressing	Toluene (%)	1.3	2.9	5.7	1.2
	Decalin (%)	0.6	1.9	2.0	0.2
	Tetralin (%)	2.0	2.6	1.7	7.9
	Benzene, alkylbenzene (%)	3.5	5.4	13.0	1.6
	Indane, alkylindane (%)	9.9	9.9	6.0	14.5
	Naphthalene (%)	52.4	45.3	38.3	47.4
	Alkylnaphthalene (%)	17.3	12.4	17.4	15.3

Typical gas-composition analysis after stressing showed all product gases to be composed of primarily methane, followed by ethane, ethylene, propane, propene, butane, and pentane in some cases.

These thermal-stressing tests were performed for the hydrogenated products. The results of thermal-stability tests will be greatly improved if the material boiling in jet-fuel range (180 to 330 °C) is distilled, and, at the same time, heavy aromatics like anthracene and phenanthrene, which are precursors to solid deposition and have boiling points higher than 330 °C, are removed.

Table 32. Examples of Composition Analysis of Hydrogenated Fuels from Reaction at 1500 psig and 350 °C in a Stirred Batch Reactor before and after Stressing

		DA/HT LCO:RCO			
Condition	Composition	3:1	1:1	1:3	0:1
Before Stressing	Decalin (%)	9.4	6.5	1.2	0.2
	Tetralin (%)	19.9	43.0	32.9	39.2
	Naphthalene (%)	6.0	7.2	34.5	38.0
After Stressing	Toluene (%)	7.1	3.8	1.7	1.3
	Decalin (%)	3.4	3.5	0.6	< 0.1
	Tetralin (%)	1.6	1.3	2.1	8.0
	Benzene, alkylbenzene (%)	13.6	7.1	2.9	1.5
	Indane, alkylindane (%)	6.2	10.6	10.5	13.5
	Naphthalene (%)	29.7	42.2	55.4	56.2
	Alkylnaphthalene (%)	13.8	11.8	13.6	10.7

9.6 Conclusions

In conclusion, hydrogenated products from reactions of DA/HT LCO:RCO 1:3 occurring at 1500 psig in the temperature range of 325 to 375°C in a stirred batch reactor have provided a fuel of the highest thermal stability, by having a large tetralin yield and a low sulfur and nitrogen content. In summary, the hydrogenated products from the hydrogenation of DA/HT LCO:RCO 1:3 at 1500 psig and 325 °C provided the optimum fuel by consisting of 50 percent (wt) tetralin, 0.06 percent (wt) sulfur, and 0.08 percent (wt) nitrogen. The hydrogen-to-carbon ratio is 1.30, and the jet-fuel yield is 80 percent.

Another advantage of coal-tar blending is the *in situ* formation of tetralin. In addition to adding tetralin as a hydrogen-donating solvent to jet fuel to improve its thermal stability, hydrogenation of coal-tar blends with refinery streams is another possible and more economical way.

9.7 Suggestions for Future Work

The data presented is from a preliminary study of an alternative process to produce thermally stable jet fuel by using coal-tar distillates as a potential source. This small-scale work can provide ideas for the scale-up of the process. Future studies will use fixed bed-catalyst techniques for pilot-scale production. The tests will be done in early 2000 by PARC Technical Services, Inc., Harmarville, PA. In a flow system, residence time will be a new factor controlling the composition of jet fuel. The design of the fixed bed-catalyst system will become critical.

The variation of pressure and temperature in a stirred batch reactor should be extended for an additional series of tests. In future work, the variation of temperature will be a key factor because each temperature condition has so far shown an inconsistent trend with each blending ratio. High temperatures such as 375 °C may easily crack some components in the 3:1 and 1:1 blends into lighter fractions having boiling points lower than the jet-fuel range (180 to 330 °C), whereas 325 °C is not adequate to hydrogenate all of the naphthalene during the hydrogenation of RCO.

Determination of hydrogen consumption in a stirred batch reactor is also an important factor in the analysis of hydrogen-to-carbon ratio, hydrogenation, desulfurization, and denitrogenation capabilities. In GC-MS analysis, the study of each individual component, e.g., naphthalene, tetralin, decalin, acenaphthylene, dibenzothiophene, carbazole, dibenzofuran, anthracene, phenanthrene, and other heavy aromatics, has to be carefully evaluated.

Another factor that would improve the quality of jet fuel is the calorific value. The calorific value of hydrogenated products will be measured, and the relationship between calorific value and chemical components in the jet fuel will be considered.

Measuring the thermal stability for products from a stirred batch reactor as a function of the residence time for thermal stressing will provide accurate results and a very useful reference. However, the results will be improved if the hydrogenated fuel components boiling in the 180 to 330 °C range are distilled prior to performing a thermal-stability test. In addition, thermal-stability tests in a flow reactor should be considered in future work as well. Finally, it should be possible to establish a relationship between the tetralin content and the thermal stability of the fuel.

10.0 REFERENCES

1. Song, C., Schmitz, A. D., *Energy & Fuels*, **11**, 656-66 (1997).
2. Stock, W. H., *J. Am. Chem. Soc. Sym. Ser.*, **634**, 379 (1996).
3. Stanislaus, A., Cooper, B. H., *Catal. Rev. Sci. Eng.*, **36**, 75-123 (1994).
4. Lin, S. D., Song, C., *Catalysis Today*, **31**, 93 (1996).
5. Hazlett, R. N., *Thermal Oxidation Stability of Aviation Turbine Fuels*, AST Monograph 1, ASTM, Philadelphia (1991), p. 163.
6. Morris, R. N., Hazlett, R. N., McIlvaine, C., L., *Ind. Eng. Chem. Res.,* **27**, 1524 (1998).
7. Moler, J. L., Steward, E. M., *Am. Chem. Soc. Div. Pet. Chem. Prepr.*, **34**, 837 (1989).
8. Edwards,T., Liberio, P. D., *Am. Chem. Soc. Div. Pet. Chem. Prepr.*, **39,** 91 (1994).
9. Edwards, T., Harrison, W. E., Schobert, H. H., 33rd AIAA/ASME/ASME/SAE Joint Propulsion Conference and Exhibit, July 6-9, 1997, Seattle, WA, Paper No. AIAA 97-2848.
10. Song, C., Eser, S., Schobert, H. H., Hatcher, P. G., *Energy Fuels*, **7**, 234 (1993).
11. Coleman, M. M., Schobert, H. H., Song, C., *Chemistry in Britain, Royal Chem. Soc.,* **29**, 760 (1993).
12. Song, C., Lai, W.C., Schobert, H. H., *Ind. Eng. Chem. Res.,* **33**, 534 (1994).
13. Eser, S., Song, C., Copenhaver, R., Parzybsju, M., *Am. Chem. Soc. Div. Pet. Chem. Prepr.*, **37**, 493 (1992).
14. Song, C., Eser, S., Schobert, H. H., Hatcher, P. G., *Am. Chem. Soc. Div. Pet. Chem. Prepr.,* **37**, 540 (1992).
15. Song, C., Lai, W.C., Schobert, H. H., *Ind. Eng. Chem. Res.*, **33**, 548 (1994).
16. Selvaraj, L., Sobkowiak, M., Song, C., Stallman, J., Coleman, M. M., *Energy Fuels*, **8**, 839 (1994).
17. Song, C., Lai, W.C., Schobert, H. H., *Am. Chem. Soc. Div. Fuel Chem. Prepr.*, **37**, 1655 (1992).
18. Yoon, E. M., Selvaraj, L., Song, C., Stallman, J. B., Coleman, M. M., *Energy Fuels*, **10**, 806 (1996).
19. Andrésen, J. M., Strohm, J. J., Coleman, M. M., Song, C., *Am. Chem. Soc. Div. Fuel Chem. Prep.,* **44**, 557 (1999).

20. Shao, J., Song, C., *16th North Am. Catal. Soc. Meeting*, Boston, May 30 - June 4 1999, Poster Program, Paper No. PII-016.
21. Schmitz, A. D., Bowers, G., Song, C., *Catal. Today*, **31**, 45 (1996).
22. Lin, S. D., Song, C., *Catal. Today*, **31**, 93 (1996).
23. Lai, W.C., Song, C., *Fuel*, **74**, 1436 (1995).
24. SCI-Expanded Database (1986-1999), Institute of Scientific Information (ISI), USA, at http://www.webofscience.com/, searched online during October 29 - November 5, 1999.
25. Vannice, M. A., *TOP CATAL*, **4**, 241 (1997).
26. Neri, G., Visco, A. M., Donato, A., Milone, C., Malentacchi, M., Gubitosa, G., *Appl. Catal. A*, **110**, 49 (1994).
27. Shawn, L. D., Song, C., *Catal. Today*, **31**, 93 (1996).
28. Li, C. L., Xue, Z. R., Cao, Z. A., Gates, B. C., *AIChE J.*, **31**, 170 (1985).
29. Song, C., Lai, W. C., Schobert, H. H., *ACS Div. Fuel Chem. Prepr.*, **37**, 1655-1663 (1992).
30. Song, C., Lai, W. C., Schobert, H. H., *Ind. Eng. Chem. Res.*, **33**(3), 548-557 (1994).
31. Khan, M. R., Reynolds, J. G., *CHEMTECH*, **26**, 56-61 (1996).
32. Song, C., Schmitz, A. D., *Energy & Fuels*, **11**, 656-661 (1997).
33. Reddy, K. M., Song, C., in *Designing Transportation Fuels for a Cleaner Environment*, Taylor & Francis Publisher, 173-185 (1999).
34. Konvalinka, J. A., Scholten, J. J. F., *J. Catal.*, **48**, 374 (1977).
35. Dorling, T.A., Moss, R. L., *J. Catal.*, **7**, 378 (1967).
36. O'Rear, D. J., Loffler, Boudart, M. J., *Catal.*, **131**, 121 (1990).
37. Card No.: 04-0880, Joint Committee on Powder Diffraction Standards, Pennsylvania (1974).
38. Card No.: 21-1272, Joint Committee on Powder Diffraction Standards, Pennsylvania (1974).
39. Tsonopoulos, C., Heidman, J. K., Hwang, S. C., *Thermodynamic and Transport Properties of Coal Liquids*, John Wiley & Sons, New York (1986).
40. Mushrush, G. W., Beal, E. J., Hardy, D. R., Hughes, J. M., *Fuel Processing Technology*, **61**, 197-210 (1999).
41. Gates, B. C., Katzer, J. R., Schuit, G. C. A., *Hydrodesulfurization Chemistry of Catalytic Processes*, McGraw Hill, New York (1979).
42. Topsoe, H., Clausen, B. S., *Catal. Rev. Sci. Eng.*, **26**(3 & 4), 395-420 (1984).

43. Topsoe, H., Clausen, B. S., *Applied Catalysis*, **25**, 273-293 (1986).
44. Chianelli, R. R., Daage, M., in *Structure/Function Relations in Transition Metal Sulfide Catalysts* Structure-Activity and Selectivity Relationships in Heterogeneous Catalysis R. K. Grasselli, A. W. Sleight eds. Elsevier Science Publishers BV, Amsterdam (1991).
45. Chianelli, R. R., Daage, M., Ledoux, M. J., *Advances in Catalysis*, **40**, 177-232 (1994).
46. Chianelli, R. R., Lyons, J. E., *Catalysis Today,* **22**, 261-396 (1994).
47. Daage, M., Chianelli, R., *Journal of Catalysis*, **149**, 414-427 (1994).
48. Topsoe, H., Clausen, B. S., Massoth, F. E., *Hydrotreating Catalysis: Science and Technology*, Springer-Verlag, Berlin (1996).
49. Vasudevan, P. T., Fierro, J. L. G., *Catal. Rev. Sci. Eng.*, **38**(2), 161-188 (1996).
50. Gates, B. C., Topsoe, H., *Polyhedron*, **16**(18), 3213-3217 (1997).
51. Prins, R., in *Hydrotreating Reactions,* Handbook of Heterogeneous Catalysis, eds. G. Ertl, H. Knözinger, and J. Weitkamp Berling, VCH **3** (1997).
52. Furimsky, E., *Applied Catalysis A: General*, **171**, 177-206 (1998).
53. Whitehurst, D. D., Isoda, T., Mochida, I., *Advances in Catalysis*, **42**, 345-471 (1998).
54. Ho, T. C., *Catalysis Review -Science and Engineering*, **30**(1), 117-160 (1988).
55. Derbyshire, F. J., *Catalysis in Coal Liquefaction*, IEA Coal Research, London, U. K. (1988).
56. Furlong, M., Fox, J., Masin, J., Production of Jet Fuels from Coal-Derived Liquids. Vol. IX-Results of Bench-Scale and Pilot Plant Testing, Fuel Science Program, The Pennsylvania State University (1989).
57. Gregory, R., Schobert, H. H., Eser, S., Song, C., Boehman, A., Coleman, M. M., Technical Report to US DOE, DE-FG22-92-PC92104, Fuel Science Program, The Pennsylvania State University (1997).
58. Gary, J. H., Handwerk, G. E., *Petroleum Refining: Technology and Economics*, Marcel Dekker, Inc., New York (1994).
59. Nishioka, M., Campbell, R. M., Lee, M. L., Castle, R. N., *Fuel*, **65**, 270 (1986).
60. Ma, X., Sakanishi, K., Isoda, T., Mochida, I., *Fuel*, **76**(4), 329-339 (1997).
61. Ma, X., Sakanishi, K., Mochida, I., *Ind. Eng. Chem. Res.*, **33**(2), 218-222 (1994).
62. Ma, X., Sakanishi, K., Mochida, I., *Ind. Eng. Chem. Res.*, **35**(8), 2487-2495 (1996).
63. Isoda, T., Nagao, S., Ma, X., Korai, Y., Mochida, I., *Energy & Fuels*, **10**, 482-486 (1996).
64. Isoda, T., Nagao, S., Ma, X., Korai, Y., Mochida, I., *Energy & Fuels*, **10**, 1078-1082 (1996).

65. Lamure-Meille, V., Schulz, E., Lemaire, M., Vrinat, M., *Applied Catalysis A: General*, **131**, 143-157 (1995).
66. Landau, M. V., Berger, D., Herskowitz, M., *Journal of Catalysis*, **158**, 236-245 (1996).
67. Takatsuka, T., Wada, Y., Inoue, S.I., *ACS Preprints*, **36**(4), 255 (1996).
68. Farag, H., Whitehurst, D. D., Mochida, I., *Industrial Engineering and Chemistry Research*, **37**(9), 3533-3539 (1998).
69. Farag, H., Sakanishi, K., Mochida, I., Whitehurst, D. D., *Energy & Fuels*, **13**, 449-453 (1999).
70. Kabe, T., Akamatsu, K., Ishihara, A., Otsuki, S., Godo, M., Zhang, Q., Qian, W., Yamada, S., *Sekiyu Gakkaishi*, **42**(3), 150-156 (1999).
71. Delmon, B., *Catalysis Letters*, **22**, 1-32 (1993).
72. Murali Dhar, G., Ramakrishna, H., Prasad, V.V. D. N., Prasada Rao,T. S. R., *Chemical Industry Digest*, 89-93 (1993).
73. Startsev, A. N., *Catal. Rev. Sci. Eng.*, **37**(3), 353-423 (1995).
74. Dolce, G. M., Savage, P. E., Thompson, L. T., *Energy & Fuels*, **11**, 668-675 (1997).
75. Van Looij, F., Van Der Laan, P., Stork, W. H. J., DiCamillo, D. J., Swain, J., *Applied Catalysis A: General*, **170**, 1-12 (1998).
76. Markel, E. J., Burdick, S. E., Leaphart II, M. E., Roberts, K. L., *Journal of Catalysis*, **182**, 136-147 (1999).
77. Ma, X., Schobert, H. H., *Journal of Catalysis*, Communicated (1999).
78. Givens, E. N., Venuto, P. B., *Preprints, Division of Petroleum Chemistry*, **15**(4), A183 (1970).
79. Houalla, M., Nag, N. K., Sapre, A. V., Broderick, D. H., Gates, B. C., *AIChE J.*, **24**(1015) (1978).
80. Clausen, B. S., Topsoe, H., Frahm, R., *Advances in Catalysis*, **42**, 315-343 (1996).
81. Knudsen, K. G., Cooper, B. H., *Applied Catalysis A: General*, Communicated (1999).
82. Wivel, C., Clausen, B. S., Candia, R., Morup, S., Topsoe, H., *J. Catal.*, **87**, 497-513 (1984).
83. Carberry, J. J., *Chemical and Catalytic Reaction Engineering*, McGraw Hill, New York (1976).
84. Chen, Y.W., Hsu, W.C., Lin, C.S., Kang, B.C., Wu, S.T., Leu, L.J., Wu, J.C., *Ind. Eng. Chem. Res.,* **29**, 1830-1840 (1990).

85. Li, C., Chen, Y.W., Yang, S.J., Wu, J.C., *Ind. Eng. Chem. Res.,* **32**, 1573-1578 (1993).
86. Chen, Y.W., Tsai, M.C., *Ind. Eng. Chem. Res.,* **36**(7), 2521-2525 (1997).
87. Farrauto, R. J., Bartholomew, C. H., *Fundamentals of Industrial Catalytic Processes*, Blackie Academic & Professional, London (1997).
88. Vanrysselberghe, V., Froment, G. F., *Ind. Eng. Chem. Res.* **35**, 3311-3318 (1996).
89. Vidal, J. L., Walker, W. E., *Inorg. Chem.*, **19**, 896 (1980).
90. Noack, K., *Spectrochim. Acta. Part A.,* **24**, 1917 (1968).
91. Alemdaroglu, N. H., Penninger, J. L. M., Oltay, E., *J. Mol. Catal.*, **1**, 27 (1967).
92. Morris, D. E., Tinker, H. B., *Rev. Sci. Instrument.*, **43**, 1024 (1977).
93. Rigby, W., Whyman, R., Wilding, K., *J. Phy. Sci. Instrument*, **2**, 27 (1970).
94. King, R. B., King, A. D., Ifbal, M. Z., Frazier, C. C., *J. Amer. Chem. Soc.,* **100**, 1687 (1978).
95. Dardas, Z., Suer, M. G., Ma, Y. H., Moser, W. R., *J. Catal.,* **159**, 204 (1996).
96. Moser, W. R., Cnossen, J. E., Wang, A. W., Krouse, S. A., *J. Catal.*, **95**, 21 (1985).
97. Yokoyama, C., Kamo, Y., Takahashi, M., Ohtaka, K., Takahashi, S., *Rev. Sci. Instrument.*, **6415**, 1369 (1993).
98. Song, C., Eser, S., Schobert, H. H., Hatcher, P. G., *Energy Fuels*, **7**, 234-243 (1993).
99. Schmitz, A., Bowers, G., Song, C., *Catal. Today*, **31**(1), 45-56 (1996).
100. Eischens, R. P., Francis, S. A., Pliskin, W. A., *J. Phys. Chem.*, **60**, 194 (1956).
101. Bradshaw, A. M., Hoffman, F. M., *Surf. Sci.,* **52**, 449 (1975).
102. Bradshaw, A. M., Hoffman, F. M., *Surf. Sci.,* **72**, 513 (1978).
103. Tanaka, K., White, J. M., *J. Catal.,* **79**, 81 (1983).
104. Vannice, M. A., Twu, C. C., Moon, S. H., *J. Catal.,* **79**, 70 (1983).
105. Topsoe, H., Clausen, B. S., *Catal. Rev.Sci. Eng.,* **26**, 395 (1984).
106. Topsoe, N.Y., Topsoe, H., Sorensen, O., Clausen, B. S., Candia, R., *Bull. Soc. Chim. Belg.* **93**(8-9), 727 (1984).
107. Gates, B. C., Ktazer, J. R., Schuit, G. C. A, *Chemistry of Catalytic Processes*, McGraw-Hill, New York (1979).
108. Peri, J. B., *J. Phys. Chem.*, **86**, 1615 (1982).
109. Segawa, K.L, Hall, W. K., *J. Catal.,* **77**, 221 (1982).
110. Valyon, J., Hall, W. K., *J. Catal.*, **84**, 216 (1983).
111. Topsoe, N.Y., Topsoe, H., *J. Catal.,* **84**, 386 (1983).

112. Portela, L., Grange, P., Delmon, B., *Bull. Soc. Chim. Belg.,* **100**, 985 (1991).
113. Kung, M. C., Kung, H. H., *Catal. Rev.Sci. Eng.*, **27**(3), 425 (1985).
114. Topsoe, N.Y., Topsoe, H., *J. Catal.*, **75**, 354 (1982).
115. O'Young, C.L., Yang, C.H., DeCanio, S. J., Patel, M. S., Storm, D. A., *J. Catal.,* **113**, 307 (1988).
116. Daly, F. P., Schmitt, J. L., Sturm, E. A., *J. Catal.*, **97**, 248 (1986).
117. Okamoto, Y., Maezawa, A., Imanaka, T., *J. Catal.*, **120**, 29 (1989).
118. Portela, L., Grange, P., Delmon, B., *Catal. Rev.Sci. Eng.,* **37**(4), 699 (1995), and references therein.
119. Topsoe, N.Y., Topsoe, H., *Bull. Soc. Chim. Belg.*, **90**(12), 1311 (1981).
120. Okamoto, Y., Katoh, Y., Mori, Y., Imanaka, T., Teranishi, S., *J. Catal.*, **70**, 445 (1981).
121. Goldwasser, J., Fang, S. M., Houalla, M., Hall, W. K., *J. Catal.*, **115**, 34 (1989).
122. Zhuang, S., Hall, W. K., Ertl, G., Knozinger, H., *J. Catal.*, **100**, 167 (1986).
123. Redey, A., Goldwasser, J., Hall, W. K., *J. Catal.*, **113**, 82 (1988).
124. Knözinger, H., in G. Ertl, H. Knözinger, and J. Weitkamp (eds.), *Handbook of Heterogenous Catalysis*, Wiley-VCH, Weinheim, Vol. 2 (1997), p. 707.
125. Bachelier, J., Duchet, J. C., Cornet, D., *Bull. Soc. Chim. Belg.*, **90**, 1301 (1981).
126. Delgado, E., Fuentes, G. A., Hermann, C., Kunzmann, G., Knozinger, H., *Bull. Soc. Chim. Belg.,* **93**, 735 (1984).
127. Zaki, M. I., Vielhaber, B., Knözinger, H., *J. Phys. Chem.*, **90**, 3176 (1986).
128. Knözinger, H., in *Transition Metal Sulfides*, T. Weber (eds.), Kluwer Academic Publishers, Netherlands (1998), p. 189.
129. Yamada, M., Koizumi, N., Yamazaki, M., *Catal. Today*, **50**, 3 (1999).
130. Yamada, M., Koizumi, N., Yamazaki, M., Hatanaka, S., *Catal. Today*, **39**, 33 (1997).
131. Fickinger, A. E., Badger, M. W., Mitchell, G. D., Schobert, H. H., *ACS Div. Of Fuel Chem.*, **44**, 684 (1999).
132. Hossain, T., Zaman, N., Jahan, S. T., Podder, J., Rashid, M. A., *J. Mech. Eng. Res. & Dev.* **16**, 47 (1994).
133. Rodriguez-Reinoso, F., Santana, P., Romero Palazon, E., Diez, M. A., *Carbon*, **36**, 105 (1998).

134. Ueda, K., Matsui, H., Song, C., Xu, W., *Journal of the Japan Petroleum Institute*, **33**, 413-417 (1990).

135. Andrésen, J. M., Strohm, J. J., Song, C., *Preprints of Papers, ACS Division of Petroleum Chemistry*, **43**(3), 412-414 (1998).

136. Strohm, J. J., Andrésen, J. M., Song, C., *Preprints of Papers, ACS Division of Petroleum Chemistry*, **44**(3), 386-390 (1999).

137. Dutta, R. P., "Catalytic Hydrogenation-Dehydrogenation of Multicyclic Compounds under Fuel Processing Conditions", *Ph.D. Thesis 1996*, The Pennsylvania State University.

138. Song, C., Lai, W., Schobert, H. H., *Preprints of Papers, ACS Division of Fuel Chemistry*, **37**(4), 1655 (1992).

139. Schobert,H. Boéhman, A. Hatcher, P. Song, C. "Coal-Based Fuel Formulation and Engineering", Prepared for U.S. Air Force, Wright Patterson Air Force Base. Contract # F33615-98-D-2802 D.O.0003. February 2000.

List of Symbols, Abbreviations, and Acronyms

Nomenclature	Definition
AAP – (p. 44)	Alumina – Alumina Phosphate
AED – (p. 42)	Atomic Emission Detector
AGO – (p. 24)	Atmospheric Gas Oil
ASTM – (p. 58)	American Standard Test Method
BP - (p. 97)	British Petroleum (Company Name)
CIR – (p. 47)	Cylindrical Internal Reflectance
DAC – (p. 37)	Data Acquisition
DBT – (p. 42)	DiBenzothiophene
DMDBT – (p. 55)	Dimethyldibenzothiophene
DRIFTS – (p. 47)	Diffuse – Reflectance Techniques
EBP – (p. 41)	End Boiling Point
FCC – (p. 41)	Fluid Catalytic Cracking
FID – (p. 59)	Flame ionization detector
FOB – (p. 89)	Free on board
FTIR – (p.47)	Fourier-transform infra red
GC-MS-(p.68)	Gas Chromatography – Mass Spectrometry
HDN – (p. 44)	Hydrodenitrogenation
HDS – (p. 54)	Hydrodesulfurization
HP – (p. 59)	Hewlett Packard
HTR – (p. 22)	High-Temperature Reduction
IBP – (p. 41)	Initial Boiling Point
IR – (p. 41)	Infra-red
LC – ((p. 41)	Liquid-Chromatography
LCO - (p. 41)	Light Cycle Oil
LECO – (p. 59)	Company Name

Nomenclature	Definition
LTR – (p. 22)	Low-Temperature Reduction
MDBT – (p. 42)	Methyldibenzothiophene
MSI – (p. 15)	Metal-Support Interactions
NSR – (p. 96)	Naphthalene Solvent Residue
PASC – (p. 43)	Polyaromatic Sulfur Compounds
PE – (p. 3)	Perkin-Elmer
Q.I. – (p. 96)	Quinoline Insolubles
RCO – (p. 96)	Refined Chemical Oil
RPM – (p. 36)	Revolutions per Minute
SMSI – (p. 22)	Strong Metal – Support Interaction
THF – (p. 60)	Tetrahydrofuran
THN – (p. 12)	Tetrahyaronaphthalene
THNOL – (p. 12)	Tetrahydronaphthol
THQ – (p. 12)	Tetrahydrquinoline
TPD – (p. 4)	Temperature-Programmed Desorption
TPR – (p. 7)	Temperature-Programmed Reduction
UHP – (p. 2)	Ultra high purity
USY – (p. 4)	Ultrastable Y (zeolite)
VGO – (p. 41)	Vacuum Gas Oils
XRD – (p. 22)	X-ray diffraction